Multiphysics modeling of deformation in biomembranes and the neuronal microenvironment, with application to Traumatic Brain Injury

by

Debabrata Auddya

A dissertation submitted in partial fulfillment of
the requirements for the degree of

Doctor of Philosophy

(Mechanical Engineering)

at the

UNIVERSITY OF WISCONSIN–MADISON

2024

Date of final oral examination: 04/22/2024

The dissertation is approved by the following members of the Final Oral Committee:

Shiva Rudraraju, Assistant Professor, Mechanical Engineering (chair)
Christian Franck, Professor, Mechanical Engineering
Alejandro Roldan-Alzate, Associate Professor, Mechanical Engineering
Corinne Henak, Assistant Professor, Mechanical Engineering
Aviad Hai, Assistant Professor, Biomedical Engineering

Inarticulo Mortis Caelitus Mihi Vires

ACKNOWLEDGMENTS

I am indebted to the University of Wisconsin-Madison for providing an opportunity to conduct my doctoral research. I am very grateful to my advisor Shiva Rudraraju for giving me a chance to work on a wide spectrum of research problems. I am thankful to the PhD committee members for their valuable time, and constructive feedback. The numerical and computational components of my research work wouldn't have been possible without the super-computing infrastructure and support provided by the Center for High Throughput Computing, compphys, and mighty "gandalf"- our lab cluster. I am thankful to my peers in the CMMG group for their valuable help in professional and personal capacities. Huge shout-out to friends who have helped me get through the thick and thins of my doctoral journey, uncertain pandemic, and lockdown. Much obliged to my mentors for their support, feedback, and mentorship at different stages of my career. I also want to thank my family members for their unconditional support and grateful to the Lord Almighty.

— Debabrata Auddya

"Last but not least, I want to thank me for believing in me, I want to thank me for doing all this hard work. I wanna thank me for having no days off. I wanna thank me for never quitting. I wanna thank me for always been a giver and trying to give more than I receive. I want to thank me for trying to do more right than wrong. I want to thank me for just being me at all times." - Snoop Dogg

CONTENTS

LIST OF TABLES

LIST OF FIGURES

ABSTRACT

Traumatic Brain Injury (TBI) is a progressively common pathological condition worldwide caused due to concussion, impact or blast to the brain. Existing challenges in TBI detection and diagnosis are partly a result of the rich microstructural complexity of the brain and the multiscale heterogeneity of the cerebral architecture. During an injury, the brain gets exposed to significant loads which fall within the pathological spectrum. Neurons and neuron clusters, which are the functional and structural units of the brain, in turn experience this mechanical strain/stress leading to a wide range of morphological and biochemical abnormalities. Due to the inherent challenges in predicting and diagnosing these loading and injury conditions, there is a growing interest in computationally modeling the neurons, and their structural and functional units. However, current coarse-scale modeling and reduced representation of the underlying sub-neuronal structures often fail to render a rich spatio-temporal representation of neuronal mechanics and subsequently capturing neuronal injury. To address these limitations, we present continuum-scale computational frameworks for modeling the neuronal microenvironment and neuron clusters. We categorize this study into two aspects: biological membranes and the neuronal microenvironment.The significance of membranes in neuronal physiology is widely acknowledged due to their crucial roles in facilitating both ionic transmission and the transport of nutrients. In order to understand the morphological modifications which biomembranes undergo to enable critical biological processes, we develop a computational framework. This numerical methodology takes into account Kirchhoff Love thin shell kinematics, Helfrich energy representation of the curvature energy and the framework of Isogeometrical Analysis to model three dimensional representations of membranes. Unlike previous axisymmetric considerations, our model admits asymmetric and

higher order, lower energy modes of deformation which are fundamental morphological adaptations that lipid bilayers seem to undergo.

In the following chapters, we present a detailed description of the neuronal microenvironment and model various mechanical and chemical metrics of injury. Initially, we present a continuum-scale computational framework for modeling the neuronal microstructure and neuronal clusters. We capture viscoelastic behaviour of the sub-neuronal proteins which provide structural and functional integrity to the neurons using representative mechanical networks. A multi-scale approach of modeling deformation of a cluster of neurons is constructed in which local sub-neuronal strain-stress metrics are estimated under various global neuronal cluster loading conditions.

In the final part of this work, we demonstrate a chemical basis of injury in which the pathological degradation of the neuronal microenvironment is considered. During a concussion or impact, beyond the initial mechanical injury (primary injury), a series of subsequent downstream pathways are set in motion, initiating a cascade of pathological biochemical processes. We have modeled some of these potential early stage (before the onset of any immune response) biochemical processes by simulating the spatio-temporal evolution of the relevant molecular biomarkers. These biomarkers are numerically modeled as coupled reaction-diffusion species that are modulated by mechanical strain/stress. This results in a comprehensive numerical framework for capturing the mechano-chemical multiphysics underlying neuronal injury, and also provides deeper insights into the spatio-temporal localization of the the mechanical metrics and the underlying biomarkers. A key highlight of this framework is the ability to obtain a computational injury curve that captures injury sensitivity of the neuronal microenvironment to rate dependent mechanical loading, and this is demonstrated using some initial (coarse) estimates of the injury envelope.

1 INTRODUCTION

The brain is considered as one of the most critical organs of the human body. It plays a central role in the functioning, organisation and maintenance of the rest of the organs. Neurons, which are the functional units of the brain, are the primary constituents of the brain matter, and their signaling activity constitutes the defining functionality of the brain. On the downside however, the brain is also the most vulnerable organ and any injury, impact or concussion to this soft biological structure jeopardizes the human physiology to various degrees. In this context, we classify such injuries arising from external loading conditions as Traumatic Brain Injury (TBI). Even though TBI itself is a broad classification of injuries, we direct our attention and investigation to sub-neuronal injuries often referred to as Diffuse Axonal Injury (DAI). The axon is a long, slender extension of the neuron and houses major structural, signal transmission and protein transport components of the neuron. During a DAI major structural and functional components of axon get affected leading to a spectrum of pathological conditions. This diffuse damage is known to persist as longtime cerebo-cranial effects from delayed brain degradation and absence of visible symptoms. One prime challenge in diagnosing and detecting injuries at the sub-neuronal scale is the increased complexity, heterogeneity and multi-scale organisation of the brain. The brain spans many orders of length scales and most of the diffuse damage manifests at the sub-neuronal scale leading to the triggering of potential biochemical pathways that may lead to the manifestation of a cascade of secondary injuries.

Due to these inherent challenges in efficiently predicting and diagnosing diffuse injuries, a widespread interest in computational modelling has garnered attention. In general, computational models mimic the process and effects of TBI. However, existing in-silico models have a coarse scale

representation of the brain architecture leading to a paucity in capturing the rich microstructural heterogeneity of the brain. Due to the reduced approximation, most models considered a homogenized version of the brain thereby skipping critical neuronal behaviour at lower scales. So, in order to address these challenges and current day limitations in efficiently modeling and comprehensively illustrating the rich spatio-temporal mechanics of the neuronal microenvironment we present a three dimensional continuum scale viscoelastic mechanical framework for the neuronal microstructure and provide a rigorous connection between brain-scale mechanical deformation and underlying neuronal-scale structural damage. We intend to develop this extensive framework in order to identify and construct key sub-neuronal elements which contribute to the structural organisation of the neuronal microenvironment. Existing literature (Ahmadzadeh et al. (2014); de Rooij and Kuhl (2018); Dubey et al. (2020); Kant et al. (2021); Lu et al. (2006)) considered elementary proteins and their corresponding mechanical role in providing structural support to neurons. These studies represented proteins as viscoelastic members and demonstrated their utility in characterizing the mechanical response of the axon during external loading. Current state-of-the-art modeling and understanding of the axonal behaviour and response during pathological and physiological loading conditions is restricted to reduced order numerical modeling of the mechanics and a limited consideration of the proteins and sub-neuronal elements that, in reality, have complex chemo-mechano-biological contributions within the neuronal microenvironment. In this work, we describe and construct a comprehensive mechanical model illustrating and explaining different proteins, building representative mechanical networks for different regions of the neuronal subdomain (cytoskeleton, extracellular matrix and membrane), demonstrating their mechanical response in transferring loads across the axon as a network and as a whole and finally developing a robust numerical scheme and solving using state-of-the-

art computational tools. The connection to chemistry and some of the underlying potential pathways is treated in the next chapter.

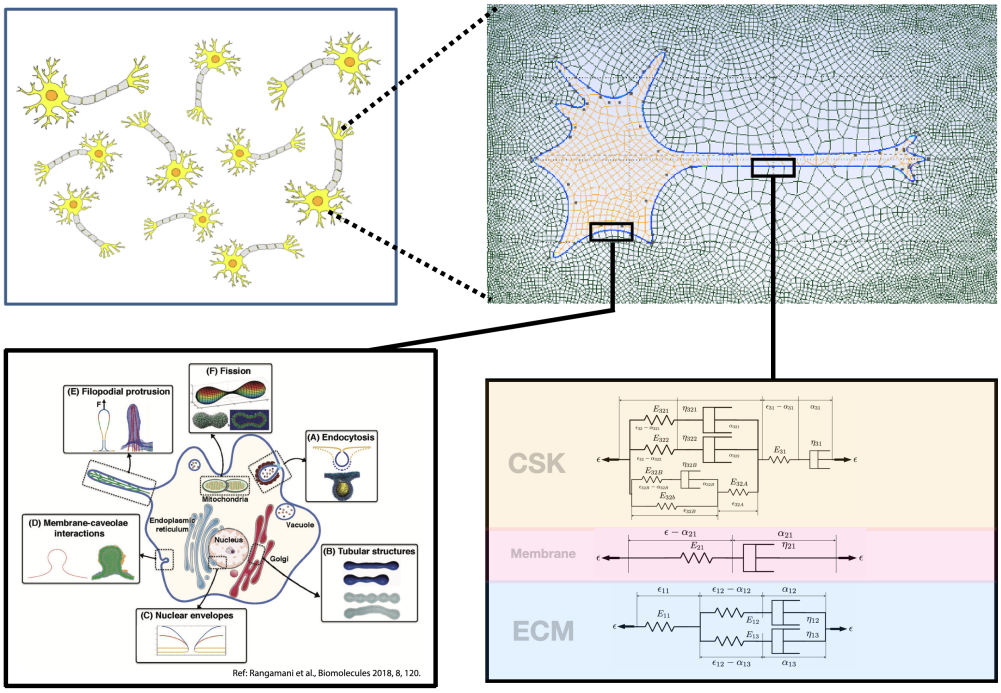

Figure 1.1: General schematic illustrating a cluster of neurons (top left), and the numerical discretization (mesh) of a single neuron in this cluster (top right) are shown. To highlight the regions of analysis, a section of the axon (bottom right) that represents the computational framework for the neuronal microstructure, and a section of the membrane region (bottom left) demonstrating various membrane bound phenomena are shown. Some of these membrane phenomena are modeled in this work using a three dimensional thin-shell framework.

As shown in Fig 1.1 the neuron microstructure has been emphasized across two different regions. The first constitutes the neuronal microenvironment which consists of the cytoskeleton, membrane and the surrounding extra-cellular matrix. The second highlights the membrane and the

multitude of morphologies that these thin structures admit. A discussion on the behaviour of membranes during various biophysical phenomena (Fig 1.1) highlights structural and functional features which is presented in **Chapter 2**. The modification in bilayer morphology leading to various biophysical phenomena is of key interest from a structural perspective. Therefore, we initially describe the morphological and functional characteristics of the membrane and demonstrate the lipid bilayer mechanics using Kirchhoff Love thin shell kinematics and Helfrich energy formulations.

The mechanics of membranes plays a central role in several biological processes such as tubule formation, cell migration, cytokinesis etc. A number of mechanisms have been identified to influence membrane bending, including geometric confinement by protein or lipid components of the membrane (intrinsic factors) and peripheral proteins and the cytoskeleton (extrinsic factors). Lipid bilayer models that assume an in-plane fluid-like behaviour and an out-of-plane solid-like behaviour have provided notable insight to investigations of such curvature generation mechanisms. Particularly, the Helfrich-Canham model has furnished mechanistic insight to shape formation of structures furnished out of large membrane deformations such as vesicles, tubules, budding etc. Despite the wealth of information provided by theoretical membrane mechanics models, an important restriction in several of these studies is the assumption of various degrees of symmetry for the membrane geometry and its deformation. The simplification of symmetry assumption in modeling membranes comes at the cost of generality and precision in identifying the underlying physics, as lower-energy, low-symmetry kinematic modes are often overlooked.

With growing interest in curvature-mediated biophysical phenomena and in 3D imaging and reconstruction methods there is a need for general purpose computational tools to enable fully three dimensional numerical simulations. Deformation of shell-like surface geometries, as is the case with biological membranes, involves tracking the underlying kinematics

and evolution of geometric configurations of a 2-manifold embedded in a 3-dimensional space. Such a geometric embedding demands a non-Euclidean framework with a curvilinear coordinate basis. With the advent of spline-based geometric representations of surfaces and the more recent development of Isogeometric Analysis (IGA) techniques allow for an exact representation of surface geometries and the use of a curvilinear coordinate basis. We build upon these developments by adopting spline-based representations of surface geometries, treatments of membrane kinematics using a curvilinear basis, and the framework of IGA to develop a comprehensive computational modeling framework for studying complex deformations in biological membranes.

In this study, we present a three-dimensional, Helfrich-energy based, Kirchhoff-Love thin-shell computational framework for modeling the deformation of biological membranes in the regime of fully nonlinear kinematics and precise geometric representations. We utilise the governing equations of Helfrich-energy based membrane mechanics and the numerical framework of IGA for solving the underlying partial differential equations. IGA methods form a numerical framework for finding approximate solutions to general partial differential equations, are a generalization of the classical Finite Element Method, and possess good numerical approximation and stability properties. As a result, we can investigate simulations of membrane deformation under conditions that are notably more general (having fewer restrictive kinematic assumptions) than those considered previously in the literature Božič et al. (2001); Alimohamadi et al. (2018).

We simulate two classical and non trivial membrane deformation phenomena: (a) formation of tubular shapes in biological membranes and (b) Piezo1-induced membrane footprint generation and gating response. In the following chapter, we present an outline of the mathematical framework and the model development, followed by a presentation of the two boundary value problems and an illustration of their three dimensional

deformation evolution along with their biophysical implications. Finally, a discussion of the framework, its utility and planned future developments is presented.

In **Chapter 3** we identify different regions of the neuronal microstructure which contribute to the structural integrity of the neuron, more specifically the axon. These regions consist of proteins which are dynamic in nature and which are constantly modeling/remodeling to adapt with the changing neuronal microenvironmental conditions. We investigate into these proteins by identifying their mechanical behaviour (stiffness, relaxation rate etc.) and idealise it using viscoelastic elements. The proteins are combined into a mechanical network for each individual region where each protein responds to their characteristic mechanical behaviour upon load transfer. Once the network is constructed we develop our continuum scale viscoelastic model using a one dimensional and three dimensional continuum approach. The fidelity of our model underlies a modular approach in which any number of fundamental sub-neuronal components can be represented in the generalised network and analytical solutions for each component obtainable. We present two approaches: the one dimensional domain, which is described for each protein component in each region and the three dimensional viscoelastic continuum formulation which has been described for a general continuum network and a detailed algorithm illustrated. The latter approach has been implemented in a finite element framework and its workflow described. Finally, we demonstrate the working fidelity of our models using a series of results and illustrations.

The other key highlight of our work is the implementation of a multiscale approach of the neuronal microenvironment. The purpose of this implementation is to highlight the principle of load transfer from the brain level (organ level) to the sub-neuronal level. Previous literature generally investigated one length scale and generated the mechanical response of

that order. However, in practice it is known that during injury the load propagates from the organ to the neuron cluster to the sub-neuronal level. Hence it is crucial to represent the mechanical behaviour at different length scales to have a broader understanding of the load transfer mechanism. The multi-neuron model is a numerical construction of a neuron cluster embedded within a substrate. A single neuronal microenvironment within the cluster of neurons is the fundamental scale and emphasizes on the sub-neuronal mechanical response.

Given the complexity of the response of this network to three dimensional loading, we gradually build the numerical model by first treating reduced order one dimensional and eventually leading to a full three dimensional representation. Overall we construct a multi-scale representation of neuronal cluster and neuronal microenvironment architecture using our high fidelity mechanical network motivated by proteins which serve as structural scaffolds. Numerical experiments on the model reveal protein level mechanical response and insights into loading rates.

In **Chapter 4** we characterize Traumatic Brain Injury (TBI) through pathological degradation at various biological length scales from a mechano-chemical perspective. To quantify the sequence of events following TBI, classically, various mechanical modeling techniques have been proposed which establish metrics that demonstrate localised to generic neuronal damage. Broadly, the two categories of degradation encompass physiological deterioration and upregulation of chemical entities such as neurotransmitters which cause initiation of downstream pathophysiological effects. The loss of structural and chemical integrity within neurons and neuron clusters release molecules which serve as critical biological markers crucial to injury diagnosis. Aberration in concentration of essential chemical components in the brain such as neurotransmitters, inflammasomes, cytokines and ionic channels lead to activation of necroptotic pathways which eventually causes neurodegeneration. Recent studies have

highlighted the pathological effects caused due to upregulation of these chemical species across the brain. The primary aim of this work is to demonstrate a continuum framework which models the multiphysics of mechano-chemical interactions underlying TBI. Using a coupled PDE (partial differential equation) formulation and FEM (finite element method) discretization, the framework highlights evolution of field variables which spatio-temporally resolves mechanical metrics and chemical species across the neuron cluster domain. Using geometric spatial localisation of specific chemical components, we illustrate dynamics of chemical field evolution across different regions of the neuronal microstructure. This enables visualisation of initiation, interaction and progression of field variables, highlighting temporal activation of different components in the downstream necroptotic pathway.

We present a novel mechano-chemical framework which models some of the potential mechanical and chemical metrics relevant to traumatic brain injury. The results demonstrate the spatio-temporal resolution of these metrics and thus provide valuable insights into some of potential critical chemical thresholds underlying neuronal necroptosis. In a first-of-its-kind representation of mechano-chemical interactions underlying neurons and neuronal clusters we have qualitatively drawn comparison between our results and existing literature, and also obtained some initial representative estimates of the injury thresholds. The fidelity of our current modeling approach allows for the inclusion of additional physics and chemical species that can provide a better resolution of injury diagnosis by linking to accepted clinical biomarkers of TBI.

2 ISOGEOMETRIC MODELING OF KIRCHHOFF-LOVE SHELL KINEMATICS: A COMPUTATIONAL FRAMEWORK FOR MODELING COMPLEX MECHANICAL DEFORMATION PATHWAYS IN BIOMEMBRANES

The contents of this chapter are a published work:

Auddya, Zhang, Gulati, Vasan, Garikipati, Rangamani, Rudraraju, "Biomembranes undergo complex non axisymmetric deformations governed by Kirchhoff-Love kinematics and revealed by a three dimensional computational framework", *Proceedings of the Royal Society A, 477.2255, 2021*.

2.1 Introduction

Membrane curvature is ubiquitous in biology McMahon and Gallop (2005). Indeed, the bending of cell membranes is a central aspect of function for cells and organelles in many cellular processes such as cell migration Zhao et al. (2013), cell membrane repair Boye et al. (2017), membrane trafficking Liu et al. (2009) and cytokinesis Schroeder (1972), as well as the maintenance of distinctive membrane shapes within internal organelles like the endoplasmic reticulum Hu et al. (2008); Shibata et al. (2006) and the Golgi complex McNiven and Thompson (2006). Some important curved structures include tubules, sheets, vesicles and cisternae Voeltz and Prinz (2007). A number of mechanisms have been identified to influence membrane bending, including geometric confinement by protein or lipid components of the membrane (intrinsic factors) Zimmerberg and Kozlov (2006); Koster et al. (2003) and peripheral proteins and the cytoskeleton (extrinsic factors) Takano et al. (2008); Cocucci et al. (2012).

These mechanisms are often coupled and are spatio-temporally regulated by biochemical signaling cascades, leading to the mechanochemical coupling of signaling and membrane deformations. Lipid bilayer models that assume an in-plane fluid-like behaviour and an out-of-plane solid-like behaviour have provided notable insight to investigations of such curvature generation mechanisms. Particularly, the Helfrich-Canham model Helfrich (1973) has furnished mechanistic insight to shape formation of liquid shells during vesiculation Miao et al. (1991); Hurley et al. (2010), tubulation Derényi et al. (2002), viral budding Tzlil et al. (2004), clathrin-mediated endocytosis Hassinger et al. (2017), and membrane neck formation Alimohamadi et al. (2018); Vasan et al. (2020). These modeling efforts have been complementary to advances in imaging techniques Choi and Lee (2009); Dupire et al. (2012); Kukulski et al. (2012), enabling a deeper appreciation of the complexity of membrane deformation.

Despite the wealth of information provided by theoretical membrane mechanics models, an important restriction in several of these studies is the assumption of various degrees of symmetry for the membrane geometry and its deformation. Indeed, the computation of membrane bending phenomena is significantly simplified with the axisymmetric assumption, but as we have shown recently Vasan et al. (2020), this may come at the cost of generality and precision in identifying the underlying physics, as lower-energy, low-symmetry kinematic modes and even entire mechanisms may be overlooked. With growing interest in curvature-mediated biophysical phenomena and in 3D imaging and reconstruction methods Lee et al. (2020a,b), there is a need for general purpose computational tools to enable fully three dimensional numerical simulations.

The continuum mechanical treatment of solids considers deformation as a mapping of the geometry (3D volume, 2D surface, or 1D curve) from its reference, undeformed configuration to a deformed current configuration under the influence of internal or external loads, of which the latter

also may appear as boundary conditions. In limited cases, the geometry, loads and boundary conditions result in a mathematical problem of deformation of a k-manifold immersed in an n-dimensional space ($\mathbb{R}^n$). A 3-manifold is a volume, 2-manifold is a surface and 1-manifold is a curve. For $k = n$, modeling solid deformation is relatively straightforward and can be accomplished in the framework of Euclidean geometry using a rectilinear coordinate basis.

However, deformation of shell-like surface geometries, as is the case with biological membranes, involves tracking the underlying kinematics and evolution of geometric configurations of a 2-manifold embedded in a 3-dimensional space Novozilov (1959). Such a geometric embedding demands a non-Euclidean framework with a curvilinear coordinate basis. While the mathematical treatment of such a framework is well-developed (beginning with the celebrated work on differential geometry by Riemann in the 19^{th} century Riemann (1854)), its application to three-dimensional modeling of biomembranes, which entails solving nonlinear partial differential equations in a curvilinear coordinate basis is relatively recent. Beginning with finite element models of Mindlin–Reissner plates Hrabok and Hrudey (1984); Arnold et al. (2005); Shi and Voyiadjis (1991); Zienkiewicz and Lefebvre (1988) and Kirchhoff-Love shells Simo and Fox (1989); Hrabok and Hrudey (1984); Yang et al. (2000); Başar and Ding (1990), initial efforts focused on developing numerical models in a rectilinear coordinate basis with approximated geometries and kinematics. However, the advent of spline-based geometric representations of surfaces and the more recent development of Isogeometric Analysis (IGA) techniques Cottrell et al. (2009) allow for an exact representation of surface geometries and the use of a curvilinear coordinate basis. Such treatments are now gaining traction in modeling structural applications Kiendl et al. (2009, 2015); Zareh and Qian (2019); Nguyen-Thanh et al. (2015) and also in the context of biological materials Tepole et al. (2015); Sauer et al.

(2017); Roohbakhshan and Sauer (2017); Sauer and Duong (2017). We build upon these developments, especially from Sauer et al. Sauer et al. (2017), by adopting spline-based representations of surface geometries, treatments of membrane kinematics using a curvilinear basis, and the framework of IGA to develop a comprehensive computational modeling framework for studying complex deformations in biological membranes.

In this work, we present a three-dimensional, Helfrich-energy based, Kirchhoff-Love thin-shell computational framework for modeling the deformation of biological membranes in the regime of fully nonlinear kinematics and accurate geometric representations. With this treatment, we are able to model membrane deformations, resolve geometric bifurcations, and explore post-bifurcation responses. The main ingredients of this framework are the governing equations of Helfrich-energy based membrane mechanics Novozilov (1959); Sauer and Duong (2017); Sauer et al. (2017); Steigmann (1999) and the numerical framework of IGA for solving the underlying partial differential equations. IGA methods form a numerical framework for finding approximate solutions to general partial differential equations Cottrell et al. (2009), are a generalization of the classical Finite Element Method Ciarlet (2002); Brenner and Scott (2007); Strang and Fix (1973), and possess good numerical approximation and stability properties Bazilevs et al. (2006). Crucially for accurate modeling of membrane biophysics, since IGA uses spline basis functions to represent the geometry and its deformation, it admits the continuity of slopes that is a characteristic of membranes in all states except for those of actual scission. As a result, we can now investigate simulations of membrane deformation under conditions that are notably more general (having fewer restrictive kinematic assumptions) than those considered previously in the literature Alimohamadi et al. (2018); Božič et al. (2001); Guckenberger and Gekle (2017); Zheng and Liu (1993); Jian-Guo and Zhong-Can (1993); Molina et al. (2020). The computational framework is implemented as an

open-source software library and provided as a resource to the biophysics community Git (2021).

To demonstrate the scope of the computational framework, we simulate two classical and non trivial membrane deformation phenomena: (a) formation of tubular shapes in biological membranes (b) Piezo1-induced membrane footprint generation and gating response. For each case, three dimensional membrane deformation is tracked, symmetry-breaking deformation pathways identified, and a few case studies of boundary conditions and loading are presented to exhibit the fidelity and modeling potential of the proposed methodology. In the following sections, we present an outline of the mathematical framework and the model development, followed by a presentation of the two boundary value problems considered, their modeling results and biophysical implications. Finally, a discussion of the framework, its utility and planned future developments is presented.

2.2 Numerical methods for biomembranes

The mathematical framework consists of surface geometry parametrization, Kirchhoff-Love membrane kinematics, Helfrich-energy based mechanics of lipid bilayers and surface partial differential equations governing mechanical deformation. Key ingredients of this framework are described below, while the more detailed mathematical derivations are provided in the SI. Using the IGA apparatus, the mathematical treatment is then cast into a numerical formulation that allows for solving the governing equations to obtain the spatial evolution of membrane deformation. These aspects of the framework are discussed under the computational implementation subsection. The mathematical treatment introduced here follows from Sauer et al. Sauer et al. (2017). Only the important results are summarized in this section, and the detailed derivations are presented in the SI.

Surface parametrization and kinematics

Consider a lipid bilayer represented as a surface (2-manifold) embedded in a 3D volume, as shown in Fig. 2.1. Let the reference (undeformed) configuration and the current (deformed) configuration of the surface geometry be denoted by Ω_0 and Ω, respectively. The configurations Ω_0 and Ω are parametrized by the coordinates ξ^1 and ξ^2 that map a flat 2D domain to the surface coordinates $\mathbf{X}$ and $\boldsymbol{x}$:

$$\mathbf{X} = \mathbf{X}(\xi^1, \xi^2) \quad \forall \quad \mathbf{X} \in \Omega_0, \qquad \boldsymbol{x} = \boldsymbol{x}(\xi^1, \xi^2) \quad \forall \quad \boldsymbol{x} \in \Omega. \tag{2.1}$$

The (covariant) tangent vectors in the reference and current configuration are given by:

$$\boldsymbol{A}_I = \frac{\partial \boldsymbol{X}}{\partial \xi^I} = \boldsymbol{X}_{,I}\,, \qquad \boldsymbol{a}_i = \frac{\partial \boldsymbol{x}}{\partial \xi^i} = \boldsymbol{x}_{,i}\,. \tag{2.2}$$

In the expressions that follow, except when indicated otherwise, uppercase letters are associated with the reference configuration and lowercase letters are associated with the current configuration.
Using the tangent vectors we define the surface normals as follows:

$$\mathbf{N} = \frac{\boldsymbol{A}_1 \times \boldsymbol{A}_2}{\|\boldsymbol{A}_1 \times \boldsymbol{A}_2\|}, \qquad \mathbf{n} = \frac{\boldsymbol{a}_1 \times \boldsymbol{a}_2}{\|\boldsymbol{a}_1 \times \boldsymbol{a}_2\|}. \tag{2.3}$$

From the triad consisting of the tangent vectors and the normal that form the local curvilinear coordinate basis, we can obtain expressions for the metric tensor,

$$A_{IJ} = \boldsymbol{A}_I \cdot \boldsymbol{A}_J \qquad a_{ij} = \boldsymbol{a}_i \cdot \boldsymbol{a}_j \tag{2.4}$$

The second order derivatives of the surface coordinates $\mathbf{X}$ and $\boldsymbol{x}$ are given by:

$$\boldsymbol{A}_{I,J} = \frac{\partial \boldsymbol{A}_I}{\partial \xi_J} \qquad \boldsymbol{a}_{i,j} = \frac{\partial \boldsymbol{a}_i}{\partial \xi_j} \tag{2.5}$$

and from them we obtain the components of the curvature tensor,

$$B_{IJ} = \boldsymbol{A}_{I,J} \cdot \mathbf{N} \qquad b_{ij} = \boldsymbol{a}_{i,j} \cdot \mathbf{n} \tag{2.6}$$

We are now able to define the primary kinematic metrics of interest: the mean and Gaussian curvature. The mean curvature and Gaussian curvature are frame invariant measures of a surface geometry, and hence are natural choices for representing the kinematics of the surface as it deforms. Using the components of the curvature tensor, we can obtain expressions for the mean curvature,

$$H = \frac{1}{2} B^{IJ} A_{IJ} \quad \text{on} \quad \Omega_0, \qquad h = \frac{1}{2} b^{ij} a_{ij} \quad \text{on} \quad \Omega \tag{2.7}$$

and the Gaussian curvature,

$$K = \frac{|B|}{|A|} \quad \text{on} \quad \Omega_0, \qquad \kappa = \frac{|b|}{|a|} \quad \text{on} \quad \Omega, \quad |\cdot| = \det(\cdot) \tag{2.8}$$

Biophysics of membrane deformation

With a focus on representing the correct deformation, a biomembrane is often modeled as a thin elastic shell governed by the classical Helfrich formulation Helfrich (1973); Kishimoto et al. (2011); Morlot et al. (2012) of membrane bending energy. In this treatment, the primary kinematic variables are the curvatures capturing the bending of the membrane, and the elastic energy density of the membrane is given by:

$$w = k_B (h - h_0)^2 + k_G \kappa \tag{2.9}$$

where k_B and k_G are the bending modulus and the Gaussian curvature modulus of the membrane, and h_0 represents the instantaneous curvature induced in the membrane.

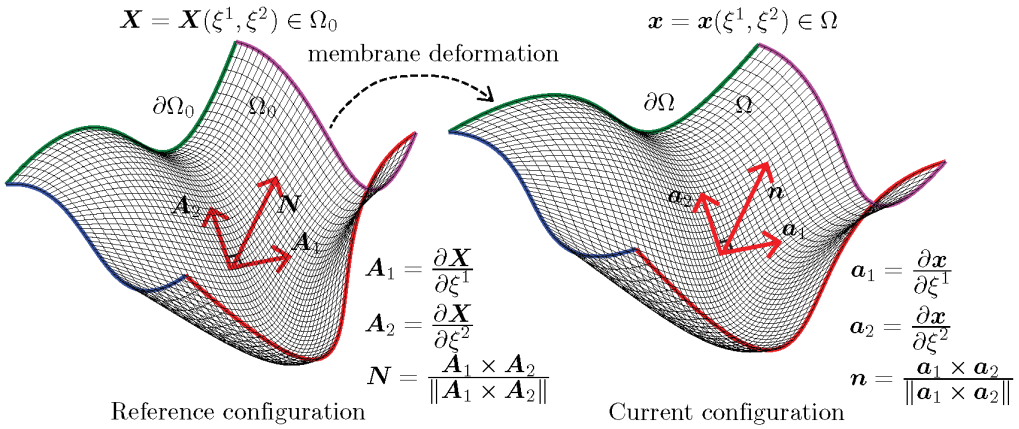

Figure 2.1: Surface parametrization of a biomembrane in the reference undeformed configuration (Ω_0) and current deformed configuration (Ω). The 2D surface, Ω_0, is bounded by the curves $\partial\Omega_0$ (highlighted with color), and embedded in a 3D volume. Here, $\mathbf{X}$ is the position vector of a point on the surface parametrized in terms of the surface coordinates (ξ^1,ξ^2) which are associated with a flat 2D domain that is then mapped to Ω_0 as $\mathbf{X} = \mathbf{X}(\xi^1, \xi^2)$. The local tangent vectors to the surface at $\mathbf{X}$ are $\mathbf{A}_1$ and $\mathbf{A}_2$, and $\mathbf{N}$ is the corresponding surface normal. The position dependent triads $\{\mathbf{A}_1,\mathbf{A}_2,\mathbf{N}\}$ and $\{\mathbf{a}_1,\mathbf{a}_2,\mathbf{n}\}$ form the local curvilinear coordinate basis for the reference undeformed configuration and current deformed configuration, respectively.

Furthermore, we assume that the membrane is area preserving (*i.e* the membrane area is constant) Evans and Skalak (1979) – a constraint that is implemented using a Lagrange multiplier field. Enforcing the area-preserving condition results in the following field expression for the elastic energy density:

$$w = k_B(h - h_0)^2 + k_G\kappa + \lambda(J - 1) \tag{2.10}$$

where λ is the point value of the Lagrange multiplier field, and J is the surface Jacobian field (ratio of an infinitesimal area element in the current configuration to the area of its pre-image in the reference configuration). Here, the Lagrange multiplier field represents the membrane tension Rangamani et al. (2014); Steigmann (1999) that enforces the area preserving property of biomembranes and thus influences the minimum energy configuration. The Lagrange multiplier field is position dependent, is obtained as part of the solution process, and thus permits non-homogeneous membrane tensions that are needed to ensure that the membrane is area preserving under general deformation conditions. In this model, we neglect in-plane fluidity of the membrane Rangamani et al. (2013); Arroyo and DeSimone (2009) and friction in the bilayer Simunovic et al. (2017); Quemeneur et al. (2014); Rahimi and Arroyo (2012), as we are interested in determining the elastic equilibrium states under quasi-static conditions and not the underlying membrane relaxation or rate processes. The augmented Helfrich Hamiltonian whose extremum is sought over the membrane surface, including the Lagrange multiplier field λ is given as:

$$E = \int_\Omega (k_B(h - h_0)^2 + k_G\kappa + \lambda(J - 1))\, da \tag{2.11}$$

where Ω is the domain of integration over the membrane surface.

Governing equations

The governing equation for quasi-static mechanical equilibrium in 3D simulations is obtained as the Euler-Lagrange condition of the Helfrich energy functional following standard variational arguments, and is given by:

$$\int_\Omega \frac{1}{2}\delta a_{ij}\sigma^{ij}\, da + \int_\Omega \delta b_{ij}M^{ij}\, da - \int_\Omega \delta\mathbf{x}\cdot\mathbf{p}\, da - \int_{\partial\Omega} \delta\mathbf{x}\cdot\mathbf{t}\, ds = 0, \tag{2.12}$$

where $\partial\Omega$ is the membrane boundary on which surface tractions and displacement boundary conditions can be applied, as shown in Chapter 2.1. Furthermore, δa_{ij} and δb_{ij} are variations of the components of the metric tensor and the curvature tensor, respectively,

Here, σ^{ij} are the components of the stress tensor, M^{ij} are components of the moment tensor (in the current configuration), $\mathbf{p}$ is the pressure applied on the membrane surface (in the case of the tube constriction boundary value problem), and $\mathbf{t}$ is the surface traction.
For a hyperelastic material model, we can express the stress and moment components in terms of the strain energy density as Sauer and Duong (2017):

$$\sigma^{ij} = \frac{2}{J}\frac{\partial w}{\partial a_{ij}}, \tag{2.13}$$

$$M^{ij} = \frac{1}{J}\frac{\partial w}{\partial b_{ij}} \tag{2.14}$$

For the Helfrich type strain energy density, these take the form:

$$\sigma^{ij} = (k_B(h-h_0)^2 - k_G\kappa)a^{ij} - 2k_B(h-h_0)b^{ij}, \tag{2.15}$$

$$M^{ij} = (k_B(h-h_0) + 2k_G h)a^{ij} - k_G b^{ij} \tag{2.16}$$

Here, it is important to note that the Helfrich elastic model inherently lacks resistance to shear deformation modes in three dimensions. This lack of shear stiffness correctly represents the fluidity of the biomembranes, but induces numerical instabilities while solving boundary value problems involving three dimensional membrane deformation. We eliminate these numerical instabilities by adding shear stabilization terms to the material model but ensure that these terms are of smaller magnitude than the bending energy terms in the Helfrich energy Sauer et al. (2017). We perform convergence studies with respect to both the underlying mesh (ensuring mesh-objectivity) and the dependence on the shear stabilization terms.

The results reported in this report are for sufficiently refined meshes. The elastic modulus corresponding to the shear stabilization is small compared to the bending modulus and is chosen to have minimal effect on the overall stiffness or the deformation energy of the membrane.

Computational implementation

In this framework, we solve the governing equation given by Equation (2.12) using the methodology of Isogeometric Analysis (IGA) Cottrell et al. (2009). As stated in the introduction, IGA is mesh-based numerical discretization scheme for finding approximate solutions to general partial differential equations Cottrell et al. (2009), and is a generalization of the classical Finite Element Method Ciarlet (2002); Brenner and Scott (2007); Strang and Fix (1973). Numerical discretization of the problem geometry in IGA is accomplished by using a spline-based C^1-continuous basis. In the context of biomembranes, this ensures accurate representation of both the reference and deformed geometries without the spurious slope discontinuities observed in more traditional finite element schemes and other grid-based numerical schemes. We developed a first of its kind in-house, parallel, C++ programming language based open-source library for membrane mechanics in three dimensions. The important components of this modular library are the implementation of membrane kinematics without any axisymmetric restrictions, Helfrich material model, weak form of the governing equations of membrane mechanics, and the setup of the global boundary value problem with biomembrane specific boundary conditions. This library sits on top of the PetIGA Dalcin et al. (2016) open source library that provides the spline (NURBS) discretization capability and the PETSC Abhyankar et al. (2018) open source library that provides a suite of data structures and routines for the scalable (parallel) solution of partial differential equations. The computational framework is implemented as an open-source software library and is provided as a

resource to the biophysics community through a GitHub repository Git (2021).

2.3 Results

We demonstrate the simulation framework using two classical membrane deformation problems: formation of tubular shapes in membrane and Piezo1-induced membrane footprint generation and gating response. Through these examples, we also demonstrate the emergence of increasingly complex membrane deformations that are beyond the scope of traditional axisymmetric formulations. These problems are described in detail below.

Formation of tubular shapes in biomembranes

Many cell organelles and cytoplasmic projections are shaped as vesicles, tubes, or elongated membrane structures. Some examples of such shapes are the filopodia protrusions, inner mitochondrial region, endoplasmic reticulum, the Golgi complex, etc. These tubular structures play an important role in the locomotion of cells, production and folding of proteins, and in the formation of vesicles for transporting proteins and lipids among others. A typical mechanism for producing these tubular shapes involves motor proteins that attach to the cell membrane and pull it along the filaments of the cytoskeleton Koster et al. (2003); Shaklee et al. (2008). From a biophysical standpoint, it is important to gain a quantitative understanding of the interaction between the proteins and the membranes by determining the deformation mechanisms, forces exerted by proteins, and kinematic constraints.

A classic benchmark problem in the understanding of elongated biomembrane structures is the analytical model of the formation and interaction of membrane tubes proposed by Derényi et al Derényi et al. (2002). Some key results of this model are the prediction of the magnitude of protein-

membrane interaction forces and tubule radius, and their dependence on the membrane bending modulus (κ_B) and surface tension (γ). The protein pulling force, t_y, and the tubule radius, r, are related to the bending modulus and surface tension of the membrane as follows: $t_y \propto \sqrt{\kappa_B \gamma}$ and $r \propto \sqrt{\kappa_B/\gamma}$. In addition to these analytical estimates, numerical solutions to the problem of membrane tube pulling, albeit with axisymmetric constraints on deformation, are available in the literature Lipowsky (2012); Bahrami and Hummer (2017) and in our earlier work Vasan et al. (2020). Given the paucity of analytical solutions to membrane deformation problems based on the Helfrich-energy model, we take advantage of the analytical estimates proposed by Derényi et al., the numerical solutions available from axisymmetric models Vasan et al. (2020), and validate the computational framework proposed in this work by comparing the load-displacement response of membrane tube pulling from these two approaches.

The boundary value problem solved, along with the spatial discretization (mesh), boundary conditions on the displacement ($\mathbf{u}$) and the membrane boundary slope (ϕ) are shown in Chapter 2.2(a). The simulation results are shown in Chapter 2.3: Chapter 2.3 (a) is the deformation profile obtained during tube pulling, and in Chapter 2.3(b) is the load-displacement response of the 3D framework compared to the asymmetric result and the equilibrium value of tube pulling force predicted by the analytical model. We note that the analytical model only predicts the final equilibrium value of the tube pulling force, and hence only a single value of the force from the analytical model is plotted. As can be seen from Chapter 2.3(b), the 3D model very closely tracks the axisymmetric solution and asymptotically approaches the equilibrium value of force from the analytical solution. Further, we show the evolution of the deformation profile with increasing tube pulling force in Chapter 2.3(c), and the dependence of the deformation profile and tubule radius on the applied surface

tension in Chapter 2.3(d). Here we note that the small deviation of the 3D model results from the axisymmetric solution in Chapter 2.3(b) is due to the fact that the 3D model boundary value problem is less constrained along the outer rim than the axisymmetric boundary value problem. For the 3D problem we enforce $u_y = 0$ along the outer rim, whereas the axisymmetric problem also enforces complete radial symmetry of the u_x and u_z displacements in addition to enforcing $u_y = 0$ (See Chapter 2.2(a)). This makes the axisymmetric problem more stiff to the applied load.

Piezo1-induced membrane footprint and gating response

We next investigate how mechanosensitive channels can deform the membrane. Mechanosensitive ion channels on the cell membrane play an important role in the mechanosensory transduction processes of the cell. These ion channels are sensitive to the forces acting on the cell membrane and respond to these forces by undergoing conformational changes. These changes result in the opening and closing of pores in the cell membrane and thereby regulate the flow of ions and solutes entering and egressing the cell. Examples of such mechanosensitive ion channels include Piezo1, MscL and TREK-2 Ridone et al. (2019). In the case of Piezo1, a gated ion channel made up of three protein subunits that induce a dome-shaped structure on the cell membrane, the gating mechanism is triggered by the membrane surface tension. The membrane deformation induced by the surface tension acts as a mechanical signal that activates the protein subunits and causes them to undergo a conformational change that results in pore opening and transport of ions and solutes Gottlieb et al. (2012); Lewis and Grandl (2015); Zhao et al. (2019).

While the exact mechanism of mechanosensory transduction effected by the Piezo1 ion channel is still an open question, the extent of the deformed shape induced by the Piezo1 dome (referred to as the membrane foot-

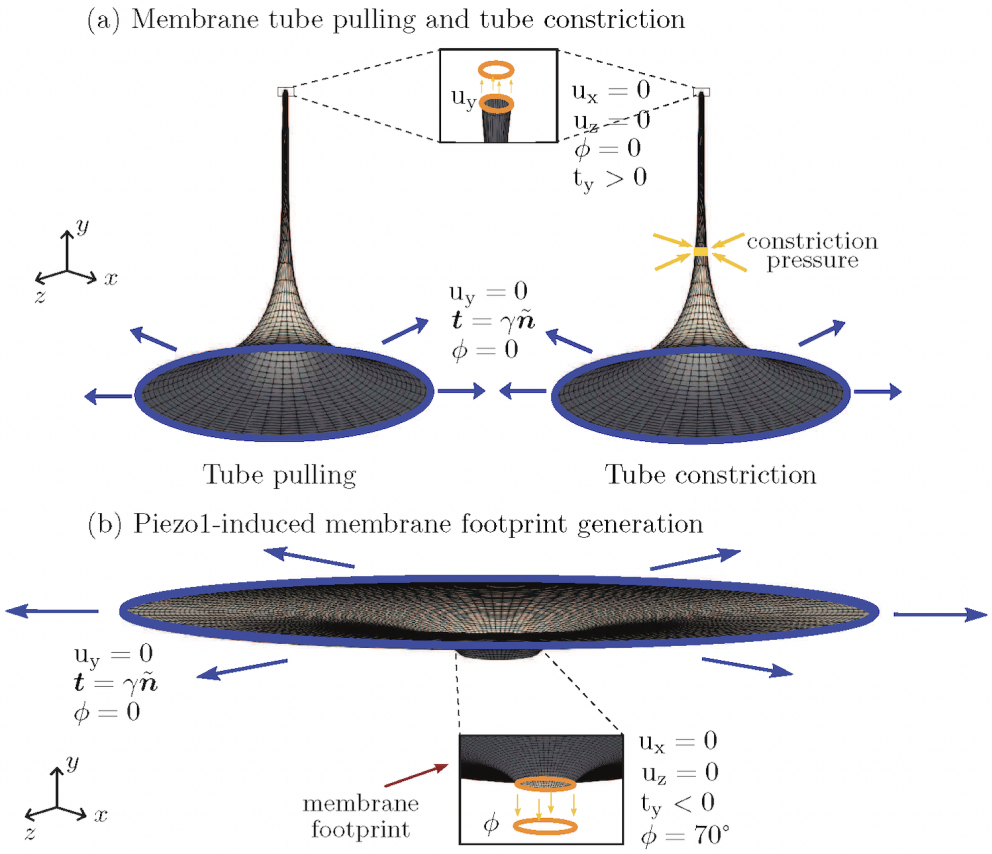

Figure 2.2: Schematic of the various membrane boundary value problems considered in this work. Shown are the geometry and boundary conditions for (a) formation of tubular shapes in biomembranes, (b) Piezo1-induced membrane footprint generation

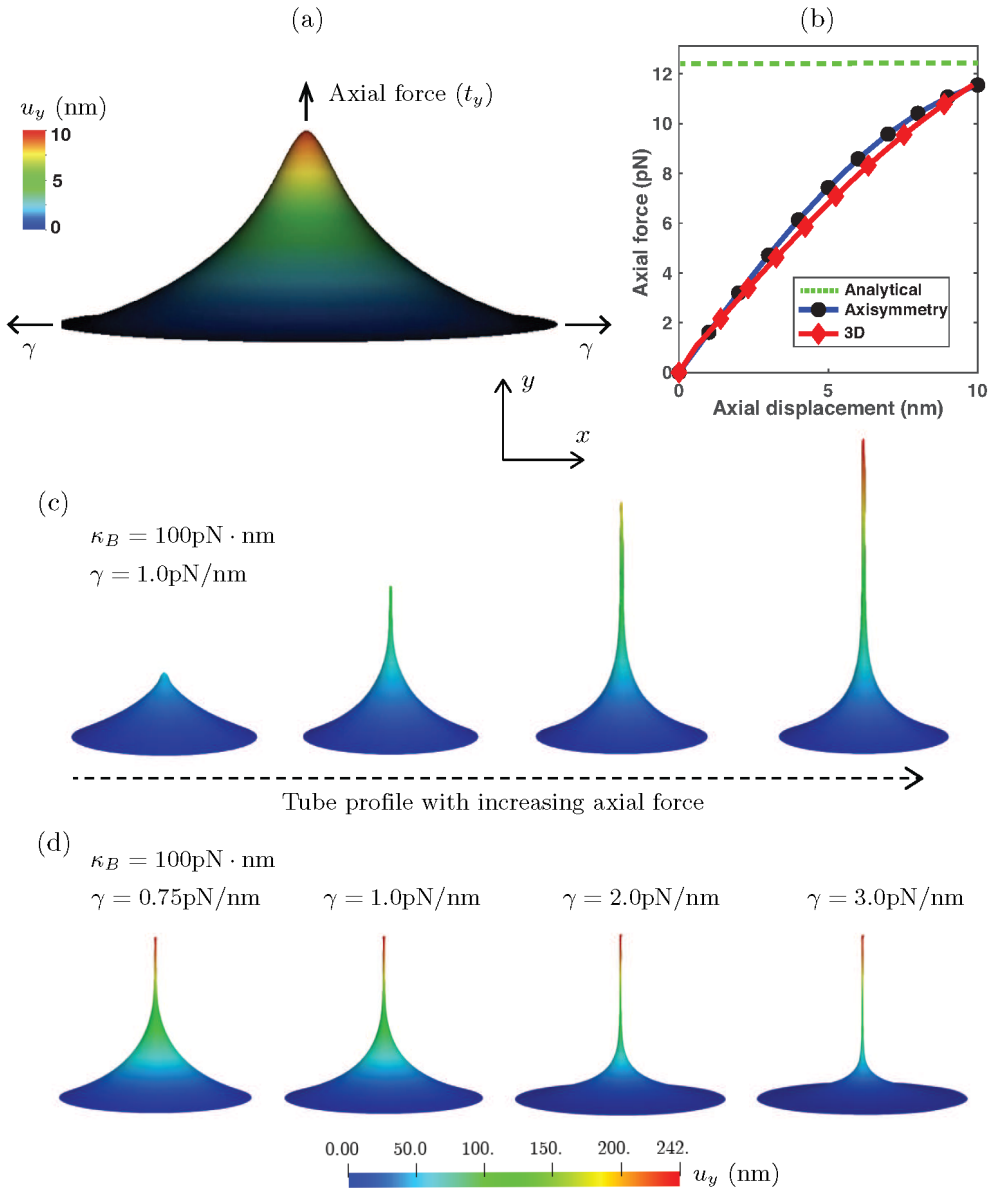

Figure 2.3: Deformation profile and force-displacement response of a membrane during tube pulling. Shown are the (a) deformation profile with the application of axial force (t_y) on a membrane with a bending modulus (κ_B) of 20 pN-nm under a surface tension (γ) of 0.1 pN/nm, (b) comparison of the 3D force-displacement response with the axisymmetric solution and the equilibrium tube pulling force predicted by the analytical model, (c) progression of tube pulling with increasing axial force, and (d) dependence of the deformation profile and tube radius on the surface tension of the membrane.

print) is understood to significantly influence the sensitivity of the gating response of the channel Haselwandter and MacKinnon (2018). As observed by Haselwandter and MacKinnon Haselwandter and MacKinnon (2018), an extended membrane footprint amplifies the sensitivity of Piezo1 subunits to respond to changes in the membrane surface tension. At the same time, increasing membrane tension significantly reduces the membrane footprint and thereby renders the Piezo1 subunits less sensitive to detect membrane mechanical signals.

In this analysis, we model the effect of surface tension on the area of the membrane footprint induced by the Piezo1 dome. Our modeling goal for this problem is to demonstrate the effect of membrane tension on: (1) the membrane footprint, and (2) the out-of-plane membrane displacement that can be interpreted as a kinematic trigger to activate the gating mechanism in the protein subunits of Piezo1. The schematic for this boundary value problem is shown in Fig 2.2(b), and the simulation results demonstrating the effect of surface tension on the membrane footprint are presented in Chapter 2.4. The plots show the 3D displacement profiles and their 2D projections under the boundary conditions enforced by the Piezo1 dome. A Piezo dome effect on the membrane is modeled by rotating the membrane (slope boundary condition) at the inner rim of the annular geometry to a value of $\phi = 70$ degrees that is chosen so as to simulate the effect of a nearly hemispherical dome (which would correspond to $\phi = 90$ degrees). This slope boundary condition assumes that the Piezo1 protein complex is a rigid dome that enforces a rotation on the surrounding membrane to ensure slope continuity between the hemispherical dome and the connected membrane. As can be seen from the subfigures Chapter 2.4(a)-(d), decreasing the surface tension increases the membrane footprint. Especially in the limit of very low surface tension ($\gamma = 0.01$ pN/nm) we see a significantly enhanced membrane footprint. The change in the out-of-plane displacement of the membrane, (u_y), shows a similar

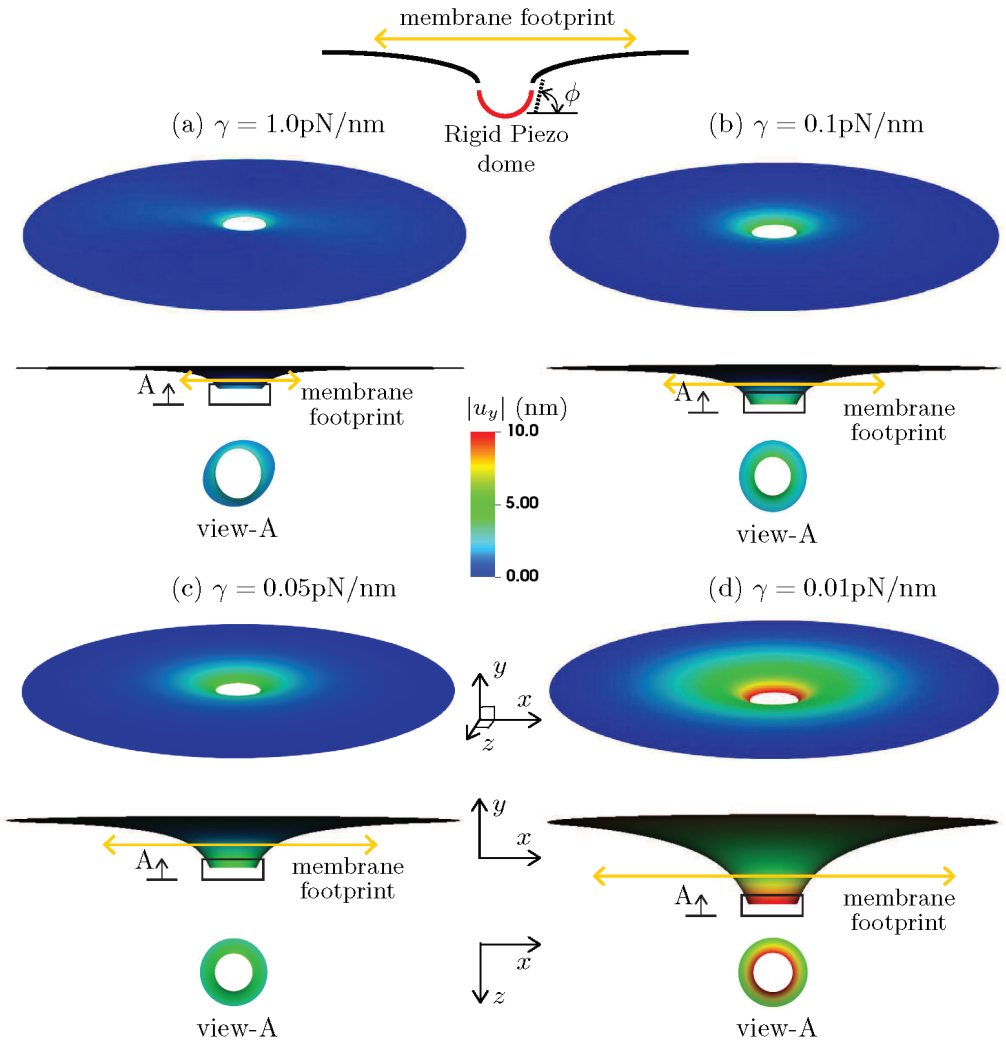

Figure 2.4: Effect of surface tension on the membrane footprint area induced by a Piezo1 dome. Plotted are the 3D displacement profile, and its projection on the $x-y$ and $z-x$ planes. The bending modulus (κ_B) of the membrane is taken to be 30 pN·nm, and a rigid Piezo dome effect is simulated by rotating the membrane (slope boundary condition) at the inner rim of the annular geometry to a value of $\phi = 70$ degrees. To clearly visualize the increasing membrane footprint with decreasing surface tension, we scale the y component of the displacement (u_y) by a factor of three in the $x-y$ oriented plots.

dependence on the surface tension. Since the out-of-plane displacement can be interpreted as a kinematic trigger to activate the gating mechanism in the protein subunits of Piezo1, this implies that at lower surface tension values, a higher value of u_y is attained, thus delivering an amplified kinematic trigger, and therefore greater sensitivity of the Piezo1 dome to changes in surface tension. These results are consistent with the observations by Haselwandter and MacKinnon Haselwandter and MacKinnon (2018) that use the classical reduced order Monge and arc-length axisymmetric parametrization methods to model the Piezo1-induced membrane deformation. Note that the deformation profile at the inner rim is, in general, non-axisymmetric, an effect that increases with membrane tension, γ. This illustrates the power of the 3D computational framework, which while it encompasses axisymmetric deformation, also admits non-axisymmetric modes. With access to the larger space, deformation profiles that are attainable at lower energies, are indeed attained since the elasticity problem results in a (local-) minimum energy configuration. Thus, while the 3D model reproduces the trends predicted by the reduced order models, its true power is in identifying more complex deformation patterns that are not accessible to the reduced order axisymmetric models.

2.4 Discussion

Biomembranes play central roles in various cell-scale and organelle-scale phenomena like locomotion of cells Zhao et al. (2013), packaging and trafficking of nutrients and signalling constituents Liu et al. (2009), maintaining organelle morphology and functionality Hu et al. (2008); Shibata et al. (2006); McNiven and Thompson (2006), etc. In almost all these processes, these surfaces are known to undergo significant deformation through bending; and the evolution of the out-of-plane bending deformation is a key mechanism of morphological evolution, besides in-plane

fluidity. Thus, many analytical and numerical approaches exist in the literature to model bending and curvature generation, especially for solving the governing equations resulting from the Helfrich-Canham Helfrich (1973) characterization of membrane elasticity.
While these widely used analytical and numerical approaches (e.g. Monge parametrization, arclength parametrization and asymptotic methods) yield solutions to a wide range of boundary value problems of membrane bending, they are intrinsically limiting in capturing the complete envelope of membrane deformations due to the underlying axisymmetric restrictions on the kinematics and boundary conditions. Since the study of biomembrane deformation draws heavily from the well established models of elastic shells Helfrich (1973); Novozilov (1959), it is only natural to look for the validity of axisymmetric approximations and for the existence of non-axisymmetric solutions in the deformation of elastic shell geometries. Interestingly, many classical elastic structures have intrinsic unstable modes (eigen modes) that lead to a snap-through buckling like deformation or collapse of structures and are associated with lower deformation energy than the corresponding axisymmetric (non-buckling) modes of deformation. Such modes are ubiquitous in elastic shells and manifest as barrelling modes of thin cylinders Azzuni and Guzey (2018), snap-through of elastic columns Brojan et al. (2007), and in folding, wrinkling, and creasing of elastic membranes Deng and Berry (2016), etc. If such modes exist, and are accessible in biomembranes, then they would naturally lead to a reduction in the load and energy barriers to membrane deformation, and may result in heretofore numerically unexplored deformation profiles and membrane morphologies. Accessing these lower symmetry modes and predicting the complex, three dimensional deformation profiles in biomembranes provided the primary motivation for developing the computational framework presented in this work.

Accordingly, in this work, we model two classical biomembrane prob-

lems: formation of tubular shapes in biomembranes and Piezo1-induced membrane footprint generation For each of these problems, we are able to validate against results and observation available in the literature for the simpler deformation modes, and also predict the more complex, less symmetric deformation profiles that are not accessible by the traditional analytical methods and axisymmetric numerical methods.

The computational framework is implemented as an open-source software library and provided as a resource to the biophysics community. It is expected that this framework will serve as a platform for exploring complex deformation mechanisms (including geometric bifurcations and post-bifurcation responses) in biomembranes, and result in an improved understanding of the mechanics underlying various biomembrane phenomena. Future extensions envisioned are support for in-plane fluidity Rangamani et al. (2013), surface diffusion (to model protein transport on the membrane) , and a contact model (to model membrane-membrane interactions). In addition, the inability of the current framework to apply non-uniform Dirichlet boundary conditions and constraints on displacement degrees of freedom inside the domain (i.e. at non-interpolatory knots of the spline surface) are significant limitations and will be addressed in future developments.

3 COMPUTATIONAL VISCOELASTIC FRAMEWORK FOR MODELING MECHANICS AND MICROSTRUCTURE UNDERLYING NEURONAL DEFORMATION AND INJURY

3.1 Introduction

The brain is considered as one of the most critical organs of the human body. It plays a central role in the functioning, organisation and maintenance of the rest of the organs. Neurons, which are the functional units of the brain, are the primary constituents of the brain matter, and their signaling activity constitutes the defining functionality of the brain. On the downside however, the brain is also the most vulnerable organ and any injury, impact or concussion to this soft biological structure jeopardizes the human physiology to various degrees. The criticality of the brain is commensurate with its vulnerability to external mechanical insults leading to concussions, neuronal degradation and injury. In this context, we classify such injuries arising from external loading conditions as Traumatic Brain Injury (TBI) Stocchetti and Zanier (2016). TBI itself can be mild or severe depending upon the severity with which the injury occur Alexander (1995). In the US alone, 1.7 million people suffer from mild to severe TBI annually, with 75-90 percent of those injuries classified as mild Georges et al. (2017); Faul et al. (2010). In the context of neuron scale modeling, TBI is also known as Diffuse Axonal Injury (DAI), characterised by swollen axonal profiles and morphological changes within the neuron ultrastructure Gennarelli et al. (1998); Johnson et al. (2013). The effects of TBI is often manifested in the form of significant physiological and cognitive degradation Neumann and Lequerica (2015) in addition to emotional, behavioural and social traumas Brenner et al. (2011); Milders (2019).

While the pathology and prognosis of severe TBI is well documented and understood in the medical fraternity, delineating standard metrics for classifying mild traumatic brain injury (mTBI) at the sub-neuronal scale is lacking. This is mainly because diagnosing a diffuse damage is more difficult than an intracranial contusion or lesion due to the absence of visible symptoms. This diffuse damage is known to result in persistent and longtime cerebo-cranial effects from delayed brain degradation Graham et al. (2021). The fundamental reason behind the limitation to detect, diagnose and treat diffuse injuries is the complex heterogeneous multiscale organisation of the brain that spans many orders of length scales from the tissue scale (10^{-1} m) to axon, dendritic spines, synapses (10^{-6} m) to the sub neuronal architecture of cytoskeleton (CSK) and cell organelles (10^{-9} m). It is at this neuronal and subneuronal scale that diffuse injury manifests and triggers potential biochemical pathways which eventually lead to neurodegenerative disorders.

Due to these inherent challenges in efficiently and accurately predicting the long term effects and current clinical limitations in conducting brain experiments on humans as well as live animal models, a widespread interest to computationally model TBI has gained much traction. Generally, computational models replicate the effects of common types of TBI and characterise the response of the brain. However coarse scale modeling of existing computational models lack a rich spatio-temporal resolution of injury evolution, especially at the sub-neuronal scale. Hereby, we refer to the complex organisation of the sub-neuronal components and its microenvironment as the neuron *microstructure*. Previously the microstructure was considered as a homogeneous mass of material to characterise its mechanical properties. In reality however, this region is an extremely complex heterogeneous constitution of proteins having a vivid distribution of composition, connectivity, physiology and functioning. Existing homogenized kinematic and mechanical metrics of brain-scale mechanical response often

do not account for the underlying heterogeneous microstructure and thus fail to provide a rigorous connection between the brain scale mechanical deformation and the underlying neuron scale damage.

The sub-cellular scale also referred here as the neuron microstructure attributes to the spatial scale of individual proteins and supporting constitutents that provide structural integrity to the axon. The role of proteins in providing structural integrity to the axon in physiological and pathological conditions serve as the foundation for modeling the neuron microstructure. Current work in neuron-scale modeling conducted loading experiments on neuron clusters to mechanically characterize the response of some of the sub-cellular structures. The viscoelastic nature of these proteins underlies much of the structural vulnerability as observed from experiments and computational modeling. Recent work on *in-silico* modeling of neuronal microstructure by characterising essential structural proteins as mechanical elements will be discussed henceforth. The axon is constituted by a microtubule-tau network assembly at the core, and this was represented by elastic rods (microtubules) and viscoelastic elements (tau) Ahmadzadeh et al. (2014). The objective was to demonstrate binding interactions of the two proteins and highlight that under low strain rates tau mitigates the stress experienced by microtubules, whereas under critical strain rates the latter undergoes rupture and there is breakdown of tau. In general the work emphasized on the viscoelastic properties of tau in mediating microtubule stabilization. Using physics-based constitutive models, the axonal microstructure was modeled and rate dependent mechanical elements were introduced to understand behaviour of elementary proteins in regulating structural integrity of the axon. Even simplistic assumptions arising from relatively recent experimental models considered neurons as a single linear solid (SLS) in the characterisation of tau protein hyperphosphorylation due to mechanical deformation Braun et al. (2020).

To investigate the role and dynamics of essential proteins such as

dynein, microtubules and actin within the axon, an analytical model was proposed de Rooij et al. (2018) which demonstrated the distribution of forces across the connecting load bearing components of the neuronal microstructure. These components, essentially proteins, were represented using viscoelastic elements and classical force-equilibrium balance equations were used to quantify the forces across them. This modeling approach served as one of the harbingers of constructing mechanical descriptions of axons considering multiple proteins which constitute the structural scaffold.

Specific studies on the binding properties within the neuronal CSK between spectrin-actin suggested unfolding of spectrin to mitigate longitudinal stresses along the axon length Dubey et al. (2020). This indicated that the axonal membrane periodic skeleton (MPS) constituted by actin rings spaced by spectrin tetramers may adapt dynamically to withstand mechanical loads using a tension buffering mechanism. Additionally the work suggests that in addition to the axonal network responding differently to loads and loading rates Bar-Kochba et al. (2016), it also exhibited a softening behaviour reminiscent of its viscoelastic characteristics. To further demonstrate the protective behaviour of the spectrin scaffold, a recent study Kant et al. (2021) measured injury regimes for different tensile loads and loading rates to the axon. A composite model of the axon was constructed with proteins contributing as mechanical elements connected together to mimic the neuronal microstructure. This mechanistic approach incorporated additional structural proteins such as myelin, spectraplakin and their linking behaviour with other subneuronal components. To summarize, the description highlighted various loading conditions applied to a structurally motivated network to evaluate mechanical metrics for quantifying injury.

In the previous studies, the biophysics of proteins highlighted a qualitative understanding of injury at the sub-neuronal scale using morphological

abnormalities and damage metrics. However, despite the progress in constructing viscoelastic models resembling the neuronal microstructure for injury prediction, the formulation is elementary, one dimensional and lacks a rich spatio-temporal resolution of the axon. Besides, there is a paucity of information on how tissue scale mechanical deformation consisting of neuron clusters influence proteins constituting the single neuron microstructure and quantifying degradation of critical axonal components which causes an irreversible progression of injury.

In this work we enhance this understanding of sub-neuronal mechanics using a three dimensional continuum viscoelastic model and a finite element implementation along the length of the neuronal axon. We construct a mechanical network of proteins resembling the cytoskeletal region of the neuronal microstructure with each protein having their stiffness and characteristic time scale. The qualitative behaviour of these proteins and the network has been utilised from existing tensile loading and loading rate experimental observations, quantitative estimates from experiments and molecular dynamics (MD) data. Two different analytical strategies have been developed, corresponding to a one dimensional (1D) and a three dimensional (3D) mathematical formulation for evaluating kinematics and mechanical metrics. The 1D model is used to demonstrate fidelity of the network in evaluating different measures of stresses/strain across each component constituting the network. Even in its simplistic representation the 1D model is used to obtain injury metrics for given strains and strain-rates. The 3D model is an extension of its 1D counterpart in which the domain considered is two dimensional and constitutes the axon along the neuronal length. We employ the finite element method (FEM) to discretize this domain and solve the underlying PDEs. The 3D formulation allows us to capture a higher order spatio-temporal representation of the stress/strain evolution in the given domain. We subject the domains to different BVPs for generic and more specific cases at different

strain and strain rates. Additionally, since the PDEs corresponding to the protein network is solved at each quadrature point, it is possible to retrieve mechanical metrics for each protein within the network. This allows comparing component stresses of the network and highlighting proteins which have significant structural contribution.

Additionally, an important feature of our model is modularity. We have constructed our existing network based on available data from literature and qualitative behaviour observed from experiments. However, it is a simplification of a generalised viscoelastic model having the utility to include additional proteins, its corresponding biophysics and interaction dynamics with other components. While previous models have elucidated on a detailed investigation of crucial proteins or larger protein networks with elementary mathematical models, our network combines the potential of these two classes of analysis and presents an enriched methodology to evaluate mechanical metrics at the sub-neuronal scale.

We develop a computational framework for modeling the mechanics of single neuron at the sub-neuronal scale primarily due to assessment of injury metrics during pathological grade loading. This injury manifests itself in the form of elevated stress or strain in a certain region of the brain leading to disruption or degeneration of proteins constituting the neuronal microstructure. However, the affected region can accommodate multiple neurons having morphological and functional differences post impact. Therefore, we model an *in-silico* representation of neuron cluster resembling a region of the brain tissue, embedded within an extracellular matrix(ECM)-like substrate and construct a domain. Akin to the neuronal microstructure, the ECM is composed of proteins which modulate neuron functionally, structurally and during development. Using viscoelastic elements to represent proteins a mechanical network is constructured to mimic the ECM response which acts as a substrate for the neurons. We use FEM to discretize the entire mesh (ECM and neurons), employ our 3D

continuum framework and solve the underlying PDEs using different BVPs. We obtain field distributions of injury-associated mechanical metrics over the domain and assess neurons having elevated levels of the same. This is the *macro* model and gives field information across a domain (globally).

Critical measures of field values such as strain, associated with a neuron within the neuron cluster, is probed by tracking temporal evolution of the field variables of interest across the different proteins constituting the single neuron microstructure. The resulting strain obtained at the point of interest is mapped to a single neuron BVP setup similar to the original problem introduced earlier, using a transformation matrix. This is the *micro* model and gives protein specific mechanical metrics. Together with the previous multi-neuron setup, this top down approach of modeling neuron clusters and the neuronal microstructure using one BVP to simulate another at different length scales, is known as the *macro-micro* approach and can be used as a computational injury assessment tool for risk prediction during TBI.

Overall, here are the key things we present in this communication. Initially, we construct a mechanical network of some structural proteins constituting the axonal region and their connectivity with other members in the network. Using a strain-driven formulation, this protein network is subjected to different BVPs to capture the sub-neuronal and protein specific response. The underlying stress developed upon strain vs strain-rate loading is derived using a 1D and 3D formulation. Using this the stress equilibrium PDEs are solved with FEM to obtain field quantities in the domain. Further a top down multiscale modeling approach is employed to study loading effects on neuron clusters. Using specific BVPs on a domain composed of multiple neurons embedded within an ECM which is modeled to exhibit a different mechanical response than the neuronal microstructure. Specific neurons are probed from this neuron cluster domain and kinematic and mechanical metrics are evaluated for each protein

constituting the chosen neuron. Using appropriate kinematic and mechanical injury thresholds for single neuron and neuron clusters a strain vs strain rate risk prediction phase space is obtained. Even though degradation of critical proteins due to mechanical deformation initiates necrotic biochemical processes and molecular pathways leading to downstream neurodegenerative processes due to injury progression, modeling such phenomena will require inclusion of diffusive chemical fields, tracking evolution of molecular pathways and mechano-chemical coupling. Ideally, addition of chemical fields to the strain and strain rate phase space will further enrich its predictive capabilities in gauging injury. However the present work considers a deformation based injury model and builds the numerical framework using an in-house C++ code (which can be extended to include additional fields and physics), using the open source deal.II Arndt et al. (2022) library, and is available to the general biophysics community. To conclude, the current work is an enhancement of the previous studies both in terms of sub-structural analysis of neurons using a rigorous 3D continuum framework along with a multi-scale approach of quantifying injury.

3.2 Viscoelastic basis of neuron microstructure

Cytoskeleton

The neuron CSK houses a plethora of subcellular components which play a foundational role in neuronal development and during injury. Broadly these subcellular components can be classified into three types of protein filaments: neurofilaments, actin filaments and microtubules. During physiological conditions these sub-structures integrate and respond to mechanical forces in a way that a stiffer component shields a weaker structure thereby protecting the neuron interior. In pathological conditions however, morphological and functional changes compromises with the structural

integrity of the neuron. This work investigates into the individual contribution of these cytoskeletal proteins and mechanistically characterizes them as load-sharing components. To capture the comprehensive mechanical properties of the subcellular components, we construct a viscoelastic network comprising fundamental neuronal proteins involved in load-sharing. The network is presented in Fig.3.1 and the components of the network are hereby discussed.

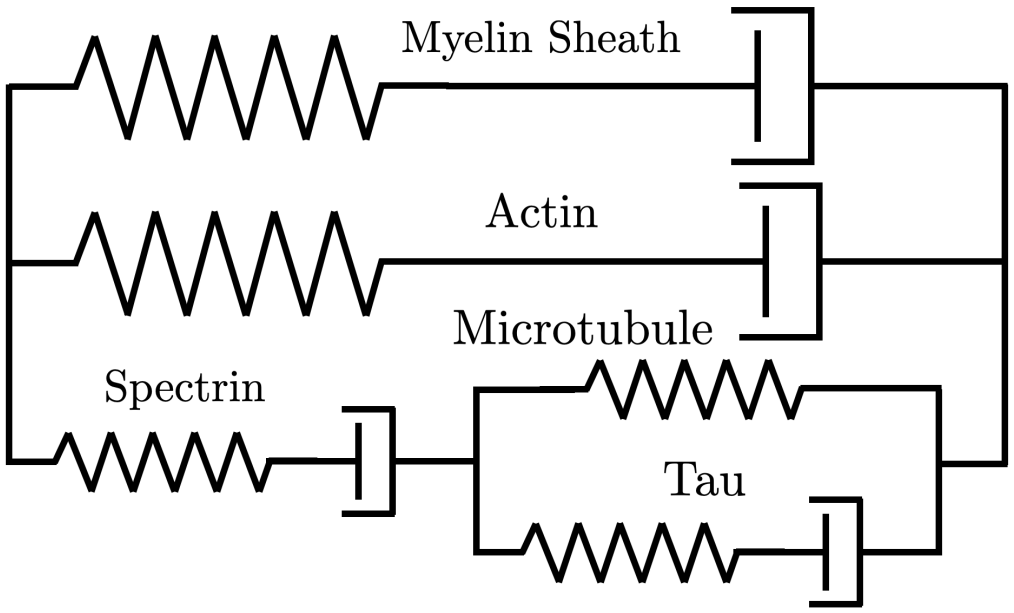

Figure 3.1: Viscoelastic representation of proteins constituting the CSK region of the neuronal microstructure. In this illustration five different proteins are shown namely myelin, short filament actin, spectrin, tau and microtubules. A strain based formulation is used to obtain the constitutive equation for the above network.

Myelin Sheath

The myelin sheath, produced from oligodendrocytes and Schwann cells, is a lipid bilayer which coats the axon along its length and is structurally characterized by Schwann cells, myelin and Nodes of Ranvier. Its primary function is to efficiently expedite electrical impulses across neurons and provide electrical insulation to the nerve cell. Besides, it also provides mechanical support and integrates with the axonal cortex to form a scaffold around the microtubule-tau assembly. In order to capture the mechanical properties, this load sharing capability of the myelin sheath has been characterized as a standard viscoelastic Maxwell element.

Actin Filaments

The actin is an eukaryotic, globular 42kD protein and under sufficient buffer condtions its monomeric isoform (G-actin) naturally aggregate into actin filaments (F-actin). Actin generally operates in tandem with other proteins called actin binding proteins (ABP) which exhibit specific roles in axonal dynamics and organisation Letourneau (2009). In this work we consider *spectrin* which anchors the actin rings and forms a support skeleton around the tubular inner axonal cortex. Actin filaments along with ABPs play a key role in withstanding a wide spectrum of strain and strain rates by mechanically stabilizing the axolemma and the inner cortex. Mechanistically, the actin filament has been represented as a Maxwell element to capture the dynamical mechanical properties.

Spectrin

In the neuronal microstructure, spectrin forms tetramers and attaches with actin rings to coaxially form a scaffold. Lack of spectrin has been shown to produce morphological aberrations in the axon upon deformable loads Krieg et al. (2014). Besides, one of the biochemical markers following

stress induced activation of calpain (leading to calpain proteolysis) are αII and βII spectrin breakdown products commonly known as SBDP Kant et al. (2021). Degradation of spectrin has also been shown to affect structural integrity of the neuronal microstructure. We estimate the contribution and mechanical properties of spectrin by a Maxwell viscoelastic element across actin which mimics the contribution of the actin-spectrin coaxial skeleton.

Microtubules

Microtubules are slender cylindrical structures that arrange itself paraxially along the length of the neuronal CSK. Two types of dimers namely αtubulin and βtubulin constitute these structures. Microtubules are highly dynamic in nature and undergo constant remodelling in the form of poylmerization and depolymerization. Morphologically they cluster themselves in a hexagonal configuration about the axonal length and connect themselves via the *tau* protein. Microtubules play a key role in determining neuronal fate during pathological conditions. For instance long microtubules undergo swelling, undulations and disassembly of the microtubule-tau core resulting in downstream effects Ahmadzadeh et al. (2014). We model the microtubule as a linear elastic spring element to capture critical mechanical thresholds which affect the neuronal physiology.

Tau

Tau (tubulin associated unit) proteins are primarily composed of amino acid chains and are microtubule binding proteins which confer structural support to the neuronal CSK, promotes microtubule growth and mediates axonal transport Weingarten et al. (1975). While tau phosphorylation plays a key role during physiological processes such as neuronal development, during pathological conditions such as TBI, there is an increased activity of this phenomena referred to as hyperphosphorylation. Morphologically,

the tau-microtubule bond starts to disintegrate and the axonal integrity starts debilitating. In order to gain mechanistic insight into the behaviour of tau proteins at certain injury thresholds we characterize it as another linker protein with similar viscoelastic elements.

Membrane

The neuron membrane is a selectively permeable double layer of phospholipid molecules with proteins embedded within, which serve a multitude of functions such as ion channels, pumps, and receptors. Additionally, this lipid bilayer plays a vital role in generating and transmitting electrical signals, facilitating cell adhesion, communication, and shielding the neuron from functional damage. The mechanical characteristics of the neuronal lipid bilayer is attributed to the ion channels and receptors, that are embedded within it. For instance, when a neuron is subjected to mechanical stress, such as stretching or compression, the viscoelastic properties of the membrane enable it to resist deformation and return to its original configuration, allowing it to maintain structural integrity. The mechanical network, illustrated in Fig.3.2, representing the membrane is comprised of a spring and a dampener Rand (1964).

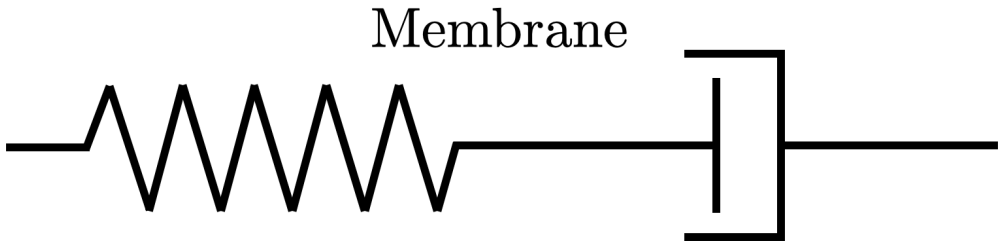

Figure 3.2: Maxwell model representating the mechanical network of a membrane within the neuronal microstructure.

Extracellular Matrix

The neuronal ECM comprises of proteins such as collagen, glycosaminoglycans (GAG), fibronectin, laminin, vitronectin and other molecules which are secreted by the neuron itself and by neighboring cells such as astrocytes and oligodendrocytes. This network of proteins form a scaffold and provide support and structural integrity to the neurons. During physiological conditions, the ECM helps maintain shape and stability of neurons, modulate growth factors thereby regulating synaptic plasticity and provides a substrate for enhanced neural migration. Nonfibrillar structures such as proteoglycans(PG) and hyaluronic acid (HA) provide structural support in the ECM during physiological conditions while fibrillar structures such as fibronectin, vitronectin and collagen increase during pathological conditions Lam et al. (2019); Keating and Cullen (2021). The mechanical network representing the ECM is illustrated in Fig.3.3, which is similar to the work of Wang et al. (2022) primarily because of the mechanistic consideration and availability of ECM specific data. Additionally, we discuss features of one of these fundamental structural proteins which provide support architecture to neurons, which is considered as a linear elastic element within the viscoelastic network.

Type IV Collagen

Type IV Collagen provides a physical network of fibers that help anchor neurons in place and maintain integrity of neural circuits. Collagen fibers are long, thin, and highly ordered, providing resistance to tensile forces and contributing to the overall stiffness of the ECM. Additionally, collagen interacts with neuronal cell surface receptors and promotes adhesion of neuron and their components to each other. During an injury, fibrillar components such as collagen is recruited to mechanically support neurons, suggesting a change in stiffness in ECM. While ECM is known to have a low stiffness due to weak presence of non-fibrillar structures, an increase

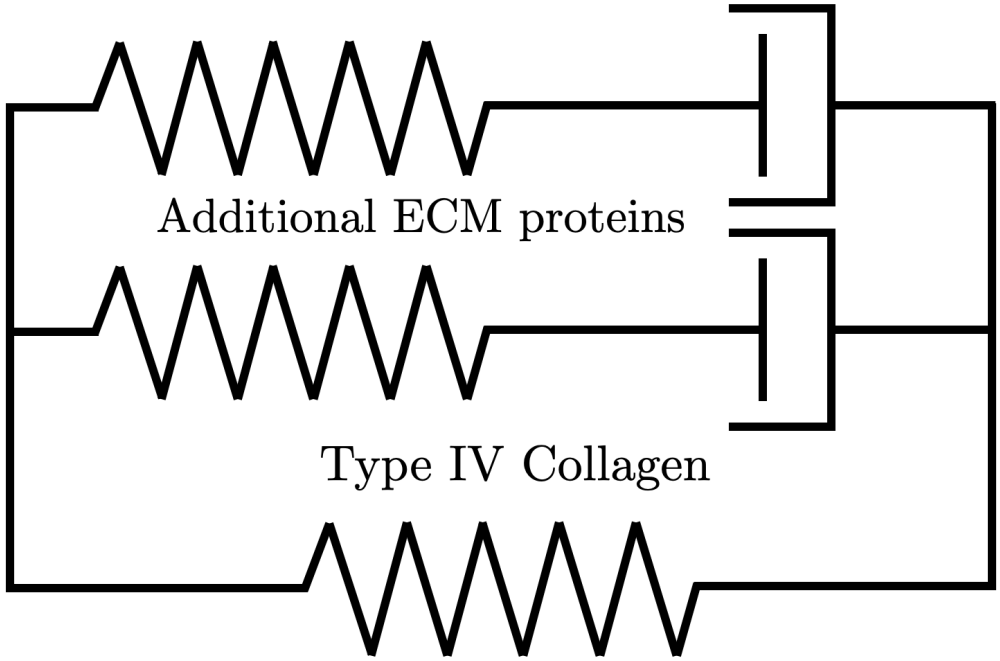

Figure 3.3: Multimode Maxwell model representing the viscoelastic model underlying ECM. Collagen is modeled and a linear elastic spring and the other ECM proteins conferring structural integrity are modeled as two Maxwell elements in parallel. The structure and values considered for this network have been derived from Wang et al. (2022)

in fibrillar composition naturally leads to an increase in ECM stiffness.

3.3 A representative viscoelastic network

The mechanical representation of the structural support provided by the sub-neuronal proteins within the axonal CSK is illustrated in the following figure. Individual proteins have distinctive viscoelastic properties as investigated from literature which were either obtained from experiments or estimated using MD simulations. Three different protein networks

have been constructed to highlight the contribution of neuronal ECM, membrane and CSK, underlying the difference in mechanical response during loading conditions. For CSK, the mathematical formulation has been presented initially for a single quadrature point using zeroth order tensor to represent the mechanical properties of the structural elements, eventually leading to a 1D representation of the mechanical response from the network. In the second case, a three dimensional formulation is presented to model a spatio-temporal evolution of the mechanical metrics across the domain length. The extension is patterned based on the earlier formulation, using three dimensional nonlinear elasticity. The constitutive relationship thus obtained in the latter case, is incorporated into the strong form and subsequently transformed into the weak form using appropriate boundary conditions. FE results are presented to demonstrate the fidelity of the CSK network in tracking metrics for individual proteins in 1D and 3D cases respectively. The specific form of the strain energy functional and 3D formulation used in this presentation is based on the generalised theory of viscoelastic networks from the seminal work of Simo and Hughes (2006).

Mathematical formulation - 1D

The 1D formulation developed for Fig. 3.4 is presented. The inelastic strain developed in branches 1,2 across the damping element due to the applied strain ϵ is given as:

$$E_i(\epsilon - \alpha_i) = \eta_i \dot{\alpha}_i \qquad \alpha_i = \epsilon - \int_{-\infty}^{t} \dot{\epsilon}(s) e^{(-(t-s)/\tau_i)} ds \qquad \tau_i = \frac{\eta_i}{E_i}$$

$$\alpha_i = \epsilon^{n+1} - (e^{-(\Delta t)/(\tau_i)} h_n^i + e^{-(\Delta t)/(2\tau_i)} (\epsilon^{n+1} - \epsilon^n))$$

$$h_{n+1}^i = (e^{-(\Delta t)/(\tau_i)} h_n^i + e^{-(\Delta t)/(2\tau_i)} (\epsilon^{n+1} - \epsilon^n)) \qquad \text{for} \quad i = 1, 2$$

Stress developed is obtained as:

$$\sigma_i = E_i(\epsilon - \alpha_i) \qquad \text{for} \quad i = 1, 2 \tag{3.1}$$

For branches 3 and 5 the expression for inelastic strain is given as:

$$\begin{aligned}
\alpha_3 &= \epsilon_1^{n+1} - (e^{-(\Delta t)/(\tau_3)} h_n^3 + e^{-(\Delta t)/(2\tau_3)}(\epsilon_1^{n+1} - \epsilon_1^n)) \\
h_{n+1}^3 &= (e^{-(\Delta t)/(\tau_3)} h_n^3 + e^{-(\Delta t)/(2\tau_3)}(\epsilon_1^{n+1} - \epsilon_1^n)) \\
\alpha_5 &= \epsilon_2^{n+1} - (e^{-(\Delta t)/(\tau_5)} h_n^5 + e^{-(\Delta t)/(2\tau_5)}(\epsilon_2^{n+1} - \epsilon_2^n)) \\
h_{n+1}^5 &= (e^{-(\Delta t)/(\tau_5)} h_n^5 + e^{-(\Delta t)/(2\tau_5)}(\epsilon_2^{n+1} - \epsilon_2^n))
\end{aligned}$$

The stress obtained in the three branches is given as:

$$\sigma_3 = E_3(\epsilon_1 - \alpha_3), \quad \sigma_4 = E_4\epsilon_2, \quad \sigma_5 = E_5(\epsilon_2 - \alpha_4) \tag{3.2}$$

where $\sigma_3 = \sigma_4 + \sigma_5$ and $\epsilon = \epsilon_1 + \epsilon_2$ as shown in Fig. 3.5.

Mathematical formulation - 3D

Constitutive relationship in nonlinear elasticity

The 3D formulation for the illustration in Fig. 3.4 is presented as follows. The stress developed in branch 1, represented by mechanical elements E_1 and η_1. τ_1 represents the relaxation time given by the expression $\tau_1 =$

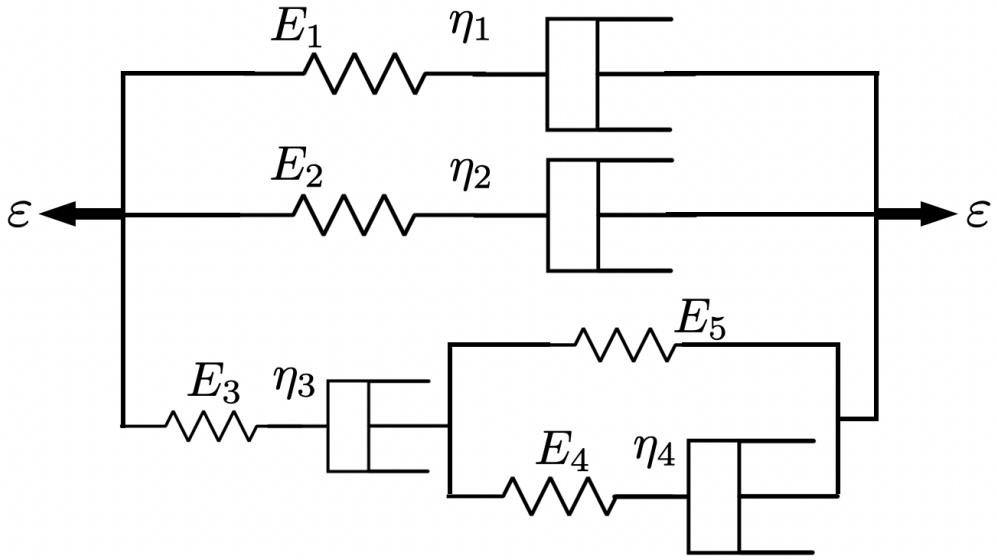

Figure 3.4: Viscoelastic representation of proteins constituting the CSK region of the neuronal microstructure. In this illustration five different proteins are shown namely myelin-1, short filament actin-2, spectrin-3, tau-4 and microtubules-5. A strain based formulation is used to obtain the constitutive equation for the above network.

$\frac{\eta_1}{E_1}, \gamma = 1, \mu_1 = E_1$.

$$\sigma_1(n+1) = \gamma h_1(n+1)$$

$$h_1(n+1) = e^{-\frac{\Delta t}{\tau_1}} h_1(n) + \frac{1 - e^{-\frac{\Delta t}{\tau_1}}}{\frac{\Delta t}{\tau_1}} (s_1^0(n+1) - s_1^0(n))$$

$$s_1^0(n+1) = 2\mu_1 \boldsymbol{e}(n+1)$$

$$\boldsymbol{e} = \text{dev}(\varepsilon(n+1)) = \varepsilon(n+1) - \frac{1}{3}\text{trace}(\varepsilon(n+1))\mathbf{1}$$

Similarly the stress developed in branch 2, represented by mechanical elements E_2 and η_2. τ_2 represents the relaxation time given by the expression

$\tau_2 = \frac{\eta_2}{E_2}, \gamma = 1, \mu_2 = E_2$.

$$\sigma_2(n+1) = \gamma h_2(n+1)$$
$$h_2(n+1) = e^{-\frac{\Delta t}{\tau_2}} h_2(n) + \frac{1 - e^{-\frac{\Delta t}{\tau_2}}}{\frac{\Delta t}{\tau_2}} (s_2^0(n+1) - s_2^0(n))$$
$$s_2^0(n+1) = 2\mu_2 \boldsymbol{e}(n+1)$$

Stress developed in Branch 3, represented by mechanical elements E_3 and

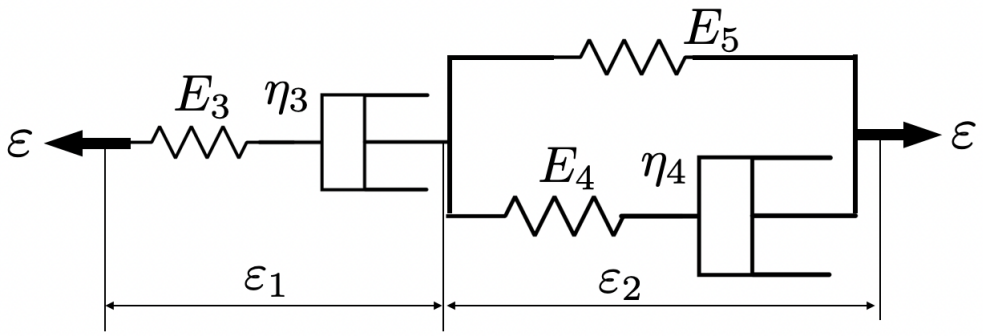

Figure 3.5: The applied strain profile ε is split into ε_1 and ε_2

η_3. The formulation is driven on modified strain represented as ε_1.$\gamma = 1, \mu_3 = E_3$. The applied strain is split additively into two components as mentioned in Fig. 3.5.

$$\sigma_3(n+1) = \gamma h_3(n+1)$$
$$h_3(n+1) = e^{-\frac{\Delta t}{\tau_3}} h_3(n) + \frac{1 - e^{-\frac{\Delta t}{\tau_3}}}{\frac{\Delta t}{\tau_3}} (s_3^0(n+1) - s_3^0(n))$$
$$s_3^0(n+1) = 2\mu_3 \boldsymbol{e}_1(n+1)$$
$$\boldsymbol{e}_1 = \text{dev}(\varepsilon_1(n+1)) = \varepsilon_1(n+1) - \frac{1}{3}\text{trace}(\varepsilon_1(n+1))\mathbf{1}$$

Stress developed in branch 3 is the same as that in the single linear solid (SLS) comprising branch 4 and 5, which is given by the following expression. Here $\gamma_0 = \frac{E_4}{E_4+E_5}, \gamma_\infty = \frac{E_5}{E_4+E_5}, \mu_4 = E_4 + E_5$

$$\sigma_4(n+1) = \gamma_\infty s_4^0(n+1) + \gamma_0 h_4(n+1)$$
$$h_4(n+1) = e^{-\frac{\Delta t}{\tau_4}} h_4(n) + \frac{1 - e^{-\frac{\Delta t}{\tau_4}}}{\frac{\Delta t}{\tau_4}}(s_4^0(n+1) - s_4^0(n))$$
$$s_4^0(n+1) = 2\mu_4 \boldsymbol{e}_2(n+1)$$
$$\boldsymbol{e}_2 = \mathrm{dev}(\varepsilon_2(n+1)) = \varepsilon_2(n+1) - \frac{1}{3}\mathrm{trace}(\varepsilon_2(n+1))\mathbf{1}$$

To obtain a relationship between $\varepsilon, \varepsilon_1$ and ε_2 the stresses in branch 3 and network 4 are equated. The following relation is obtained.

$$h_3(n+1) = \gamma_\infty s_4^0(n+1) + \gamma_0 h_4(n+1)$$
$$\mathrm{dev}(\varepsilon_1(n+1)) = \mathrm{dev}(\varepsilon(n+1))C_1 - C_2$$

where,

$$C_1 = \frac{2\mu_4\gamma_\infty + 2\mu_4\gamma_0 \frac{1-e^{-\frac{\Delta t}{\tau_4}}}{\frac{\Delta t}{\tau_4}}}{2\mu_3 \frac{1-e^{-\frac{\Delta t}{\tau_3}}}{\frac{\Delta t}{\tau_3}} - 2\mu_3 \frac{1-e^{-\frac{\Delta t}{\tau_4}}}{\frac{\Delta t}{\tau_4}}} \qquad C_2 = \frac{D}{2\mu_3 \frac{1-e^{-\frac{\Delta t}{\tau_3}}}{\frac{\Delta t}{\tau_3}} - 2\mu_3 \frac{1-e^{-\frac{\Delta t}{\tau_4}}}{\frac{\Delta t}{\tau_4}}}$$

$$D = 2\mu_4 \frac{1 - e^{-\frac{\Delta t}{\tau_4}}}{\frac{\Delta t}{\tau_4}} \mathrm{dev}(\varepsilon(n)) - \gamma_0 e^{-\frac{\Delta t}{\tau_4}} h_4(n) + 2\mu_4 \mathrm{dev}(\varepsilon_1(n)) \frac{1 - e^{-\frac{\Delta t}{\tau_4}}}{\frac{\Delta t}{\tau_4}} +$$
$$e^{-\frac{\Delta t}{\tau_3}} h_3(n) - 2\mu_3 \frac{1 - e^{-\frac{\Delta t}{\tau_3}}}{\frac{\Delta t}{\tau_3}} \mathrm{dev}(\varepsilon_1(n))$$

The total stress response σ is obtained from the above network by summation of the individual branch contributions :

$$\sigma = \sigma_1 + \sigma_2 + \sigma_3 \quad \text{or} \quad \sigma = \sigma_1 + \sigma_2 + \sigma_4 \tag{3.3}$$

Material matrix for the network

The algorithmic tangent moduli (C) for each branch, is required in the FE implementation during the construction of stiffness matrix (K) for computing degrees of freedom of the global field variable at every node of the discretized domain. For Branch 1 and 2 the deviatoric tensor of elastic moduli in linear isotropic elasticity is given as:

$$\frac{\partial s_i^0(n+1)}{\partial \varepsilon(n+1)} = \bar{C}_i^0 = 2\mu_i(\mathbf{I} - \mathbf{1} \otimes \mathbf{1}) \qquad i = 1, 2$$

For Branch 3 the matrix is modified as:

$$\bar{C}_3^0 = \frac{\partial s_3^0(n+1)}{\partial \varepsilon_1(n+1)} = \frac{\partial s_3^0(n+1)}{\partial \varepsilon(n+1)} \frac{\partial \varepsilon(n+1)}{\partial \varepsilon_1(n+1)} = 2\frac{\mu_3}{C_1}(\mathbf{I} - \mathbf{1} \otimes \mathbf{1})$$

followed by the algorithmic tangent moduli given as:

$$C = \sum_i \frac{\partial \sigma_i^0(n+1)}{\partial \varepsilon(n+1)} = \sum_i \frac{1 - e^{-\frac{\Delta t}{\tau_i}}}{\frac{\Delta t}{\tau_i}} \bar{C}_i^0 \tag{3.4}$$

FE Implementation

The domain used in our simulations is 2D and represents the axonal region along the neuronal length. Additionally, we have obtained a constitutive relationship for stress-strain in the previous section for network. The following algorithm 1 is presented to demonstrate a stress-update algorithm in a strain-driven formulation. Once the constitutive equations have been established, the governing equation (Conservation of Linear Momentum)

Algorithm 1 Stress update in a 3D formulation

Require: $n \geqslant 0$

Ensure: $t_{n+1} \leqslant T, \epsilon_n = \text{given}$

$\boldsymbol{e}(t_{n+1}) = \text{dev}(\epsilon(t_{n+1}))$

$s^0_{n+1} = \text{dev}(\partial_{\boldsymbol{e}} W^0(\boldsymbol{e}(t_{n+1})))$

$h_{n+1} = e^{(-\Delta t_n/\tau)} h_n + \frac{1-e^{(-\Delta t_n/\tau)}}{\Delta t_n/\tau}(s^0(t_{n+1}) - s^0(t_n))$

$\sigma_{n+1} = U^{0'}(\Theta) + \gamma_\infty s^0_{n+1} + \gamma h_{n+1}$

in the weak formulation suitable for a FEM implementation takes the form:

$$R = \int_\Omega w_{i,j}\sigma_{ij}\,dV - \int_{\partial\Omega_h} w_i t_i\,dS = 0 \tag{3.5}$$

where $\partial\Omega_h$ denotes the Neumann boundary of the boundary value problem, and $\mathbf{t}$ is the corresponding boundary traction.

3.4 Results

Single axon loading

Using the mathematical formulation as described above, we perform numerical simulations on a representative axon, which is characterized by its three distinct regions: CSK, membrane and ECM. Fig.3.6 highlights the axon and the underlying viscoelastic networks which govern the mechanical response of each region considered. Using BVPs we obtain mechanical metrics which are compared against each region and within each protein of a particular region. This gives us a comprehensive ballpark of mechanical estimates at specific loads and loading rates. Initially, we demonstrate stress developed within the neuronal microstructure during strain rate dependent loading followed by relaxation as plotted in Fig.3.7.

Additionally the mechanical stress developed within each region can be split into individual protein contributions to distinguish their presence

Table 3.1: Viscoelastic parameters constituting the neuronal microstructure

Parameter	Protein	Value	Reference
E_{00}	Collagen	3 MPa	Wang et al. (2022)
E_{01}	ECM Protein 1	130 MPa	Wang et al. (2022)
E_{02}	ECM Protein 2	1 MPa	Wang et al. (2022)
$\tau_{01}(\frac{\eta_{01}}{E_{01}})$	ECM Protein 1	16s	Wang et al. (2022)
$\tau_{02}(\frac{\eta_{02}}{E_{02}})$	ECM Protein 2	400s	Wang et al. (2022)
E_2	Membrane	1 MPa	Rand (1964)
$\tau_2(\frac{\eta_2}{E_2})$	Membrane	1s	Rand (1964)
E_{11}	Myelin Sheath	10 MPa	Shin et al. (2020)
E_{12}	Actin	400 MPa	Khan et al. (2021a)
E_{13}	Spectrin	80 MPa	(estimated)
E_{14}	Tau	10 MPa	Khan et al. (2021b)
E_{15}	Microtubules	600 MPa	Memet et al. (2018)
$\tau_{11}(\frac{\eta_{11}}{E_{11}})$	Myelin Sheath	1s	(estimated)
$\tau_{12}(\frac{\eta_{12}}{E_{12}})$	Actin	0.2s	Maxian et al. (2021)
$\tau_{13}(\frac{\eta_{13}}{E_{13}})$	Spectrin	20s	(estimated)
$\tau_{14}(\frac{\eta_{14}}{E_{14}})$	Tau	0.35s	Ahmadzadeh et al. (2014)

and impact on the neuronal microstructure. To demonstrate this, we have resolved the stress values for individual proteins and illustrated in Fig 3.8.

Multi neuron cluster loading

A more realistic representation of neurons is achieved through neuron-cluster loading. In this instance, we construct a computational domain comprising of mechanistic version of axons, as demonstrated previously, and orient them at random angles within the domain. This allows us to obtain a spatially heterogeneous distribution of axons which is similar to neuron-cluster experimental studies. Using a similar BVP for the larger domain, we have been able to plot stress distributions for different neurons within the domain. This enables us to understand the amount of

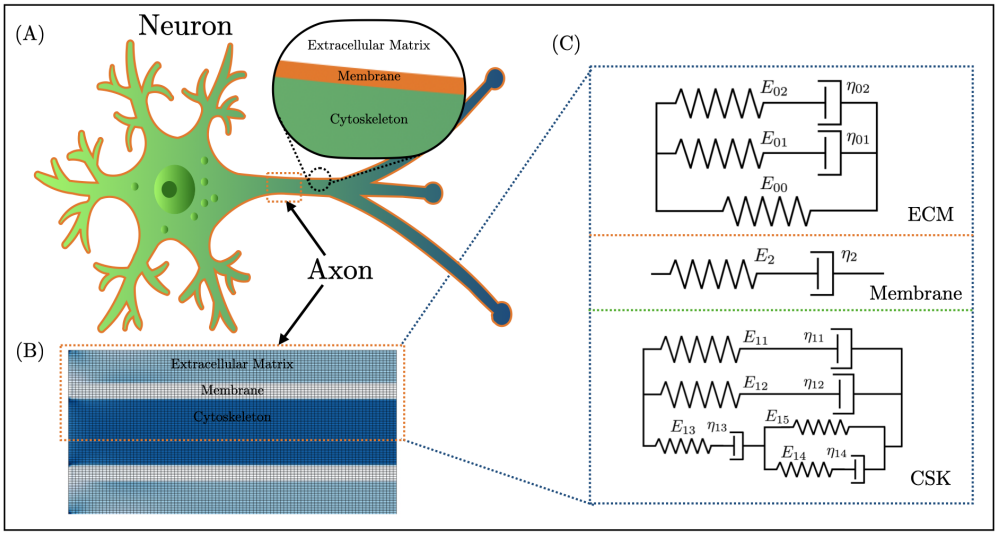

Figure 3.6: (**A**) The axon is highlighted within a graphical illustration of a neuron showing the different layers. (**B**) The chosen region, with dimensions 10 µm X 5 µm, is discretized using a mesh which enables finite element simulations. (**C**) Every Gaussian point of each region has an underlying viscoelastic network which captures its mechanical behaviour upon loading. The mechanical properties of the viscoelastic elements used in the networks have been obtained or estimated from literature, and is given in Table.3.1

stress localisation within each neuron within the cluster, upon mechanical loading. We have illustrated this in Fig.3.9, consisting of a schematic and some mechanics metrics obtained from the BVP simulations.

3.5 Conclusion

We have presented a three dimensional continuum based viscoelastic model of the neuronal microstructure for single and multi-neuron cases. The key highlight of this work is the consideration of different regions

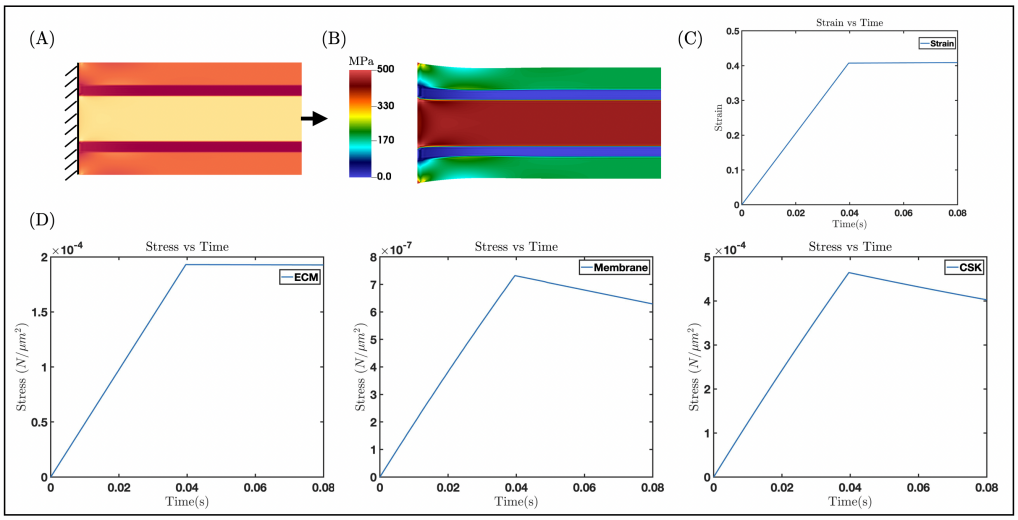

Figure 3.7: (**A**) The BVP shows one end of the axon is fixed while the other end undergoes displacement based loading. A strain rate of 1e+2 s^{-1} is applied up to a strain of 0.4, corresponding to a time of 40ms and held at that value for another 40ms to enable relaxation. (**B**) The maximum stress field distribution is plotted across the spatial region of the neuronal microstructure. (**C**) A plot of strain against time is shown to highlight loading behaviour (**D**) Stress against time plots are shown for (Left to Right) ECM, Membrane and CSK respectively. As evident from the strain plot, stresses increase according to the underlying viscoelastic networks and eventually relaxes when the displacement load is held at the given strain.

within the axonal sub-structure consisting of different proteins which contribute towards structural integrity. These proteins are further expressed as viscoelastic elements and investigated according to their specific contributions towards mechanical strength of the axon. The computational framework presented in this study captures the spatio-temporal evolution of mechanical metrics within neuronal clusters.

This work is fundamental in understanding cellular and sub-cellular scale mechanics of neurons during TBI. Using different strain rate de-

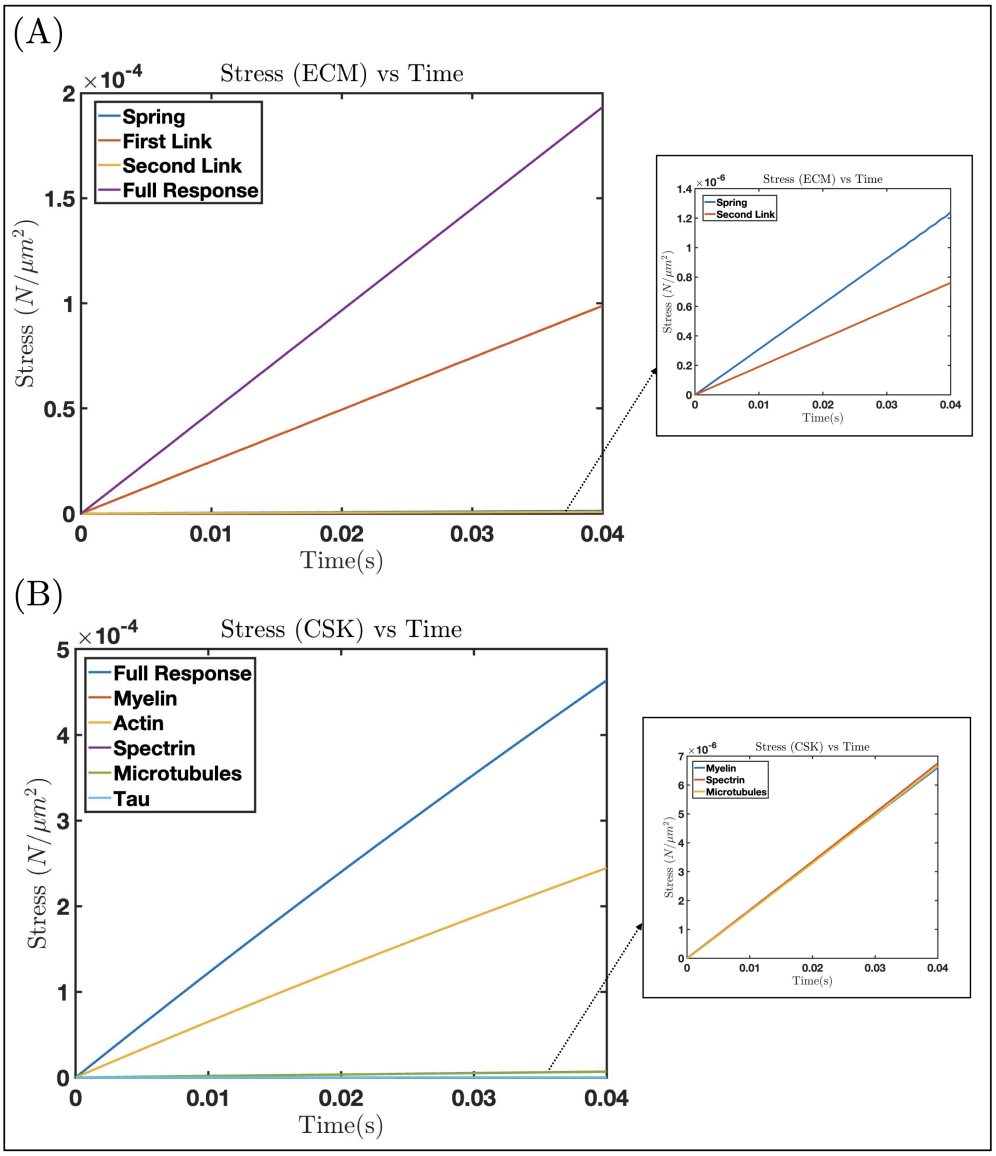

Figure 3.8: Stress developed across individual proteins resolved from the overall stress response of the regions: (**A**) ECM and (**B**) CSK

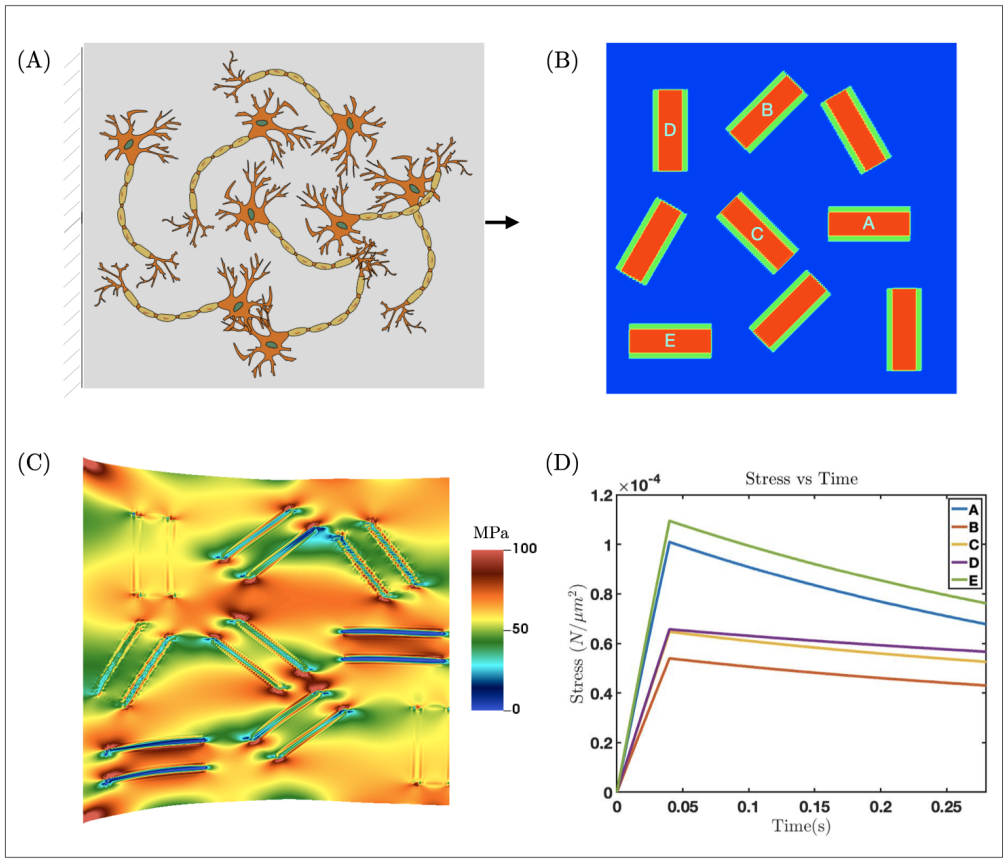

Figure 3.9: (**A**) Graphical representation of neurons embedded within a cluster. Additionally it also highlights a BVP with the left end fixed and the right end subjected to displacement based loading condition. (**B**) Computational estimation of neurons. As the figure indicates, the red regions correspond to the CSK, green represents membrane and blue, ECM. For simplicity the mechanical properties of all the neurons are same. (**C**) Upon a strain-dependent loading rate of 1e+2 s^{-1} upto a strain of 15 percent applied over 40 ms and held constant upto 350 ms, the stress field distribution for the domain is obtained and plotted as shown. The heterogeneity observed in the stress values for individual neurons is captured in (**D**). For neurons marked A through E in sub figure (**B**), the stresses developed in their respective CSK is plotted against time.

pendent loading conditions and incorporating appropriate injury based neuronal thresholds it is possible to construct injury maps which indicate survivability of neurons and neuron clusters. Additionally our mathematical model can be extended to include additional CSK or ECM proteins, having their characteristic viscoelastic descriptions which could improve the fidelity of injury assessment. We extend this study to include chemical fields in addition to mechanical fields in Chapter 4 to demonstrate the multiphysics capabilities of our numerical framework.

4 SPATIO TEMPORAL MODELING OF BIOMARKER EXPRESSION IN NEURONAL CLUSTERS DURING TRAUMATIC BRAIN INJURY

4.1 Introduction

A broad classification of injuries caused due to an impact or concussion to the head is referred as TBI. The difficulty in TBI diagnoses stems from the heterogeneity of the brain, structural complexity of the neuronal microstructure and the complex interplay of proteins at different length and time scales. TBI is generally manifested as primary and secondary, with primary referring to the immediate mechanical response of the brain and the secondary type culminating as a biochemical response. The initiation of the secondary injury is triggered by a pathological grade of mechanical load and as the initial trauma unfolds, a cascade of complex cellular and molecular events follow, potentially exacerbating the damage inflicted during the primary injury. The injury progression involves upregulation of critical neurotransmitters, inflammasomes and prolonged activation of ionic channels which are crucial to maintaining physiological homeostasis within neurons and neuronal clusters. Identifying the cascade of these molecular events in accelerating neurological degradation remains as a fundamental challenge in post injury diagnoses. In this work we aim to qualitatively and quantitatively demonstrate one of the many pathways underlying secondary injury across the labyrinth of TBI to predict and possibly mitigate its devastating consequences.

Previous studies have highlighted key biomarkers relevant to TBI which are clinically calibrated as a metric for facilitating potential downstream pathological pathways. Recent studies highlight activation of the transmembrane channel proteins Pannexin-1 (Panx1) Seo et al. (2021) present

in neurons and glial cells, due to an increase in mechanical strain Albalawi et al. (2017), which are key mediators of ATP (Adenosine Triphosphate) release into the extracellular region, thereby facilitating neuroinflammation. An increase in extracellular ATP, which is widely known for its role in energy metabolism, activates trimeric purinergic receptors P2X which are ATP-sensitive ion channels present in the microglia Hattori and Gouaux (2012). Xing et al. (2016) quantitatively highlighted the influence of increasing extracellular ATP concentration on P2X and P2Y receptor sensitivity and highlighted activation dynamics of the P2X7 receptor, whose expression has been associated with inflammation Andrejew et al. (2020); Rotondo et al. (2022). P2X7 receptor activation causes outflux of K^+ ions from the intra-cellular to the extra-cellular neuronal microenvironment causing a deficit in ionic concentration, which assists in formation of the nucleotide-binding domain, leucine-rich-containing family, pyrin domain-containing 3 (NLRP3) inflammasome and activation of Caspase 1, also known as Interleukin-1 converting enzyme (ICE)Pelegrin (2021). Additionally the P2X7 receptor also assists in production and release of TNF-α (Tumor Necrosis Factor), another major pro-inflammatory cytokine, responsible for triggering an inflammatory response You et al. (2021); Barberà-Cremades et al. (2017). One aspect of its influence involves its potential contribution to excitotoxicity, a process where excessive activation of receptors for excitatory neurotransmitters like glutamate leads to cell damage or death. TNF-α has been implicated in modulating glutamate transmission and excitotoxicity in the brain and can increase the release of glutamate, promoting excitotoxicity by several mechanisms Olmos et al. (2014). It can enhance the expression and function of certain glutamate receptors, such as the NMDA receptor, which is heavily involved in excitotoxic processes Jara et al. (2007). Moreover, TNF-α can disrupt the balance of glutamate and its clearance mechanisms in the brain, leading to increased levels of this neurotransmitter and subsequent excitotoxic

damage to neurons Takeuchi et al. (2006). The clinical consequences originating from the pathological response due to increased expression of these molecules causes initiation of neuronal degradation in the form of irregular signal transmission across neurons, initiation of necrotic pathways and uncontrolled inflammation in cells all of which eventually lead to neurodegeneration.

To address this complexity in resolving and quantifying critical biomarkers involved in spatial and temporal regulation of the pathological downstream pathways, we propose a possible molecular cascade following primary injury. While previous studies have investigated into the individual molecular contributions and expression within the sequence of events, we aim to unify clinically identified biomarkers as an ensemble of chemical species constituting secondary injury. Additionally, there is a paucity in demonstrating spatial localisation behaviour of these species and their downstream influence on associated elements within the pathway. Therefore, our objective is to quantify the gap between isolated molecular events at the cellular scale and neurodegeneration at the tissue scale using a qualitative narrative.

Our approach of quantifying the mechanotransduction process underlying TBI is structured into two components. Initially, we construct a cascade of molecular biomarkers implicating necroptosis during secondary injury followed by numerical estimation of these species within the chemical pathway. Firstly, we construct a mechano-chemical formulation consisting of relevant chemical and mechanical fields which dictate the multi-physics of secondary injury. Secondly, we numerically develop geometrical domains resembling neurons, microglia and extracellular matrix (ECM) to spatially represent localisation and evolution of chemical species within a larger neuronal cluster domain. This enhances a comprehensive visualisation of the interactions between mechanical and chemical fields and their spatio-temporal resolution with single and multiple neuron-

microglia-ECM assembly. Finally, the mechano-chemical formulation is mathematically modelled using partial differential equations (PDE) with appropriate boundary conditions relevant to TBI. This first-of-a-kind study provides useful insights into approximating molecular behaviour upon deformation based injury at distinct spatial and temporal scales from neuronal microstructure to system-level.

Underlying the multiphysics setup for approximating mechanotransduction, the mechanical response has been modeled using a three dimensional viscoelastic network consisting of proteins which confer structural stability to the neuron-microglia-ECM assembly. The chemical response has been modeled using advection-diffusion equations with chemical fields representing molecular species (ATP, TNF-α, P2X7, glutamate) and geometrical localisation accounting for the spatial heterogeneity of these constituents across the domain. The finite element (FE) method has been used to discretize the underlying coupled PDE formulation. Using appropriate sets of loading conditions across the domain, we demonstrate spatio-temporal evolution of biomarkers and characterize mechano-chemical basis of injury thresholds. We also construct an enhanced description of an injury curve considering critical chemical fields in addition to the existing mechanical metrics.

To summarize we propose a multiphysics model of molecular mechanotransduction and capture the mechano-chemical dynamics arising out of secondary injury. In Section 2 we provide a comprehensive description of the chemical pathway proposed. In Section 3 we introduce the biomarkers and quantify them using PDEs. This is followed by numerical formulation of the multiphysics setup. In Section 4 we discuss about specific boundary value problems (BVPs) similar to TBI conditions and demonstrate mechano-chemical interactions. Additionally, we construct a computational injury curve and increase the phase spectrum for TBI diagnoses. We conclude with Section 5 with a brief discussion and directions for future

possibilities in the computational treatment of TBI.

4.2 Chemical pathway of necroptosis

TBI is often addressed as a "biphasic injury" having a primary and a secondary component Ng and Lee (2019). While experimental studies have addressed and clinical studies established treatment strategies for primary injury, a detailed understanding of secondary injury remains unclear. The paucity in injury resolution is often attributed to the myriad of necrotic biochemical pathways which trigger and persist for days, weeks to months Maas et al. (2008). Enhancing treatment strategies for the biochemical irregularities associated with TBI necessitates identifiable mechanisms and measurable biomarkers. This study aims to elucidate the mechanisms driving secondary injury, focusing on identifying, quantifying biomarkers, and spatio-temporally modeling the proposed pathway that culminates in necroptosis Hu et al. (2022).

Cell death, traditionally categorized into three primary types namely apoptosis, autophagy, and necrosis showcases distinct morphological and biochemical transformations, each illuminating unique pathways in the landscape of cellular degradation Healy et al. (1998). In the context of TBI, cellular damage is characterized through apoptosis and necrosis Fink and Cookson (2005). Apoptosis refers to an orchestrated cellular self-deconstruction without instigating inflammation thereby preserving the integrity of surrounding tissues Akamatsu and Hanafy (2020). Necrosis, on the other hand, unfolds as a passive and unintended fate for cells, arising from external disruptions and environmental effects causing uncontrolled release of inflammatory cellular components. In the realm of secondary injury, emerging research Nie et al. (2022); Hu et al. (2022) suggests the presence of a meticulously regulated form of cell death, poised as the governing mechanism regulating downstream pathways known

as necroptosis. The distinguishing feature of this programmed cell death is in its controlled activation and orchestrated process by inflammatory proteins compared to the uncontrolled and accidental nature of necrosis Dhuriya and Sharma (2018). In this communication, our objective is to intricately delineate and quantify a possible chemical pathway governing necroptosis.

Following an insult, a cascade of downstream molecular pathways initiate within the brain causing an upregulation of several critical biomarkers responsible for modulating chemical and electrical signalling. Crucial to biomarker expression is the activation of microglia, the resident immune cells of the central nervous system. Microglia mediates the neuroinflammatory response and causes production and release of several molecules. Recent findings have identified multi-protein complexes such as NLRP3 inflammasome O'Brien et al. (2020), pro-inflammatory cytokines such as interleukins Yan et al. (1996), TNF-α Woodcock and Morganti-Kossmann (2013); Longhi et al. (2013) and neurotransmitters such as glutamate Guerriero et al. (2015) most of which are expressed in varying degrees during pathophysiological conditions. These biomarkers play a central role as essential indicators in injury assessment and diagnosis, serving as foundational elements for modeling the mechanisms underlying subsequent downstream processes.

The principal challenges in formulating a hypothesis for a biochemical pathway underlying secondary injury essentially revolve around the identification of relevant molecules integral to the pathway and the acquisition of experimental evidence enabling precise quantification of specific biomarkers. To fulfill our primary aim, we have assembled a set of molecules crucial in secondary injury, commonly recognized as biomarkers in clinical diagnoses. Leveraging these, we've proposed a potential molecular pathway, illustrated in Fig.4.1 as part of our hypothesis. In this section we develop a qualitative understanding of the molecular pathway and

describe how each component unfolds spatio-temporally in response to its predecessor. The pathway begins with a concussion to the brain characterized by mechanical deformation within neurons and neuron clusters and terminates with glutamate excitotoxicity, a classic indicator suggestive of neuronal degeneration Armada-Moreira et al. (2020).

Initiating the molecular cascade upon concussion, mechanosensitive receptor channels identified as Pannexins become activated as the first elemental response in the pathway Bao et al. (2004). Pannexin proteins, particularly pannexin-1 (Panx1), are transmembrane channels found in the plasma membrane of many cell types, including neurons and astrocytes. These channels play a crucial role in the exchange of ions, metabolites, and signaling molecules between the intracellular and extracellular environments. Opening of pannexin channels in response to mechanical strain represents a significant aspect of cellular communication and signaling in various physiological and pathological conditions. Recent studies have demonstrated the influence of mechanical deformation in prolonged activation of pannexin channels which trigger excessive release of energy molecules such as ATP from the intracellular to the extracellular milieu Albalawi et al. (2017); Xia et al. (2012).

Excess extracellular ATP, beyond its normal physiological levels, can trigger several detrimental effects including neuronal excitotoxicity Choi et al. (2021), inflammation Cauwels et al. (2014), oxidative stress Cruz et al. (2007) and impaired synaptic function Vroman et al. (2014). This surplus ATP present in the extracellular space can overstimulate purinergic receptors, leading to dysregulated signaling pathways. Purinergic receptors are a class of cell surface receptors that are activated by purines, particularly ATP, and are widely expressed in microglia Calovi et al. (2019). Of particular interest is the P2X7 receptor, a distinct member of the purinergic receptor family of ligand-gated ion channels which plays multifaceted roles in various physiological and pathological processes Andrejew et al.

(2020). Xing et al. (2016) provided a comprehensive characterization of P2X receptor responses across varying concentrations of ATP, examining both human and rodent receptors. Their findings not only provide valuable insights into the intricacies of purinergic signaling but also serve as a fundamental quantitative tool crucial for refining and constructing our modeling processes. Activation of these receptors, typically at high concentrations of ATP, leads to the opening of non-selective cation channels, allowing the influx of calcium and sodium ions and subsequent efflux of potassium ions Piccini et al. (2008); Xu et al. (2020). Elevated extracellular potassium concentration is known to cause a multitude of events such as alteration of electrochemical homeostasis across neuronal membrane Schaefer et al. (1995), hyperexcitability Florence et al. (2012), altered synaptic activity Tagluk and Tekin (2014) and neuronal degradation Muñoz-Planillo et al. (2013); Koumangoye (2022).

A reduction in intracellular potassium concentration is associated with the activation of the NLRP3 inflammasome Muñoz-Planillo et al. (2013). This drop in potassium levels serves as a signal for NLRP3 activation in microglia, triggering the assembly and activating the inflammasome complex Xu et al. (2020), consequently leading to the processing and release of pro-inflammatory cytokines Blevins et al. (2022). These mature cytokines are then released into the neuronal extracellular region, fostering an inflammatory response that exacerbates tissue damage which perpetuates neuroinflammation. In addition to the molecular pathway under consideration, numerous studies underscore a significant pathophysiological occurrence subsequent to TBI, which is, heightened production of reactive oxygen species (ROS) attributable to an increased post-injury oxygen consumption rate in the brain Fesharaki-Zadeh (2022). The imbalance between cellular ROS generation and the body's antioxidant defenses results in oxidative stress, a crucial factor implicated in the development and progression of numerous human diseases. Oxidative stress plays a signifi-

cant role in modulating the transcription factor nuclear factor-κB (NF-κB) pathway, a fundamental signaling cascade involved in the regulation of inflammation and immune responses Lingappan (2018). ROS-induced activation of the NF-κB pathway not only triggers the formation of the NLRP3 inflammasome but also directly stimulates the production of inflammatory mediators such as TNF-α, pro-interleukins and various other inflammatory factors Liang et al. (2017).

TNF-α is a pleiotropic pro-inflammatory cytokine which is primarily released by activated microglia and other immune cells in the brain during secondary injury. It's production contributes significantly to the intricate cascade of inflammatory processes observed in these conditions, a hallmark associated with various neurological disorders. Interestingly, despite its predominantly recognized pro-inflammatory role, TNF-α also serves various beneficial functions within the body such as immune defense, tissue repair and regulation of immune cells Shohami et al. (1999); Francisco et al. (2015). In this study however, our focus remains constrained to understanding the pathophysiological impacts of this cytokine and its influence on other molecules within the specific chemical pathway under investigation. Various inflammatory stimuli, like the cytokine interferon-gamma Hanisch (2002), act as triggers for microglial activation during neuroinflammation. These stimuli influence distinct signaling pathways, including the p38 mitogen-activated protein kinase (p38 MAPK) and NF-κB pathways Kim et al. (2013), orchestrating the upregulation of TNF-α expression Olmos et al. (2014).

TNF-α's detrimental impact within the molecular pathway manifests notably through its influence on glutamate excitotoxicity. Glutamate, the most abundant amino acid in the body, beyond its role as the primary excitatory neurotransmitter of the brain, holds a multifaceted significance in the physiology of the central nervous system. Often revered as the "commander" of the brain Mattson (2023), glutamate orchestrates several

pivotal functions crucial for neuronal signalling Reiner and Levitz (2018), synaptic plasticity Nadler (2012), memory and cognition Pal (2021). Neurons initiate the process of glutamate synthesis by transforming glutamine into glutamate and subsequently releasing it to astrocytes which capture the released amino acid, converting it back into glutamine before transporting it back to neurons. During pathophysiological conditions, TNF-α downregulates the expression and function of glutamate transporters on astrocytes, such as excitatory amino acid transporters (EAATs). The interference of the inflammatory cytokine with glutamate uptake by astrocytes leads to increased extracellular glutamate levels, contributing to excitotoxicity and neuronal damage Olmos et al. (2014); Guerriero et al. (2015).

Glutamate excitotoxicity unfolds through multiple layers, involving interconnected mechanisms within the landscape of neurons and its microenvironment. Within glial cells, the activation of tumor necrosis factor receptor 1 (TNFR1) by TNF-α elicits a dual effect. Firstly it stimulates the process of glutamate removal from astrocytes and secondly it impedes their ability to efficiently clear glutamate from the synaptic cleft. In neurons, the TNF-α/TNFR1 interaction increases the excitatory synaptic strength. This effect stems from the induction of heightened Ca^{2+} permeability in ionotropic glutamate receptors α-amino-3-hydroxy-5-methyl-4-isoxazolepropionic acid (AMPA) and N-methyl-D-aspartate (NMDA) receptors, intensifying excitatory transmission. Simultaneously, TNF-α decreases the surface presence of inhibitory gamma aminobutyric acid (GABA)-A receptors, further tipping the balance towards increased neuronal excitability Pribiag and Stellwagen (2013).

The accumulation of excessive calcium, underlying glutamate excitotoxicity, inside neurons emerges as a key process triggering necroptosis. NMDA receptors, upon activation, facilitate the entry of extracellular calcium through specialized channels. When these glutamate receptors are

overly stimulated, it results in an overload of calcium within neurons, setting the stage for cellular damage due to an overwhelming influx of this essential yet potentially harmful ion. Stimulation of glutamate receptors leads to the influx of calcium causing the neuronal cell membrane to depolarize. This depolarization triggers the activation of voltage-dependent calcium channels which facilitate more calcium entry, compounding the intracellular calcium overload initiated by the excessive stimulation of glutamate receptors Mark et al. (2001).

In this envisioned molecular pathway illustrated in Fig.4.1, as we witness a sequence of pathophysiological occurrences including the generation of reactive oxygen species (ROS), heightened calcium levels, and the activation of cellular degradation via TNF, we employ the term "necroptosis" to encapsulate and define the subsequent biochemical process. This designation signifies a specific form of programmed cell death as described and marked by these collective events within the pathway Arrazola et al. (2019); Li et al. (2008). The consequences of glutamate excitotoxicity commences at the molecular level, where dysregulated glutamate signaling disrupts neuronal homeostasis and triggers a cascade of downstream events. These molecular abnormalities, characterized by excessive calcium influx, oxidative stress and neuronal damage, gradually evolves and contributes to the progression of lifelong neurodegenerative disorders. The sustained impact of excitotoxicity over time contributes to chronic neurodegeneration, culminating in conditions such as Alzheimer's disease Wang and Reddy (2017), Parkinson's disease Iovino et al. (2020), Huntington's disease André et al. (2010), and others. These disorders manifest progressively, characterized by the gradual loss of neuronal function and structure, leading to long-term cognitive decline, motor impairments, and various neurological deficits. Incorporating the qualitative insights from the proposed pathway we have developed a PDE based multiphysics (mechano-chemical) framework. This is used to capture and emulate the

intricate chemical processes triggered by both initial molecular perturbations and mechanical loading. We use our framework primarily to model neurons, neuron clusters and their microenvironment to visualise and resolve the spatio-temporal dynamics of the molecular biomarkers.

Reduced pathway considered for quantification of chemical species

Given the challenges and complexities in mathematically modeling the entire pathway in Fig.4.1, primarily due to insufficient quantifiable data for every element, we suggest a more succinct approach. Our proposal involves a reduced pathway focusing on major components within the cascade, supported by substantial experimental validation found in the literature. We aim to quantify the reduced envisioned pathway, presented in Fig.4.2 into a set of governing equations motivated by evolution of chemical species' concentrations as primary field variables. The shortened pathway consists of fundamental chemical elements, identified as critical biomarkers during secondary TBI and modeled as diffusive fields.

As illustrated in Fig.4.2 the cascade initiates with mechanical deformation, manifested as strain within neurons and neuron clusters. Mathematically, the imposed boundary condition is treated as deformation while the corresponding strain response is obtained from the viscoelastic constitutive network of the underlying neuronal microstructure. Using this strain field generated across the domain of interest (neurons or neuron clusters), we use it as an input for driving ATP generation. This assumption is hypothesized from the phenomena that mechanical deformation causes activation of Panx1 channels leading to ATP release from the microglia to the extracellular region.

Excess concentration of extracellular ATP causes activation of the purinergic P2X7 receptors situated in the microglia. These receptors play a fundamental role in facilitating formation of pro-inflammatory complexes

and therefore has been modeled in the proposed pathway. Recent findings Xing et al. (2016) have quantified the effect of ATP on members of the P2X and P2Y receptor family. These studies play a pivotal role in correlating the effect of ATP concentration with P2X7 receptor opening probability. In the modeling process, the purinergic receptor channel has been estimated numerically as a phase field. The consequences of this activation leads to production of enzymes, formation of inflammasomes and release of cytokines from the microglia. Among these one of the central molecules, also recognised as a clinical biomarker, is TNF-α.

The release of this inflammatory cytokine is regulated heavily by modulation of the P2X7 receptor. Studies have indicated increase in concentration of TNF-α due to receptor activation. This inflammatory molecule is mathematically modeled as a diffusive chemical field and driven by a function which depends on the P2X7 phase field. While there are a number of crucial elements preceding the formation and release of TNF$-\alpha$, they have not been considered in the reduced pathway due to a paucity in quantifiable data relating intermediate molecules with any of the cascade components considered.

TNF$-\alpha$ causes initiation of a number of downstream events following its activation and release, primarily associated with excitotoxicity. Due to the increased extracellular concentration of this inflammatory cytokine, the microglial uptake of glutamate reduces in the glial cells and subsequently increases in the post synaptic region. Since glutamate is the principal excitatory neurotransmitter of the brain, an increase in its concentration causes a spectrum of neurodegenerative disorders due to the disturbed ionic homeostasis principal to neuronal signalling. In our reduced pathway, glutamate is also modeled as a diffusive chemical field localised in the neuronal synapses. Our modeling process is facilitated by data associating TNF$-\alpha$ with glutamate, where evolution of the latter is driven by a function relating the former.

We discuss the multiphysics of the functional dependencies of all of the above chemical species' and derive reaction terms which demonstrate quantifiable relations between them. The shortened pathway brings together critical elements necessary for spatio-temporal resolution of the necroptotic pathway while highlighting a strong correlation between the chemical species. The idea is to present a novel mathematical framework incorporating a first-of-its-kind necroptotic pathway modeled with a rigorous numerical implementation using state-of-the-art scientific computing tools in FEM and demonstrate mechanical and chemical metrics underlying secondary injury. The computational framework is made available to the wider research community as an open source library Git (2024).

4.3 Mathematical formulation

The first step in the multiphysics formulation is identifying the biological species constituting the molecular mechanotransduction pathway and characterizing their diffusive dynamics, sources and chemo-mechanical interactions. We consider concentrations of the following chemical species as the primary fields: ATP (c_a), TNF-α (c_t), Glutamate (c_g) and ionic channels represented as a phase field: P2X7 (ϕ_p). The idea behind a phase field assumption of ionic channels is the appoximation of gating probability (0-closed, 1-open) due to concentration sensitivity of certain chemical species. The evolution of these chemical fields are modeled using

the following advection-diffusion equations:

$$\frac{\partial c_a(\mathbf{x},t)}{\partial t} = \nabla \cdot (D_a \nabla c_a) + f(\epsilon, \dot{\epsilon}), \quad \mathbf{x} \in \Omega \tag{4.1}$$

$$\frac{\partial c_t(\mathbf{x},t)}{\partial t} = \nabla \cdot (D_t \nabla c_t) + f(c_a, \phi_p), \quad \mathbf{x} \in \Omega \tag{4.2}$$

$$\frac{\partial c_g(\mathbf{x},t)}{\partial t} = \nabla \cdot (D_g \nabla c_g) + f(c_t), \quad \mathbf{x} \in \Omega \tag{4.3}$$

$$\phi_p = \Phi(c_a) \tag{4.4}$$

where the source terms are expressed as $f(\epsilon, c_a, c_t, \dots)$ and Φ represents receptor sensitivity as a function of concentration of ATP. The diffusivity terms are expressed as D_x where the subscript x refers to individual species.

In order to model the mechanical response of the underlying neuronal microstructure, a viscoelastic network consisting of three dimensional springs and dampeners have been considered. The network illustrated in Fig.4.3, capable of mimicing the extracellular matrix is similar to the work of Wang et al. (2022) who have characterised the mechanical properties of the elements constituting the network. Finally, the governing equation for the evolution of the deformation is the standard statement of the conservation of linear momentum.

$$\nabla \cdot \sigma = 0 \tag{4.5}$$

Variational Formulation

Casting the above governing equations in their variational (integral/weak) form. This formulation is used to solve these equations within a standard finite element method framework. We consider treatment of the chemical species dynamics followed by the mechanical equilibrium equations.

Find the primal concentration fields $\{c_a, c_t, c_g, \phi_p, \mathbf{u}\}$ where,

$$c_i \in \mathscr{S}_{c_i}, \quad \mathscr{S}_{c_i} = \{c_i \in \mathscr{H}^1(\Omega) \ \ | c_i = \bar{c_i} \ \ \forall \ \ \mathbf{X} \in \Gamma_g^{c_i}\} \tag{4.6}$$

where $i \in \{\text{ATP}, \text{TNF-}\alpha, \text{Glutamate}\}$ and the phase field,

$$\phi_p \in \mathscr{S}_{\phi_p}, \quad \mathscr{S}_{\phi_p} = \{\phi_p \in \mathscr{H}^1(\Omega) \ \ | \phi_p = \bar{\phi_p} \ \ \forall \ \ \mathbf{X} \in \Gamma_g^{\phi_p}\} \tag{4.7}$$

finally displacement,

$$\mathbf{u} \in \mathscr{S}_{\mathbf{u}}, \quad \mathscr{S}_{\mathbf{u}} = \{\mathbf{u} \in \mathscr{H}^1(\Omega) \ \ | \mathbf{u} = \bar{\mathbf{u}} \ \ \forall \ \ \mathbf{X} \in \Gamma_g^{\mathbf{u}}\} \tag{4.8}$$

such that for all variations,

$$w_{c_i} \in \mathscr{V}_{c_i}, \quad \mathscr{V}_{c_i} = \{w_{c_i} \in \mathscr{H}^1(\Omega) \ \ | w_{c_i} = 0 \ \ \forall \ \ \mathbf{X} \in \Gamma_g^{c_i}\} \tag{4.9}$$

$$w_{\phi_p} \in \mathscr{V}_{\phi_p}, \quad \mathscr{V}_{\phi_p} = \{w_{\phi_p} \in \mathscr{H}^1(\Omega) \ \ | w_{\phi_p} = 0 \ \ \forall \ \ \mathbf{X} \in \Gamma_g^{\phi_p}\} \tag{4.10}$$

$$w_{\mathbf{u}} \in \mathscr{V}_{\mathbf{u}}, \quad \mathscr{V}_{\mathbf{u}} = \{w_{\mathbf{u}} \in \mathscr{H}^1(\Omega) \ \ | w_{\mathbf{u}} = 0 \ \ \forall \ \ \mathbf{X} \in \Gamma_g^{\mathbf{u}}\} \tag{4.11}$$

we have,

$$\int_\Omega w_{\mathbf{u}} \sigma dV - \int_{\Gamma_h^{\mathbf{u}}} w_u \mathbf{t} dS = 0 \tag{4.12}$$

$$\int_\Omega w_{c_i} \frac{\partial c_i}{\partial t} dV + \int_\Omega (D_{c_i} \nabla w_{c_i} \nabla c_i - w_{c_i} f(c_j, \epsilon)) dV - \int_{\Gamma_h^{c_i}} w_{c_i} (\nabla c_i \cdot \mathbf{n}) dS = 0 \tag{4.13}$$

$$\int_\Omega w_{\phi_p} (\Phi(c_a) - 1.0) dV = 0 \tag{4.14}$$

where w_{c_i}, w_{ϕ_p} are the variations in chemical concentrations and phase field respectively, $w_{\mathbf{u}}$ is the variation in displacement and $i \neq j$. Ω is the

problem domain,$\{\Gamma_g^{c_i}, \Gamma_g^{\phi_p}, \Gamma_g^{\mathbf{u}}\}$ are the Dirichlet boundaries for the chemical concentration fields, phase field and displacement vector respectively. Similarly, $\Gamma_h^{c_i}$ and $\Gamma_h^{\mathbf{u}}$ are the Newmann boundaries for the chemical fields and displacment respectively and $\mathbf{n}$ is the unit normal vector. In this formulation, we assume that there are traction boundary conditions $\mathbf{t}$ for the displacement boundaries and no chemical species flux at all the boundaries ($\nabla c_i \cdot \mathbf{n} = 0$).

The mechanical and chemical properties which have been used from literature are summarized in Table 4.1.

Table 4.1: Mechanical and chemical properties

Property	**Value**	**References**
E_0	3 $\mu N/\mu m^2$	Wang et al. (2022)
E_1	1 $\mu N/\mu m^2$	Wang et al. (2022)
E_2	130 $\mu N/\mu m^2$	Wang et al. (2022)
τ_1	16 s	Wang et al. (2022)
τ_2	400 s	Wang et al. (2022)
bulk	1000 $\mu N/\mu m^2$	Konno et al. (2021)
D_a	300 $\mu m^2/s$	Bennett et al. (1995),Zhang et al. (2018)
D_t	150 $\mu m^2/s$	Ross and Pompano (2018), Goodhill (1997)
D_g	460 $\mu m^2/s$	Rusakov et al. (2011),Moussawi et al. (2011)

Multiphysics of Reaction Terms

The equations representing evolution of the chemical species are driven by source terms which depend on evolution characteristics of other chemical fields. In our formulation, we have introduced four different chemical species and a displacement variable, which are related to each other sequentially. Based on the quantitative evidence from recent literature, the functional dependence of each primary field with others have been established.

ATP

As discussed earlier, when an injury manifests, it does so by activating pannexin channels embedded in the microglia which causes excess energy molecules, ATP, to efflux. While we have established a qualitative relationship between external mechanical deformation and spatial modulation of ATP concentration, there is a lack of quantitative evidence on specific metrics which relates the two phenomena. Therefore, we propose a linear relationship between the amount of mechanical strain and strain rate obtained from the underlying constitutive framework and the amount of ATP produced subsequently. The mathematical relation between the source term in Eq.4.1 driving ATP evolution and mechanical deformation is expressed as:

$$f(\epsilon, \dot{\epsilon}) = K_1 f(\epsilon) + K_2 f(\dot{\epsilon}) \tag{4.15}$$

where K_1 and K_2 are fitting constants with units M and M-sec respectively. The functions $f(\epsilon)$ and $f(\dot{\epsilon})$ are plotted in Fig.4.4. The evolution profile is presented in Fig.4.5(A).

P2X7 Receptor

Xing et al. (2016) demonstrated a critical concentration of ATP beyond which the purinergic P2X7 receptor activates leading to increased probability of inflammasome complex formation. Based on the quantitative data provided in their experiments, a tan hyperbolic function has been used to recreate the normalised response of the receptor. We have illustrated (Fig.4.5(B)) and compared the data with our proposed function as a mathematical source term for P2X7 receptor channel properties. The specific expression used in Eq.4.4 to quantify the phase field evolution

representing the purinergic receptor is given as:

$$\Phi_p = \tanh(Af(c_a)) \tag{4.16}$$

where $A = 10^{2.25}M^{-1}$ and $f(c_a)$ varies between $10^{-8} - 10^{-1}$ M, which is considered keeping in view the typical ballpark of ATP produced during pathological conditions.

TNF-α

Upon P2X7 receptor activation, a cascade of events unfolds, of which the pivotal step involves release of pro-inflammatory molecules namely TNF-α. Based on the work of Barberà-Cremades et al. (2017), a relationship between amount of this cytokine release upon P2X7 receptor activation over time has been shown. We compare the experimental findings with another tanh function tailored to incorporate contribution of the purinergic receptor as illustrated in Fig.4.5(B). In this comparison, TNF-α accumulates as a function of time and saturates at a certain concentration. We propose a mathematical model which formulates a source term, as mentioned in Eq.4.2 by associating the P2X7 receptor based on the experimental findings and spatio-temporally resolving the maximum limits of this chemical species.

$$f(c_a, \phi_p) = B\phi_p \tag{4.17}$$

where $B = 0.1$ and a critical concentration of ATP (c_a) is considered as a trigger for TNF-α evolution. The reaction profile is shown in Fig.4.5(C).

Glutamate

Once the concentration of TNF-α increases, glutamate uptake by nearby astrocytes decreases and post synaptic presence increases. This leads to

excitotoxicity of the primary neurotransmitter. We have identified a study by Zou and Crews (2005) which presents some evidence of glutamate uptake reduction due to increase in cytokine concentration. Since there is no explicit data measuring excitotoxicity, we have hypothesized a metric which states that the reduction in uptake is inversely proportional to the increase in extracellular glutamate concentration. Using this principle we have quantified the increase in glutamate as a function of TNF-α. The specific mathematical form representing the source term for Eq.4.3 is expressed as:

$$f(c_t) = Cc_t \tag{4.18}$$

where $C = 100M^{-1}$ and is a fitting parameter. The reaction profile is highlighted in Fig.4.5(D).

4.4 Results

Outline of BVPs

We proceed onto numerically implementing the multiphysics based variational formulation in a standard FE setting in two dimensions. In order to achieve visualisation of the chemical species' evolution firstly we need to geometrically allocate regions within the given domain. These localised domains will signify neurons, microglia and the ECM and will correspond to presence of specific chemical fields in those regions. In order to construct a geometry which resembles a neuron-microglia-ECM assembly at single and multi-neuron length scale we subdivide a given domain into realistic shapes highlighted by the Gaussian point. This approach allow spatio-temporal visualisation of chemical species' diffusion and interaction with the underlying mechanics in a realistic morphological setting, as observed in biological systems. Furthermore, simulation of

boundary value problems enables a wide class of kinematics/mechanics driven mechano-chemical phenomena to be analysed.

Single neuron-microglia-ECM morphology

We have illustrated a morphological representation of single neuron-glia-ECM assembly (Fig.4.6). This consists of neuron synapses indicated by red, padded on both sides by microglia painted in green. The microglia is a pivotal region in numerical simulations, as it facilitates release of ATP to the ECM, houses the P2X7 receptor and modulates channel sensitivity and finally enables production of inflammatory cytokines. All the above mentioned chemical fields are spatially localised in the microglial region and the numerical framework allows diffusion across the ECM. For a single neuron-glia-ECM assembly we observe the effects of various mechanical loading conditions on this domain through evolution of the underlying chemical and mechanical fields. Upon tensile loading, the biomarkers represented by chemical fields diffuse across the illustrated domain.

Multiple neuron-microglia-ECM geometry

In a more realistic setting, the length scale of the domain is increased to accommodate more number of neuron-glia-ECM assemblies which illustrate a better representation of neuron clusters (Fig.4.7). As we observe from this construction, more assemblies have been added at random orientations each having the characteristic spatial localisation as mentioned in the single neuron setup. For simplicity we have considered all neuron assemblies of the same type, meaning, the chemical and mechanical properties are the same for all assembly configurations. Primarily, this improvised structure allows us to visualise the spatio-temporal heterogeneity of chemical field evolution and capture essential chemical and mechanical injury metrics across the domain. Similar to the previous setup, we perform different BVPs on this domain and observe field evolution characteristics.

Simulations

For single and multiple neuron-microglia-ECM assembly, we demonstrate key results based on unaxial tension numerical simulations. For single assembly, as shown in Fig.4.8(A), the domain is fixed at one end and a displacement-type load is applied across a spectrum of strain and strain-values. In this simulation we highlight results obtained at a strain rate of $10^2 s^{-1}$ upto 80% strain. A fundamental metric of deformation based loading problems is strain; accordingly the axial strain field (ϵ_{11}), obtained from the underlying mechanical network is plotted for the domain as given in Fig.4.8(B). Using a combination of strain and strain-rates, an array of results are presented in Fig.4.8(C). The strain field induces ATP to release from the microglia to the ECM. From left to right, field characteristics for ATP due to the above mentioned strain field is shown. As observed, ATP diffuses out of the microglia into the ECM demonstrating the heterogeneous nature of field distribution. The following sub-figure shows P2X7 characteristics which is operating at maximum potential as the critical concentration of ATP, needed to trigger the receptor, has already reached. To its right, TNF-α field plot is shown, which depends on P2X7 receptor opening probability and diffuses out of the microglia. The final sub-plot highlights glutamate concentration due to the influence of TNF-α. The neurotransmitter is localised at the synaptic region and diffuses into the ECM. While Fig.4.8(C) demonstrates full field profiles for each chemical entity, Fig.4.8(D) illustrates field evolution characteristics for increasing strain-rates from 10^{-3} up to 10^3 keeping the maximum strain fixed at 0.8 for each simulation. The following sub-plots (left to right) describe the nature of evolution of ATP (near the microglia), P2X7 (within the microglia), TNF-α (near the microglia) and Glutamate (near the synapse). The particular strain and strain-rate combination used for the full field plots has been highlighted by an arrow in each sub-plot. The maximum magnitude of the chemical species' concentrations are comparable with

pathological estimates and presented in Table.4.2.

A key highlight of the spatio-temporal resolution of these chemical fields is the construction of an injury curve. Considering maximum ATP concentration across the spatial domain at specific strain and strain-rates a dataset is established. The data set is plotted against strain vs strain-rate as illustrated in Fig.4.9 and allows visual representation of field values at specific loading conditions. A cutoff for critical extracellular ATP is chosen based on the concentration at which purinergic receptors (P2X7) activate Browne (2013), which is about $6e-3$ mM Xing et al. (2016). The proposition is, if the maximum concentration of ATP stays above this number, the neuronal micro environment is susceptible to chemical degradation, which is also how we define chemical injury. Using this metric, two regions are shown representing pathway induced injury (red boxes) and uninjured region (green boxes). It is a first order estimation of how mechanical loading conditions can influence downstream pathways and elevate critical molecular concentrations.

Unaxial tensile loading numerical simulations using rate-dependent loading are performed for multi-neuron assemblies. Using variable orientations for individual single neuron-microglia structures, a neuron cluster is constructed and a boundary value problem is setup as illustrated in Fig.4.10(A). We have chosen two essential field variables namely ATP (Fig.4.10(B)) and glutamate (Fig.4.10(C)) to demonstrate the heterogeneity and interactions within this assembly. The results consisting of these field profiles are generated using a strain rate of $10^2 s^{-1}$, applied up to a strain of 0.4.

A heterogeneous distribution of micro-glia and neurons has been presented in Fig.4.11. In this example the number of neuron synapses are reduced and a more dense population of micro-glia has been shown. The figure illustrates ATP release from the micro-glia throughout the ECM upon mechanical deformation.

Table 4.2: Comparison of chemical concentrations

Species	Pathological estimate	Numerical results
ATP	1e-2 M (Xing et al. (2016))	7e-2 M
P2X7	0 - 1 (Xing et al. (2016))	0 - 1
TNF-α	2.4 mM (Mogi et al. (1994))	1.8 mM
Glutamate	1-2 μM (Mark et al. (2001))	0.5 μM

4.5 Conclusion

We have proposed and quantified an injury based pathway beginning with mechanical deformation and culminating in necroptosis. The proposed pathway based model incorporates a finite element PDE oriented multiphysics formulation for investigating mechano-chemical interactions during TBI at the cellular scale. The fidelity of our numerical modeling framework involves a first-of-its-kind representation of neuronal microenvironment as a viscoelastic network coupled with an ensemble of molecular biomarkers represented as chemical fields. Using our modeling framework, we have demonstrated field behaviour for single neuron-glia assembly along with neuron-glia clusters highlighting localisation of biomarkers. Our results agree closely with clinical estimates of molecular concentrations during pathological conditions.

We believe that the idea of a mechano-chemical framework utilised to capture pathway induced injury opens up avenues of research directions in injury specific biomarker identification. Although our modeling approach relies on limited availability of biomarker datasets, experimental quantification for injury metrics in human subjects and generic assumptions on field evolution characteristics, it provides a robust numerical and computational base for further improvements. Additionally, our model is capable of incorporating additional biophysics at the neuronal scale including ionic conduction Gulati and Rudraraju (2023), nutrient transport and inter-neuronal interactions which possess immense potential in

understanding crucial neurodegenerative disorders.

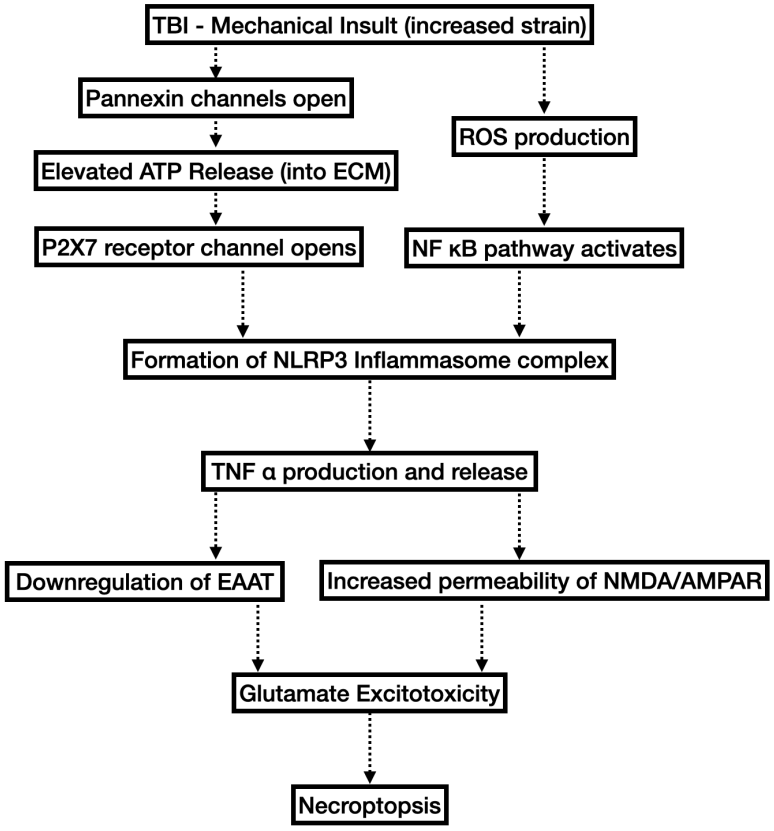

Figure 4.1: Proposed pathway of necroptosis underlying secondary injury during TBI. The pathway begins with mechanical deformation manifested as increased strain to the brain, which triggers opening of the pannexin channels leading to massive ATP efflux into the extracellular region. Increased ATP causes purinergic receptors to activate, particularly the P2X7R, which causes potassium efflux from the intra- to extracellular milieu. Decrease in ionic concentration of potassium initiates formation of the NLRP3 inflammasome complex. Simultaneously there is a heightened increase in the demand for oxygen causing oxidative stress and production of reactive oxygen species. This causes the NFκB pathway to trigger, also leading to intracellular formation of the NLRP3 inflammasome complex. This complex is responsible for modulating formation of pro-inflammatory products mainly cytokines such as TNF-α and ILs. TNF-α causes dysregulation in neuronal signalling by blocking EAAT's on astrocytes thereby reducing glutamate uptake. It also intensifies excitatory transmission by increasing permeability of the glutamate receptors to calcium ions. Increased glutamate concentration in the post synaptic region causes excitotoxicity and is considered as the pivotal step towards necroptosis.

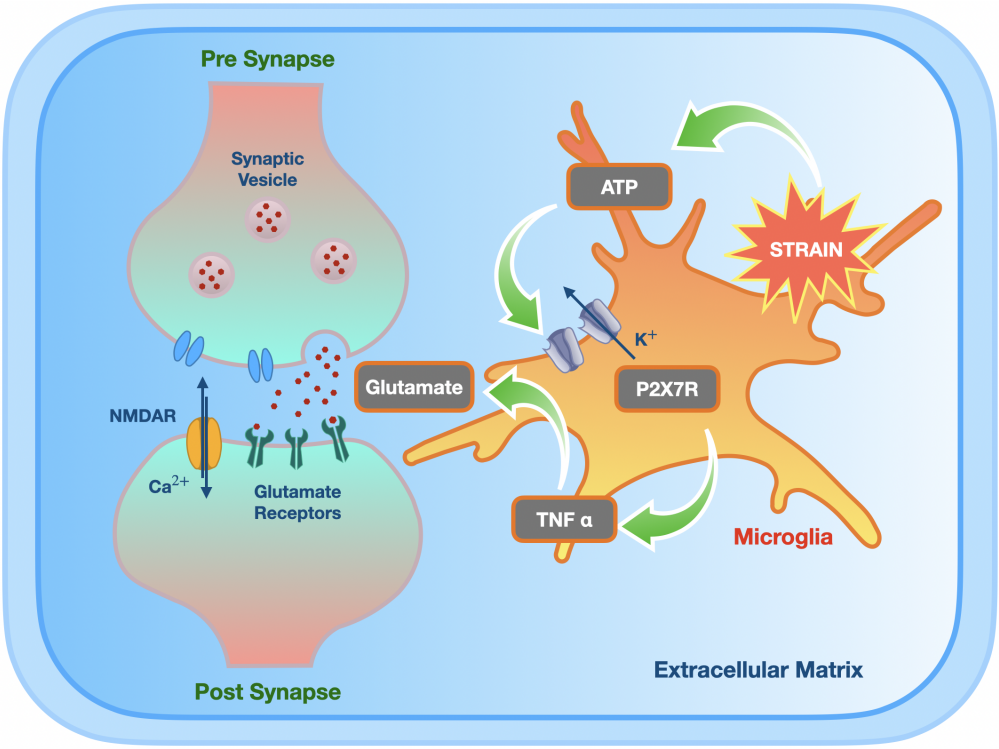

Figure 4.2: Representation of a reduced pathway consisting of quantifiable elements which contribute towards necroptosis. Illustrated in this pathway are ATP, TNF-α and glutamate classified as chemical concentration fields and the P2X7 receptor mathematically as a phase field. This is attributed qualitatively to the opening probability of the channel upon prolonged activation by ATP. The shortened pathway enables formulation of diffusive equations to spatio-temporally resolve the chemical species across the inhomogenous neuronal landscape.

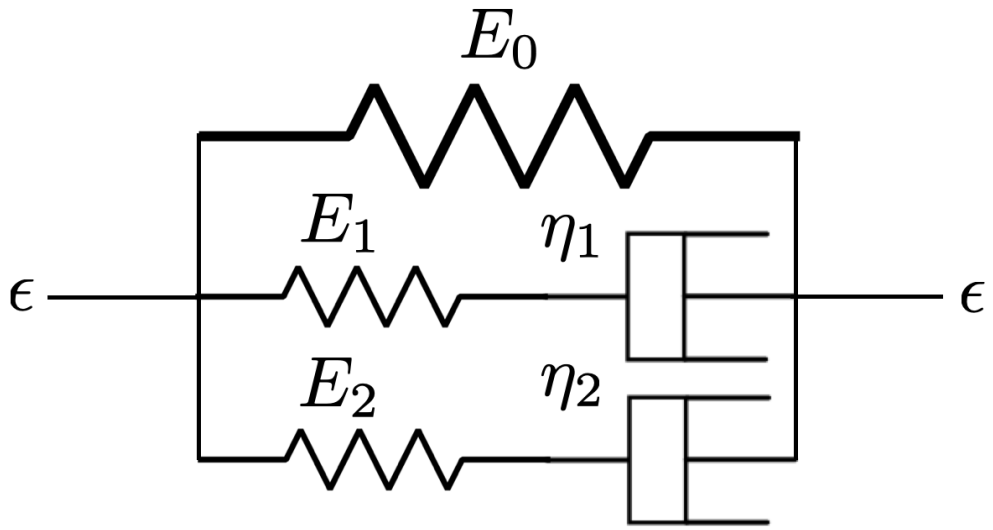

Figure 4.3: Mechanical network representing the neuronal microenvironment. The mechanical estimates of springs and dampeners are obtained from Wang et al. (2022)

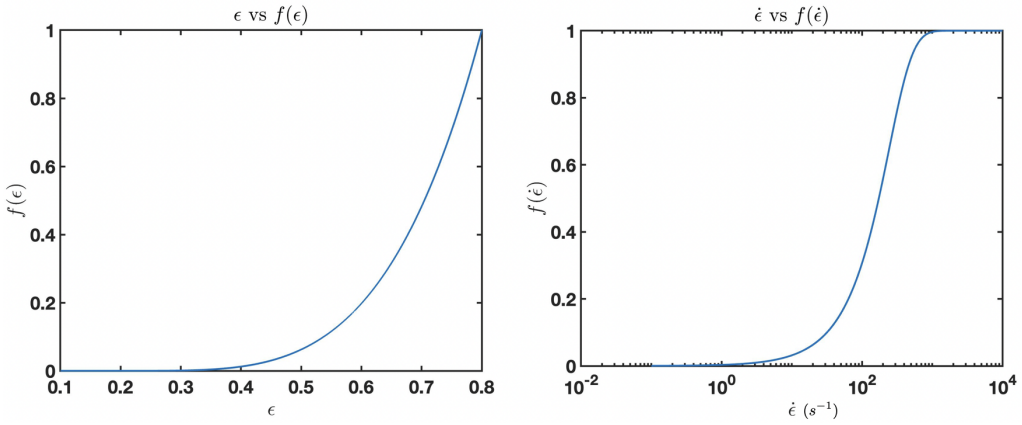

Figure 4.4: (Left) Dependence of f(ϵ) with ϵ. (Right) Dependence of f(ė) with ė.

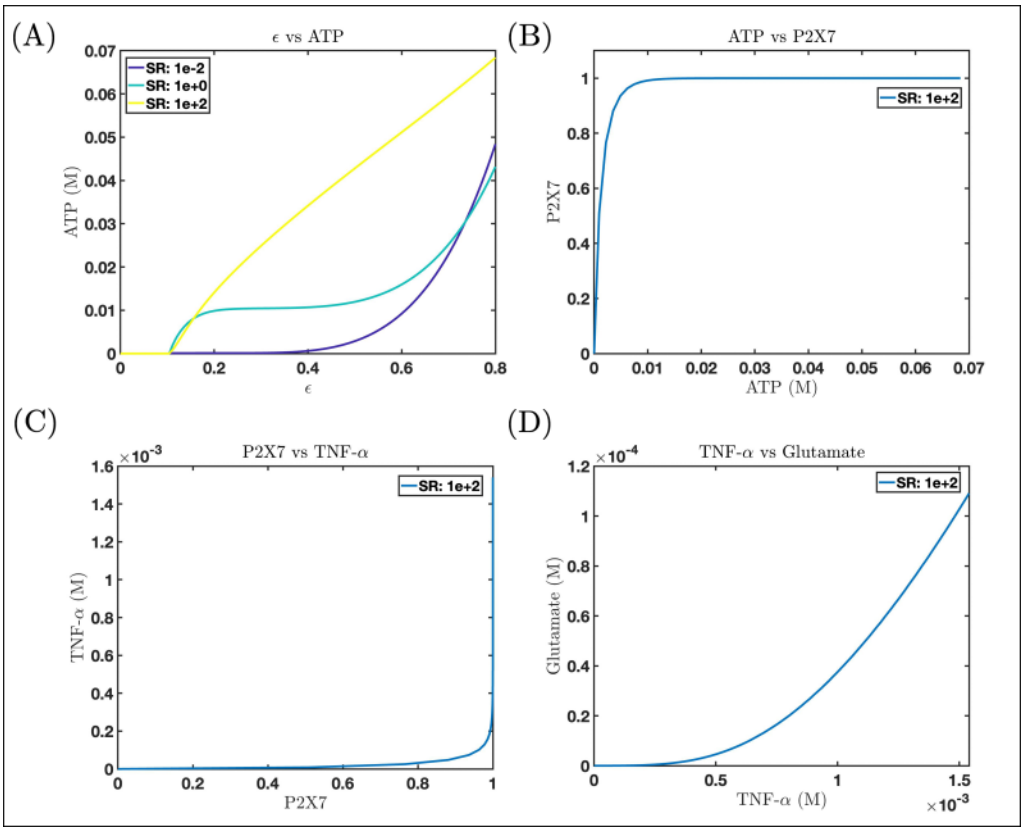

Figure 4.5: (**A**) ATP evolution against increasing strain (upto 80 percent) has been shown here with different strain rates. In particular, the strain rate $10^2 s^{-1}$ has been chosen to further illustrate correlations between the chemical fields. (**B**) P2X7 receptor opening probability is plotted against ATP evolution for the aforementioned strain rate. Furthermore, this data suggests a positive agreement with the findings of Xing et al. (2016) for estimating P2X7 receptor probability with change in ATP. (**C**) TNF-α evolution with change in receptor opening characteristics has been demonstrated in this plot. It is observed that at a relatively higher value of P2X7, TNF-α diffuses out and continues evolving with time. (**D**) Glutamate excitotoxicity in the extracellular region, influenced by increased presence of inflammatory cytokines like TNF-α can be observed in this plot. These results are compared with the findings of Zou et al. Zou and Crews (2005) and show significant resemblance in the nature of glutamate evolution.

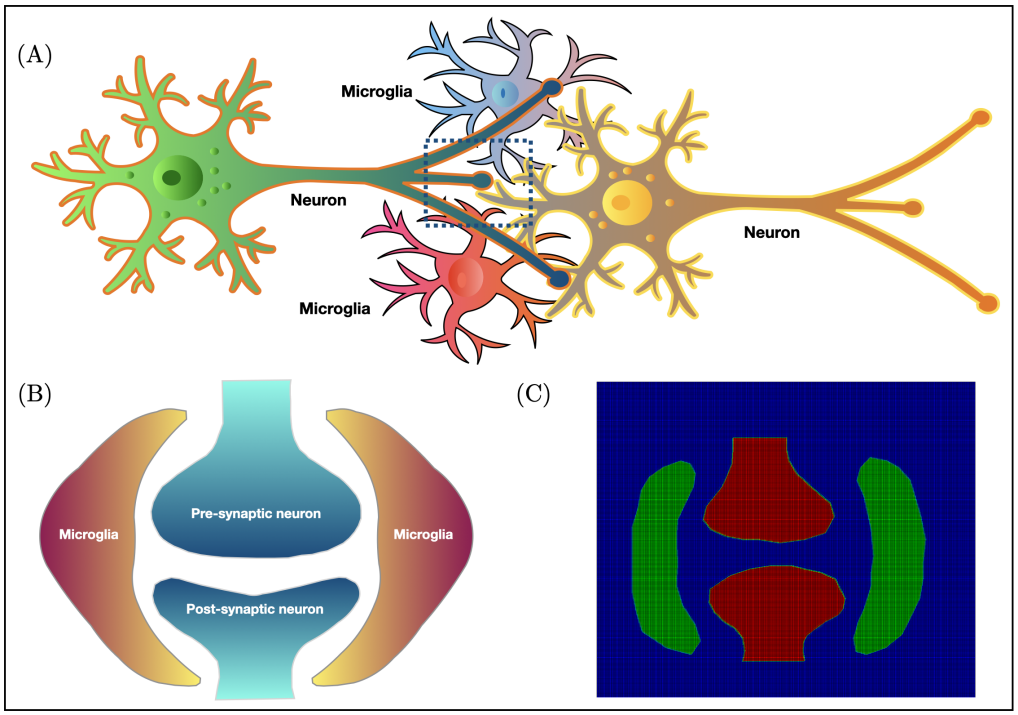

Figure 4.6: The design of the computational domain has been adapted from a realistic representation of the neurons and the surrounding microglia. As illustrated in (**A**) a specific region consisting of neuron synapses and microglia has been considered which has been magnified in (**B**). A schematic of pre-synaptic and post-synaptic neurons are shown flanged on both sides by microglia. This design has been incorporated as our computational domain (**C**) to facilitate localisation of chemical fields, visualization of diffusive behaviour of fields and understand interactions between these species at different length and time scales. A meshed version of the numerical domain has been shown with colors (green: microglia,blue: ECM,red: synapse) indicating distinct regions of interest.

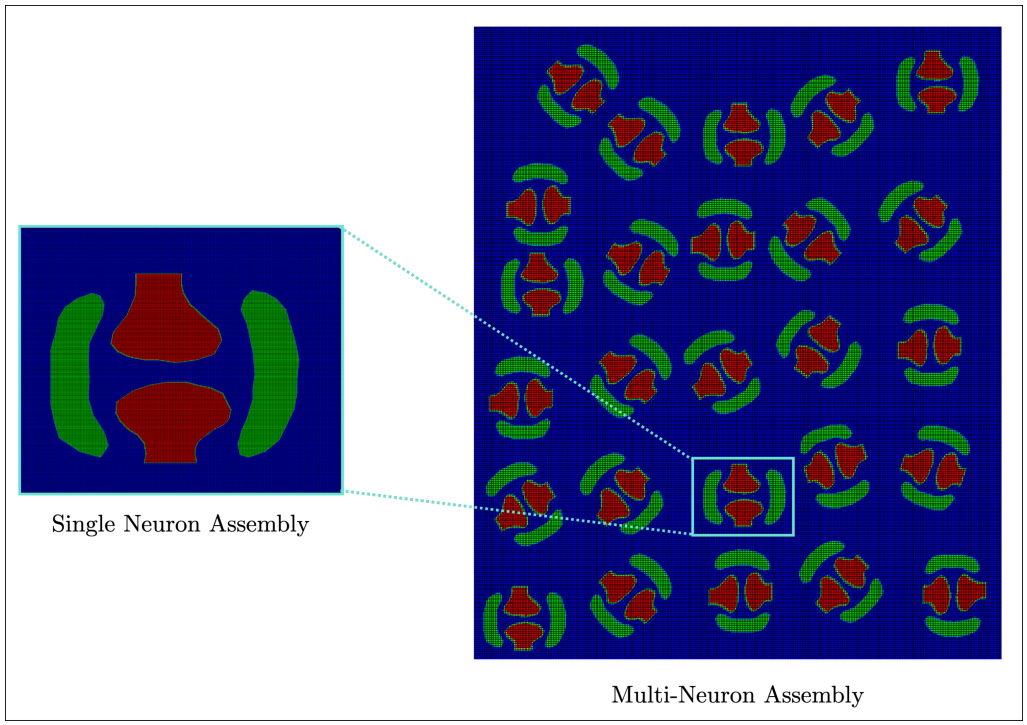

Figure 4.7: Illustration of a meshed neuron cluster domain (single neuron assembly) in a random spatial distribution of single neuron-microglia assemblies at different orientations (multi-neuron assembly). The dimensions of the single neuron domain are 12μm X 10μm and that of the larger domain are 60μm X 72μm

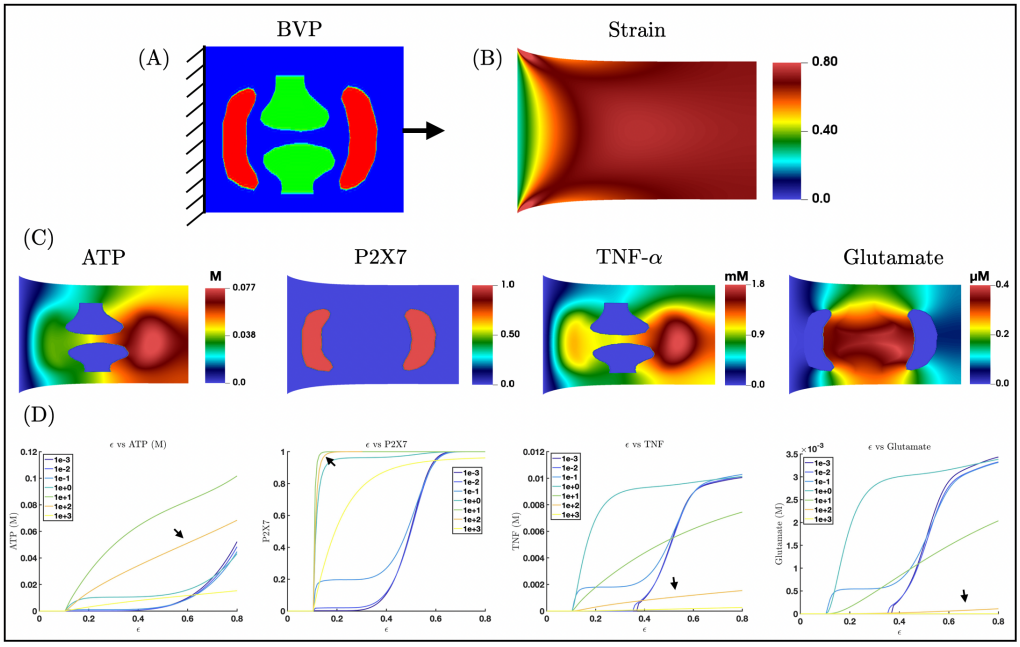

Figure 4.8: **(A)** Boundary value problem demonstrating simple tension on a computational domain represented by neuron synapse (green), microglia (red) and ECM (blue). The domain is fixed at one end, while the other end is displaced through a combination of strain and strain-rate loading conditions. **(B)** Uniaxial strain (ϵ_{11}) field profile obtained from the underlying viscoelastic network by applying displacement through a strain rate of $10^2 s^{-1}$ upto a strain of 0.8. **(C)** Chemical field evolution profiles representing (left to right) ATP (originating from microglia), P2X7 (localized in microglia), TNF-α (originating from microglia) and Glutamate (originating from neuron synapses). **(D)** Field evolution plots against a strain of 0.8 has been illustrated for increasing strain rates spanning over six orders of magnitude (10^{-3} - 10^3). The strain rate measure for which the field plots are highlighted is indicated in each subplot and mentioned accordingly.

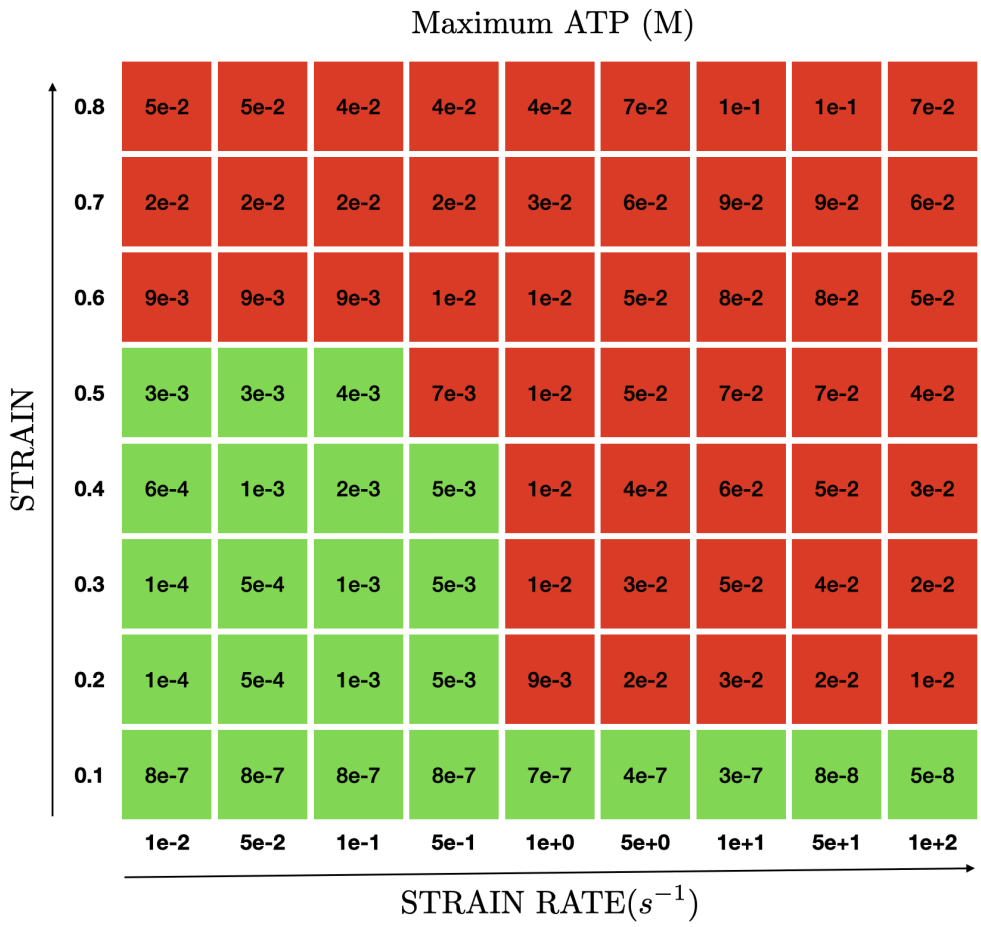

Figure 4.9: Maximum concentration of ATP within the field distribution is recorded for a spectrum of strain and strain-rates. The resulting data set obtained is utilised to construct a computational injury curve. Using a specific cut-off for ATP concentration $(6e-3M)$ two regions are obtained. The red one represents pathway induced injury while the green one reflects uninjured regimes.

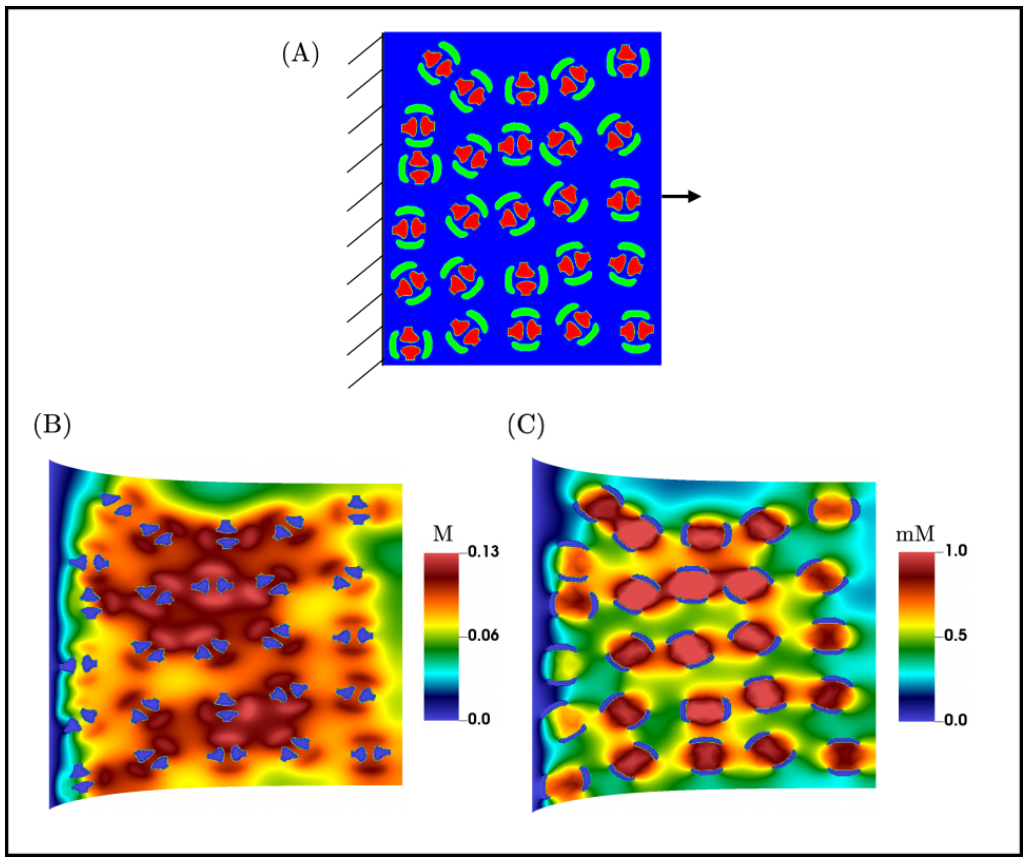

Figure 4.10: (**A**) Boundary value problem of multi neuron-microglia-ECM assembly is shown. Similar to the single neuron assembly, the larger domain is fixed at one end and displacement based loading is applied at the other end as indicated. (**B**) ATP evolution for multiple assemblies are shown as induced by the underlying strain field. The heterogeneous nature of field evolution is a hallmark characteristic for such larger domains and can be spatio-temporally resolved to better understand neuron-cluster based experiments. (**C**) Glutamate evolution is highlighted which is localised near the neuron synapses. Cluster based spatio-temporal resolution of chemical fields such as glutamate serve as key indicators in excitoxicity prediction.

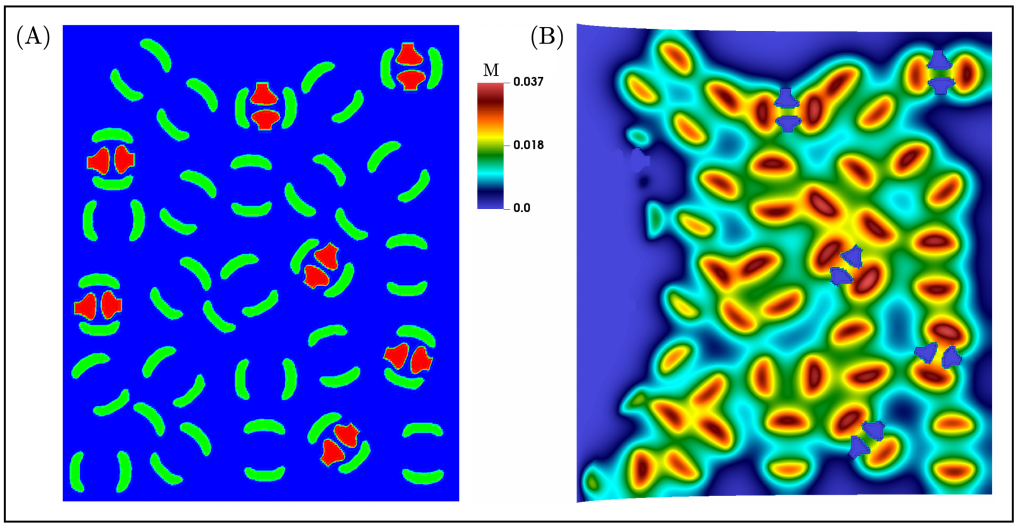

Figure 4.11: (**A**) Phase field demarcation of a heterogeneous distribution indicating neuronal synapse and microglia (**B**) ATP evolution for multiple assemblies are shown as induced by the underlying strain field.

5 CONCLUSION

In this dissertation, we have demonstrated three different biophysics problems which are computationally modeled using robust numerical frameworks. Although a significant volume of the thesis is dedicated to understanding neuronal scale behaviour upon mechanical loading, we have also described the structural and functional modifications which membranes undergo during biophysical processes. **Chapter 2** begins with a mathematical framework for modeling biological membranes using Kirchhoff Love thin shell kinematics. Using state-of-the-art modeling techniques we have been able to demonstrate two classical biomembrane problems: formation of tubular shapes in biomembranes and Piezo1-induced membrane footprint generation. For each of these problems we are able to validate against results and experimental observations for the simpler deformation modes, and also predict the complex deformation profiles that are not accessible by traditional analytical and numerical methods. The key highlight of our work is the prediction of complex, three dimensional deformation profiles in biomembranes which often lead to reduction in the load and energy barriers to membrane deformation, and reveals numerically unexplored deformation profiles and membrane morphologies.

In **Chapter 3** we investigate into the neuronal microenvironment and characterize neurons and neuronal clusters. In a first of its kind representation the neurons have been spatially localised into CSK, ECM and membrane each having its characteristic viscoelastic network. These networks are constructed based on physiological and experimental observations of proteins which contribute towards the structural integrity of those regions. For single neuron simulations we have demonstrated distribution of mechanical loads for individual proteins within each spatial region. The advantage of resolving cellular scale metrics into a sub-cellular scale reveals insights into vulnerability of proteins to damage or degradation. We

have also extended the single neuron description into a multi-neuron cluster numerical domain, which enables visualization of the spatio-temporal evolution of essential field variables relevant to injury. Our computational framework is able to capture protein specific information for tissue-scale rate dependent loading, often used in injury assessment and diagnoses.

We improvise our understanding of the mechanical basis of injury in the previous chapter by expanding our generalisation of the pathological degradation to incorporate chemical fields in addition to mechanical fields. In this mechano-chemical framework established in **Chapter 4** we consider the biochemical pathways which trigger due to induced deformation within the neuronal microenvironment. Characterising these pathways often involve macromolecules, neurotransmitters and inflammasomes which operate in tandem towards necrosis. In our study we identify a potential chemical pathway, supported by biophysical arguments, which potentially leads to necroptosis. Within this pathway we have quantified a couple of biomarkers as chemical fields and constructed a numerical framework taking into account neurons, microglia and ECM. Using spatial localisation, we have demonstrated spatio-temporal evolution of these biomarkers upon strain and strain-rate based loading. Our results have been incorporated into an injury map which reveals a kinematic spectrum of injury probability based on chemical concentrations of certain biomarkers. Our numerical framework also extends towards multi neuron-glia-ECM assembly and illustrates realistic evolution of chemical fields. In a first of its kind study our mechano-chemical model demonstrates a chemical basis of injury based on concentration thresholds of critical biomarkers. We believe that this model can be extended to include additional relevant chemical and mechanical fields backed by literature and experimental observations which can enrich injury detection and diagnoses.

REFERENCES

2021. Code repository for kirchhoff-love shell kinematics and applications to mechanics of biological membranes. https://github.com/cmmg/biologicalMembraneMechanics.

2024. Code repository for spatio temporal modeling of biomarkers to demonstrate mechano-chemical interactions during tbi. https://github.com/cmmg/mechanoChemistry.

Abhyankar, Shrirang, Jed Brown, Emil M Constantinescu, Debojyoti Ghosh, Barry F Smith, and Hong Zhang. 2018. Petsc/ts: A modern scalable ode/dae solver library. *arXiv preprint arXiv:1806.01437*.

Ahmadzadeh, Hossein, Douglas H Smith, and Vivek B Shenoy. 2014. Viscoelasticity of tau proteins leads to strain rate-dependent breaking of microtubules during axonal stretch injury: predictions from a mathematical model. *Biophysical journal* 106(5):1123–1133.

Akamatsu, Yosuke, and Khalid A Hanafy. 2020. Cell death and recovery in traumatic brain injury. *Neurotherapeutics* 17:446–456.

Albalawi, Farraj, Wennan Lu, Jonathan M Beckel, Jason C Lim, Stuart A McCaughey, and Claire H Mitchell. 2017. The p2x7 receptor primes il-1β and the nlrp3 inflammasome in astrocytes exposed to mechanical strain. *Frontiers in cellular neuroscience* 11:227.

Alexander, Michael P. 1995. Mild traumatic brain injury: pathophysiology, natural history, and clinical management. *Neurology*.

Alimohamadi, Haleh, Ritvik Vasan, Julian E Hassinger, Jeanne C Stachowiak, and Padmini Rangamani. 2018. The role of traction in membrane curvature generation. *Molecular biology of the cell* 29(16):2024–2035.

André, Véronique M, Carlos Cepeda, and Michael S Levine. 2010. Dopamine and glutamate in huntington's disease: A balancing act. *CNS neuroscience & therapeutics* 16(3):163–178.

Andrejew, Roberta, Ágatha Oliveira-Giacomelli, Deidiane Elisa Ribeiro, Talita Glaser, Vanessa Fernandes Arnaud-Sampaio, Claudiana Lameu, and Henning Ulrich. 2020. The p2x7 receptor: central hub of brain diseases. *Frontiers in Molecular Neuroscience* 13:124.

Armada-Moreira, Adam, Joana I Gomes, Carolina Campos Pina, Oksana K Savchak, Joana Gonçalves-Ribeiro, Nádia Rei, Sara Pinto, Tatiana P Morais, Robertta Silva Martins, Filipa F Ribeiro, et al. 2020. Going the extra (synaptic) mile: excitotoxicity as the road toward neurodegenerative diseases. *Frontiers in cellular neuroscience* 14:90.

Arndt, Daniel, Wolfgang Bangerth, Marco Feder, Marc Fehling, Rene Gassmöller, Timo Heister, Luca Heltai, Martin Kronbichler, Matthias Maier, Peter Munch, Jean-Paul Pelteret, Simon Sticko, Bruno Turcksin, and David Wells. 2022. The `deal.II` library, version 9.4. *Journal of Numerical Mathematics* 30(3):231–246.

Arnold, Douglas N, Franco Brezzi, and L Donatella Marini. 2005. A family of discontinuous galerkin finite elements for the reissner–mindlin plate. *Journal of Scientific Computing* 22(1-3):25–45.

Arrazola, Macarena S, et al. 2019. Compartmentalized necroptosis activation in excitotoxicity-induced axonal degeneration: a novel mechanism implicated in neurodegenerative disease pathology. *Neural Regeneration Research* 14(8):1385–1386.

Arroyo, Marino, and Antonio DeSimone. 2009. Relaxation dynamics of fluid membranes. *Physical Review E* 79(3):031915.

Azzuni, Eyas, and Sukru Guzey. 2018. A perturbation approach on buckling and postbuckling of circular rings under nonuniform loads. *International Journal of Mechanical Sciences* 137:86 – 95.

Bahrami, Amir Houshang, and Gerhard Hummer. 2017. Formation and stability of lipid membrane nanotubes. *ACS Nano* 11(9):9558–9565.

Bao, Li, Silviu Locovei, and Gerhard Dahl. 2004. Pannexin membrane channels are mechanosensitive conduits for atp. *FEBS letters* 572(1-3): 65–68.

Bar-Kochba, Eyal, Mark T Scimone, Jonathan B Estrada, and Christian Franck. 2016. Strain and rate-dependent neuronal injury in a 3d in vitro compression model of traumatic brain injury. *Scientific reports* 6(1):1–11.

Barberà-Cremades, Maria, Ana I Gómez, Alberto Baroja-Mazo, Laura Martínez-Alarcón, Carlos M Martínez, Carlos de Torre-Minguela, and Pablo Pelegrín. 2017. P2x7 receptor induces tumor necrosis factor-α converting enzyme activation and release to boost tnf-α production. *Frontiers in immunology* 8:862.

Başar, Yavuz, and Yunhe Ding. 1990. Finite-rotation elements for the non-linear analysis of thin shell structures. *International Journal of Solids and Structures* 26(1):83–97.

Bazilevs, Yuri, L Beirao da Veiga, J Austin Cottrell, Thomas JR Hughes, and Giancarlo Sangalli. 2006. Isogeometric analysis: approximation, stability and error estimates for h-refined meshes. *Mathematical Models and Methods in Applied Sciences* 16(07):1031–1090.

Bennett, MR, L Farnell, WG Gibson, and S Karunanithi. 1995. Quantal transmission at purinergic junctions: stochastic interaction between atp and its receptors. *Biophysical journal* 68(3):925–935.

Blevins, Hallie M, Yiming Xu, Savannah Biby, and Shijun Zhang. 2022. The nlrp3 inflammasome pathway: a review of mechanisms and inhibitors for the treatment of inflammatory diseases. *Frontiers in aging neuroscience* 14:879021.

Boye, Theresa Louise, Kenji Maeda, Weria Pezeshkian, Stine Lauritzen Sønder, Swantje Christin Haeger, Volker Gerke, Adam Cohen Simonsen, and Jesper Nylandsted. 2017. Annexin a4 and a6 induce membrane curvature and constriction during cell membrane repair. *Nature communications* 8(1):1–11.

Božič, B, V Heinrich, S Svetina, and B Žekš. 2001. Shapes of nearly cylindrical, axisymmetric bilayer membranes. *The European Physical Journal E* 6(1):91–98.

Braun, Nicholas J, Katherine R Yao, Patrick W Alford, and Dezhi Liao. 2020. Mechanical injuries of neurons induce tau mislocalization to dendritic spines and tau-dependent synaptic dysfunction. *Proceedings of the National Academy of Sciences* 117(46):29069–29079.

Brenner, Lisa A, Lisa M Betthauser, Beeta Y Homaifar, Edgar Villarreal, Jeri EF Harwood, Pamela J Staves, and Joseph A Huggins. 2011. Posttraumatic stress disorder, traumatic brain injury, and suicide attempt history among veterans receiving mental health services. *Suicide and Life-Threatening Behavior* 41(4):416–423.

Brenner, Susanne, and Ridgway Scott. 2007. *The mathematical theory of finite element methods*, vol. 15. Springer Science & Business Media.

Brojan, Miha, A Puksic, and Franc Kosel. 2007. Buckling and postbuckling of a nonlinearly elastic column. *ZAMM-Journal of Applied Mathematics and Mechanics/Zeitschrift für Angewandte Mathematik und Mechanik: Applied Mathematics and Mechanics* 87(7):518–527.

Browne, Susan E. 2013. When too much atp is a bad thing: a pivotal role for p2x7 receptors in motor neuron degeneration.

Calovi, Stefano, Paula Mut-Arbona, and Beáta Sperlágh. 2019. Microglia and the purinergic signaling system. *Neuroscience* 405:137–147.

Cauwels, Anje, Elke Rogge, Benjamin Vandendriessche, S Shiva, and Peter Brouckaert. 2014. Extracellular atp drives systemic inflammation, tissue damage and mortality. *Cell death & disease* 5(3):e1102–e1102.

Choi, Ji-in Vivien, Boriana K Tchernookova, Wasan Kumar, Lech Kiedrowski, Calla Goeke, Marina Guizzetti, John Larson, Matthew A Kreitzer, and Robert Paul Malchow. 2021. Extracellular atp-induced alterations in extracellular h+ fluxes from cultured cortical and hippocampal astrocytes. *Frontiers in Cellular Neuroscience* 15:640217.

Choi, Yong-Seok, and Sang-Joon Lee. 2009. Three-dimensional volumetric measurement of red blood cell motion using digital holographic microscopy. *Applied optics* 48(16):2983–2990.

Ciarlet, Philippe G. 2002. *The finite element method for elliptic problems*. SIAM.

Cocucci, Emanuele, François Aguet, Steeve Boulant, and Tom Kirchhausen. 2012. The first five seconds in the life of a clathrin-coated pit. *Cell* 150(3):495–507.

Cottrell, J. Austin, Thomas J. R. Hughes, and Yuri Bazilevs. 2009. *Isogeometric Analysis*. John Wiley & Sons, Ltd.

Cruz, Cristiane M, Alessandra Rinna, Henry Jay Forman, Ana LM Ventura, Pedro M Persechini, and David M Ojcius. 2007. Atp activates a reactive oxygen species-dependent oxidative stress response and secretion of proinflammatory cytokines in macrophages. *Journal of Biological Chemistry* 282(5):2871–2879.

Dalcin, Lisandro, Nathaniel Collier, Philippe Vignal, AMA Côrtes, and Victor M Calo. 2016. Petiga: A framework for high-performance isogeometric analysis. *Computer Methods in Applied Mechanics and Engineering* 308:151–181.

Deng, Shikai, and Vikas Berry. 2016. Wrinkled, rippled and crumpled graphene: an overview of formation mechanism, electronic properties, and applications. *Materials Today* 19(4):197 – 212.

Derényi, Imre, Frank Jülicher, and Jacques Prost. 2002. Formation and interaction of membrane tubes. *Physical review letters* 88(23):238101.

Dhuriya, Yogesh K, and Divakar Sharma. 2018. Necroptosis: a regulated inflammatory mode of cell death. *Journal of neuroinflammation* 15(1):1–9.

Dubey, Sushil, Nishita Bhembre, Shivani Bodas, Sukh Veer, Aurnab Ghose, Andrew Callan-Jones, and Pramod Pullarkat. 2020. The axonal actin-spectrin lattice acts as a tension buffering shock absorber. *Elife* 9: e51772.

Dupire, Jules, Marius Socol, and Annie Viallat. 2012. Full dynamics of a red blood cell in shear flow. *Proceedings of the National Academy of Sciences* 109(51):20808–20813.

Evans, EA, and R Skalak. 1979. Mechanics and thermodynamics of biomembranes: part 1. *CRC critical reviews in bioengineering* 3(3):181–330.

Faul, M, L Xu, MM Wald, V Coronado, and Ann M Dellinger. 2010. Traumatic brain injury in the united states: national estimates of prevalence and incidence, 2002–2006. *Injury Prevention* 16(Suppl 1):A268–A268.

Fesharaki-Zadeh, Arman. 2022. Oxidative stress in traumatic brain injury. *International Journal of Molecular Sciences* 23(21):13000.

Fink, Susan L, and Brad T Cookson. 2005. Apoptosis, pyroptosis, and necrosis: mechanistic description of dead and dying eukaryotic cells. *Infection and immunity* 73(4):1907–1916.

Florence, Gerson, Tiago Pereira, and Jürgen Kurths. 2012. Extracellular potassium dynamics in the hyperexcitable state of the neuronal ictal activity. *Communications in Nonlinear Science and Numerical Simulation* 17(12):4700–4706.

Francisco, Ngiambudulu M, Nai-Jen Hsu, Roanne Keeton, Philippa Randall, Boipelo Sebesho, Nasiema Allie, Dhirendra Govender, Valerie Quesniaux, Bernhard Ryffel, Lauriston Kellaway, et al. 2015. Tnf-dependent regulation and activation of innate immune cells are essential for host protection against cerebral tuberculosis. *Journal of neuroinflammation* 12(1): 1–14.

Gennarelli, Thomas A, Lawrence E Thibault, and David I Graham. 1998. Diffuse axonal injury: an important form of traumatic brain damage. *The Neuroscientist* 4(3):202–215.

Georges, Alan, et al. 2017. Traumatic brain injury.

Goodhill, Geoffrey J. 1997. Diffusion in axon guidance. *European Journal of Neuroscience* 9(7):1414–1421.

Gottlieb, Philip A, Chilman Bae, and Frederick Sachs. 2012. Gating the mechanical channel piezo1: a comparison between whole-cell and patch recording. *Channels* 6(4):282–289.

Graham, Neil SN, Karl A Zimmerman, Federico Moro, Amanda Heslegrave, Samia Abed Maillard, Adriano Bernini, John-Paul Miroz, Cornelius K Donat, Maria Yanez Lopez, Niall Bourke, et al. 2021. Axonal marker neurofilament light predicts long-term outcomes and progres-

sive neurodegeneration after traumatic brain injury. *Science translational medicine* 13(613):eabg9922.

Guckenberger, Achim, and Stephan Gekle. 2017. Theory and algorithms to compute helfrich bending forces: A review. *Journal of Physics: Condensed Matter* 29(20):203001.

Guerriero, Réjean M, Christopher C Giza, and Alexander Rotenberg. 2015. Glutamate and gaba imbalance following traumatic brain injury. *Current neurology and neuroscience reports* 15:1–11.

Gulati, Rahul, and Shiva Rudraraju. 2023. Spatio-temporal modeling of saltatory conduction in neurons using poisson–nernst–planck treatment and estimation of conduction velocity. *Brain Multiphysics* 4:100061.

Hanisch, Uwe-Karsten. 2002. Microglia as a source and target of cytokines. *Glia* 40(2):140–155.

Haselwandter, Christoph A, and Roderick MacKinnon. 2018. Piezo's membrane footprint and its contribution to mechanosensitivity. *Elife* 7: e41968.

Hassinger, Julian E, George Oster, David G Drubin, and Padmini Rangamani. 2017. Design principles for robust vesiculation in clathrin-mediated endocytosis. *Proceedings of the national academy of sciences* 114(7):E1118–E1127.

Hattori, Motoyuki, and Eric Gouaux. 2012. Molecular mechanism of atp binding and ion channel activation in p2x receptors. *Nature* 485(7397): 207–212.

Healy, Edel, Mark Dempsey, Christine Lally, and Michael P Ryan. 1998. Apoptosis and necrosis: mechanisms of cell death induced by cyclosporine a in a renal proximal tubular cell line. *Kidney international* 54(6):1955–1966.

Helfrich, Wolfgang. 1973. Elastic properties of lipid bilayers: theory and possible experiments. *Zeitschrift für Naturforschung C* 28(11-12):693–703.

Hrabok, MM, and TM Hrudey. 1984. A review and catalogue of plate bending finite elements. *Computers & Structures* 19(3):479–495.

Hu, Junjie, Yoko Shibata, Christiane Voss, Tom Shemesh, Zongli Li, Margaret Coughlin, Michael M Kozlov, Tom A Rapoport, and William A Prinz. 2008. Membrane proteins of the endoplasmic reticulum induce high-curvature tubules. *Science* 319(5867):1247–1250.

Hu, Xinli, Yu Xu, Haojie Zhang, Yao Li, Xiangyang Wang, Cong Xu, Wenfei Ni, and Kailiang Zhou. 2022. Role of necroptosis in traumatic brain and spinal cord injuries. *Journal of Advanced Research* 40:125–134.

Hurley, James H, Evzen Boura, Lars-Anders Carlson, and Bartosz Różycki. 2010. Membrane budding. *Cell* 143(6):875–887.

Iovino, L, ME Tremblay, and L Civiero. 2020. Glutamate-induced excitotoxicity in parkinson's disease: The role of glial cells. *Journal of pharmacological sciences* 144(3):151–164.

Jara, Javier H, Brij B Singh, Angela M Floden, and Colin K Combs. 2007. Tumor necrosis factor alpha stimulates nmda receptor activity in mouse cortical neurons resulting in erk-dependent death. *Journal of neurochemistry* 100(5):1407–1420.

Jian-Guo, Hu, and Ou-Yang Zhong-Can. 1993. Shape equations of the axisymmetric vesicles. *Physical Review E* 47(1):461.

Johnson, Victoria E, William Stewart, and Douglas H Smith. 2013. Axonal pathology in traumatic brain injury. *Experimental neurology* 246:35–43.

Kant, Aayush, Victoria E Johnson, John D Arena, Jean-Pierre Dollé, Douglas H Smith, and Vivek B Shenoy. 2021. Modeling links softening of

myelin and spectrin scaffolds of axons after a concussion to increased vulnerability to repeated injuries. *Proceedings of the National Academy of Sciences* 118(28):e2024961118.

Keating, Carolyn E, and D Kacy Cullen. 2021. Mechanosensation in traumatic brain injury. *Neurobiology of disease* 148:105210.

Khan, Md Ishak, Sheikh Fahad Ferdous, and Ashfaq Adnan. 2021a. Mechanical behavior of axonal actin, spectrin, and their periodic structure: A brief review. *Multiscale Science and Engineering* 1–20.

Khan, Md Ishak, Kathleen Gilpin, Fuad Hasan, Khandakar Abu Hasan Al Mahmud, and Ashfaq Adnan. 2021b. Effect of strain rate on single tau, dimerized tau and tau-microtubule interface: A molecular dynamics simulation study. *Biomolecules* 11(9):1308.

Kiendl, Josef, K-U Bletzinger, Johannes Linhard, and Roland Wüchner. 2009. Isogeometric shell analysis with kirchhoff–love elements. *Computer Methods in Applied Mechanics and Engineering* 198(49-52):3902–3914.

Kiendl, Josef, Ming-Chen Hsu, Michael CH Wu, and Alessandro Reali. 2015. Isogeometric kirchhoff–love shell formulations for general hyperelastic materials. *Computer Methods in Applied Mechanics and Engineering* 291:280–303.

Kim, Byung-Wook, Sushruta Koppula, Seong-Su Hong, Sae-Bom Jeon, Ji-Hye Kwon, Bang-Yeon Hwang, Eun-Jung Park, and Dong-Kug Choi. 2013. Regulation of microglia activity by glaucocalyxin-a: attenuation of lipopolysaccharide-stimulated neuroinflammation through nf-κb and p38 mapk signaling pathways. *PloS one* 8(2):e55792.

Kishimoto, Takuma, Yidi Sun, Christopher Buser, Jian Liu, Alphée Michelot, and David G Drubin. 2011. Determinants of endocytic membrane

geometry, stability, and scission. *Proceedings of the National Academy of Sciences* 108(44):E979–E988.

Konno, Ryan N, Nilima Nigam, and James M Wakeling. 2021. Modelling extracellular matrix and cellular contributions to whole muscle mechanics. *Plos one* 16(4):e0249601.

Koster, Gerbrand, Martijn VanDuijn, Bas Hofs, and Marileen Dogterom. 2003. Membrane tube formation from giant vesicles by dynamic association of motor proteins. *Proceedings of the National Academy of Sciences* 100(26):15583–15588.

Koumangoye, Rainelli. 2022. The role of cl- and k+ efflux in nlrp3 inflammasome and innate immune response activation. *American Journal of Physiology-Cell Physiology* 322(4):C645–C652.

Krieg, Michael, Alexander R Dunn, and Miriam B Goodman. 2014. Mechanical control of the sense of touch by β-spectrin. *Nature cell biology* 16(3):224–233.

Kukulski, Wanda, Martin Schorb, Marko Kaksonen, and John A G Briggs. 2012. Plasma membrane reshaping during endocytosis is revealed by time-resolved electron tomography. *Cell* 150(3):508–520.

Lam, Doris, Heather A Enright, Jose Cadena, Sandra KG Peters, Ana Paula Sales, Joanne J Osburn, David A Soscia, Kristen S Kulp, Elizabeth K Wheeler, and Nicholas O Fischer. 2019. Tissue-specific extracellular matrix accelerates the formation of neural networks and communities in a neuron-glia co-culture on a multi-electrode array. *Scientific Reports* 9(1): 1–15.

Lee, Christopher T, Justin G Laughlin, Nils Angliviel de La Beaumelle, Rommie E Amaro, J Andrew McCammon, Ravi Ramamoorthi, Michael Holst, and Padmini Rangamani. 2020a. 3D mesh processing using GAMer

2 to enable reaction-diffusion simulations in realistic cellular geometries. *PLoS Comput. Biol.* 16(4):e1007756.

Lee, Christopher T, Justin G Laughlin, John B Moody, Rommie E Amaro, J Andrew McCammon, Michael J Holst, and Padmini Rangamani. 2020b. An Open-Source mesh generation platform for biophysical modeling using realistic cellular geometries. *Biophys. J.* 118(5):1003–1008.

Letourneau, Paul C. 2009. Actin in axons: stable scaffolds and dynamic filaments. *Cell Biology of the Axon* 265–290.

Lewis, Amanda H, and Joerg Grandl. 2015. Mechanical sensitivity of piezo1 ion channels can be tuned by cellular membrane tension. *Elife* 4: e12088.

Li, Yanli, Xiaorong Yang, Cungen Ma, Jiantian Qiao, and Ce Zhang. 2008. Necroptosis contributes to the nmda-induced excitotoxicity in rat's cultured cortical neurons. *Neuroscience letters* 447(2-3):120–123.

Liang, Xiao, Di Zhang, Wenjia Liu, Yingjie Yan, Fang Zhou, Weidong Wu, and Zhen Yan. 2017. Reactive oxygen species trigger nf-κb-mediated nlrp3 inflammasome activation induced by zinc oxide nanoparticles in a549 cells. *Toxicology and Industrial Health* 33(10):737–745.

Lingappan, Krithika. 2018. Nf-κb in oxidative stress. *Current opinion in toxicology* 7:81–86.

Lipowsky, Reinhard. 2012. Spontaneous tubulation of membranes and vesicles reveals membrane tension generated by spontaneous curvature. *Faraday discussions* 161:305–331.

Liu, Jian, Yidi Sun, David G Drubin, and George F Oster. 2009. The mechanochemistry of endocytosis. *PLoS biology* 7(9).

Longhi, Luca, Carlo Perego, Fabrizio Ortolano, Silvia Aresi, Stefano Fumagalli, Elisa R Zanier, Nino Stocchetti, and Maria-Grazia De Simoni. 2013. Tumor necrosis factor in traumatic brain injury: effects of genetic deletion of p55 or p75 receptor. *Journal of Cerebral Blood Flow & Metabolism* 33(8):1182–1189.

Lu, Yun-Bi, Kristian Franze, Gerald Seifert, Christian Steinhäuser, Frank Kirchhoff, Hartwig Wolburg, Jochen Guck, Paul Janmey, Er-Qing Wei, Josef Käs, et al. 2006. Viscoelastic properties of individual glial cells and neurons in the cns. *Proceedings of the National Academy of Sciences* 103(47): 17759–17764.

Maas, Andrew IR, Nino Stocchetti, and Ross Bullock. 2008. Moderate and severe traumatic brain injury in adults. *The Lancet Neurology* 7(8): 728–741.

Mark, Leighton P, Robert W Prost, John L Ulmer, Michelle M Smith, David L Daniels, James M Strottmann, W Douglas Brown, and Lotfi Hacein-Bey. 2001. Pictorial review of glutamate excitotoxicity: fundamental concepts for neuroimaging. *American journal of neuroradiology* 22(10): 1813–1824.

Mattson, Mark P. 2023. *Sculptor and destroyer: Tales of glutamatethe brain's most important neurotransmitter*. MIT Press.

Maxian, Ondrej, Raul P Peláez, Alex Mogilner, and Aleksandar Donev. 2021. Simulations of dynamically cross-linked actin networks: morphology, rheology, and hydrodynamic interactions. *PLoS computational biology* 17(12):e1009240.

McMahon, Harvey T, and Jennifer L Gallop. 2005. Membrane curvature and mechanisms of dynamic cell membrane remodelling. *Nature* 438(7068):590–596.

McNiven, Mark A, and Heather M Thompson. 2006. Vesicle formation at the plasma membrane and trans-golgi network: the same but different. *Science* 313(5793):1591–1594.

Memet, Edvin, Feodor Hilitski, Margaret A Morris, Walter J Schwenger, Zvonimir Dogic, and L Mahadevan. 2018. Microtubules soften due to cross-sectional flattening. *Elife* 7:e34695.

Miao, Ling, Bertrand Fourcade, Madan Rao, Michael Wortis, and RKP Zia. 1991. Equilibrium budding and vesiculation in the curvature model of fluid lipid vesicles. *Physical Review A* 43(12):6843.

Milders, Maarten. 2019. Relationship between social cognition and social behaviour following traumatic brain injury. *Brain injury* 33(1):62–68.

Mogi, Makio, Minoru Harada, Peter Riederer, Hirotaro Narabayashi, Keisuke Fujita, and Toshiharu Nagatsu. 1994. Tumor necrosis factor-α (tnf-α) increases both in the brain and in the cerebrospinal fluid from parkinsonian patients. *Neuroscience letters* 165(1-2):208–210.

Molina, Rossana Rojas, Susanne Liese, and Andreas Carlson. 2020. Diffusion on membrane domes, tubes and pearling structures. *Biophysical Journal*.

Morlot, Sandrine, Valentina Galli, Marius Klein, Nicolas Chiaruttini, John Manzi, Frédéric Humbert, Luis Dinis, Martin Lenz, Giovanni Cappello, and Aurélien Roux. 2012. Membrane shape at the edge of the dynamin helix sets location and duration of the fission reaction. *Cell* 151(3):619–629.

Moussawi, Khaled, Arthur Riegel, Satish Nair, and Peter W Kalivas. 2011. Extracellular glutamate: functional compartments operate in different concentration ranges. *Frontiers in systems neuroscience* 5:94.

Muñoz-Planillo, Raúl, Peter Kuffa, Giovanny Martínez-Colón, Brenna L Smith, Thekkelnaycke M Rajendiran, and Gabriel Núñez. 2013. K+ efflux is the common trigger of nlrp3 inflammasome activation by bacterial toxins and particulate matter. *Immunity* 38(6):1142–1153.

Nadler, J Victor. 2012. Plasticity of glutamate synaptic mechanisms. *Jasper's Basic Mechanisms of the Epilepsies* [*Internet*]. *4th edition*.

Neumann, Dawn, and Anthony Lequerica. 2015. Cognitive problems after traumatic brain injury. *Archives of physical medicine and rehabilitation* 96(1):179–180.

Ng, Si Yun, and Alan Yiu Wah Lee. 2019. Traumatic brain injuries: pathophysiology and potential therapeutic targets. *Frontiers in cellular neuroscience* 13:528.

Nguyen-Thanh, Nhon, N Valizadeh, MN Nguyen, H Nguyen-Xuan, X Zhuang, P Areias, Goangseup Zi, YDLLRT Bazilevs, Laura De Lorenzis, and Timon Rabczuk. 2015. An extended isogeometric thin shell analysis based on kirchhoff–love theory. *Computer Methods in Applied Mechanics and Engineering* 284:265–291.

Nie, Zhenyu, Liming Tan, Jie Niu, and Bing Wang. 2022. The role of regulatory necrosis in traumatic brain injury. *Frontiers in Molecular Neuroscience* 15:1005422.

Novozilov, V. V. 1959. *The theory of thin shells*. Noordhoff Ltd.

Olmos, Gabriel, Jerònia Lladó, et al. 2014. Tumor necrosis factor alpha: a link between neuroinflammation and excitotoxicity. *Mediators of inflammation* 2014.

O'Brien, William T, Louise Pham, Georgia F Symons, Mastura Monif, Sandy R Shultz, and Stuart J McDonald. 2020. The nlrp3 inflammasome

in traumatic brain injury: potential as a biomarker and therapeutic target. *Journal of neuroinflammation* 17:1–12.

Pal, Mia Michaela. 2021. Glutamate: The master neurotransmitter and its implications in chronic stress and mood disorders. *Frontiers in human neuroscience* 15:722323.

Pelegrin, Pablo. 2021. P2x7 receptor and the nlrp3 inflammasome: Partners in crime. *Biochemical pharmacology* 187:114385.

Piccini, Alessandra, Sonia Carta, Sara Tassi, Denise Lasiglié, Gianluca Fossati, and Anna Rubartelli. 2008. Atp is released by monocytes stimulated with pathogen-sensing receptor ligands and induces il-1β and il-18 secretion in an autocrine way. *Proceedings of the National Academy of Sciences* 105(23):8067–8072.

Pribiag, Horia, and David Stellwagen. 2013. Tnf-α downregulates inhibitory neurotransmission through protein phosphatase 1-dependent trafficking of gabaa receptors. *Journal of Neuroscience* 33(40):15879–15893.

Quemeneur, François, Jon K Sigurdsson, Marianne Renner, Paul J Atzberger, Patricia Bassereau, and David Lacoste. 2014. Shape matters in protein mobility within membranes. *Proceedings of the National Academy of Sciences* 111(14):5083–5087.

Rahimi, Mohammad, and Marino Arroyo. 2012. Shape dynamics, lipid hydrodynamics, and the complex viscoelasticity of bilayer membranes. *Physical Review E* 86(1):011932.

Rand, RP. 1964. Mechanical properties of the red cell membrane: Ii. viscoelastic breakdown of the membrane. *Biophysical Journal* 4(4):303–316.

Rangamani, Padmini, Ashutosh Agrawal, Kranthi K Mandadapu, George Oster, and David J Steigmann. 2013. Interaction between surface shape

and intra-surface viscous flow on lipid membranes. *Biomechanics and modeling in mechanobiology* 12(4):833–845.

Rangamani, Padmini, Kranthi K Mandadap, and George Oster. 2014. Protein-induced membrane curvature alters local membrane tension. *Biophysical journal* 107(3):751–762.

Reiner, Andreas, and Joshua Levitz. 2018. Glutamatergic signaling in the central nervous system: ionotropic and metabotropic receptors in concert. *Neuron* 98(6):1080–1098.

Ridone, Pietro, Massimo Vassalli, and Boris Martinac. 2019. Piezo1 mechanosensitive channels: what are they and why are they important. *Biophysical reviews* 1–11.

Riemann, Bernhard. 1854. On the hypotheses which lie at the foundation of geometry. *A source book in mathematics* 2:411–425.

Roohbakhshan, Farshad, and Roger A Sauer. 2017. Efficient isogeometric thin shell formulations for soft biological materials. *Biomechanics and Modeling in Mechanobiology* 16(5):1569–1597.

de Rooij, Rijk, and Ellen Kuhl. 2018. Microtubule polymerization and cross-link dynamics explain axonal stiffness and damage. *Biophysical journal* 114(1):201–212.

de Rooij, Rijk, Ellen Kuhl, and Kyle E Miller. 2018. Modeling the axon as an active partner with the growth cone in axonal elongation. *Biophysical journal* 115(9):1783–1795.

Ross, AE, and RR Pompano. 2018. Diffusion of cytokines in live lymph node tissue using microfluidic integrated optical imaging. *Analytica chimica acta* 1000:205–213.

Rotondo, John Charles, Chiara Mazziotta, Carmen Lanzillotti, Chiara Stefani, Giada Badiale, Giulia Campione, Fernanda Martini, and Mauro Tognon. 2022. The role of purinergic p2x7 receptor in inflammation and cancer: Novel molecular insights and clinical applications. *Cancers* 14(5): 1116.

Rusakov, Dmitri A, Leonid P Savtchenko, Kaiyu Zheng, and Jeremy M Henley. 2011. Shaping the synaptic signal: molecular mobility inside and outside the cleft. *Trends in neurosciences* 34(7):359–369.

Sauer, Roger, Thang Duong, Kranthi Mandadapu, and David Steigmann. 2017. A stabilized finite element formulation for liquid shells and its application to lipid bilayers. *Journal of Computational Physics* 330:436–466.

Sauer, Roger A, and Thang X Duong. 2017. On the theoretical foundations of thin solid and liquid shells. *Mathematics and Mechanics of Solids* 22(3): 343–371.

Schaefer, M, J Link, L Hannemann, and K H Rudolph. 1995. Excessive hypokalemia and hyperkalemia following head injury. *Intensive care medicine* 21:235–237.

Schroeder, Thomas E. 1972. The contractile ring: Ii. determining its brief existence, volumetric changes, and vital role in cleaving arbacia eggs. *The Journal of cell biology* 53(2):419–434.

Seo, Joon Ho, Miloni S Dalal, and Jorge E Contreras. 2021. Pannexin-1 channels as mediators of neuroinflammation. *International journal of molecular sciences* 22(10):5189.

Shaklee, Paige M, Timon Idema, Gerbrand Koster, Cornelis Storm, Thomas Schmidt, and Marileen Dogterom. 2008. Bidirectional membrane tube dynamics driven by nonprocessive motors. *Proceedings of the National Academy of Sciences* 105(23):7993–7997.

Shi, Guangyu, and George Z Voyiadjis. 1991. Efficient and accurate four-node quadrilateral c0 plate bending element based on assumed strain fields. *International Journal for Numerical Methods in Engineering* 32(5): 1041–1055.

Shibata, Yoko, Gia K Voeltz, and Tom A Rapoport. 2006. Rough sheets and smooth tubules. *Cell* 126(3):435–439.

Shin, Andrew, Joseph Park, Alan Le, Vadims Poukens, and Joseph L Demer. 2020. Bilaminar mechanics of the human optic nerve sheath. *Current eye research* 45(7):854–863.

Shohami, Esther, Irene Ginis, and John M Hallenbeck. 1999. Dual role of tumor necrosis factor alpha in brain injury. *Cytokine & growth factor reviews* 10(2):119–130.

Simo, Juan C, and David D Fox. 1989. On a stress resultant geometrically exact shell model. i: Formulation and optimal parametrization. *Computer Methods in Applied Mechanics and Engineering* 72(3):267–304.

Simo, Juan C, and Thomas JR Hughes. 2006. *Computational inelasticity*, vol. 7. Springer Science & Business Media.

Simunovic, Mijo, Jean-Baptiste Manneville, Henri-François Renard, Emma Evergren, Krishnan Raghunathan, Dhiraj Bhatia, Anne K Kenworthy, Gregory A Voth, Jacques Prost, Harvey T McMahon, et al. 2017. Friction mediates scission of tubular membranes scaffolded by bar proteins. *Cell* 170(1):172–184.

Steigmann, DJ. 1999. Fluid films with curvature elasticity. *Archive for Rational Mechanics and Analysis* 150(2):127–152.

Stocchetti, Nino, and Elisa R Zanier. 2016. Chronic impact of traumatic brain injury on outcome and quality of life: a narrative review. *Critical Care* 20(1):1–10.

Strang, Gilbert, and George J Fix. 1973. *An analysis of the finite element method*. Prentice-hall.

Tagluk, M Emin, and Ramazan Tekin. 2014. The influence of ion concentrations on the dynamic behavior of the hodgkin–huxley model-based cortical network. *Cognitive neurodynamics* 8:287–298.

Takano, Kazunari, Kiminori Toyooka, and Shiro Suetsugu. 2008. Efc/f-bar proteins and the n-wasp–wip complex induce membrane curvature-dependent actin polymerization. *The EMBO journal* 27(21):2817–2828.

Takeuchi, Hideyuki, Shijie Jin, Jinyan Wang, Guiqin Zhang, Jun Kawanokuchi, Reiko Kuno, Yoshifumi Sonobe, Tetsuya Mizuno, and Akio Suzumura. 2006. Tumor necrosis factor-α induces neurotoxicity via glutamate release from hemichannels of activated microglia in an autocrine manner. *Journal of Biological Chemistry* 281(30):21362–21368.

Tepole, Adrián Buganza, Hardik Kabaria, Kai-Uwe Bletzinger, and Ellen Kuhl. 2015. Isogeometric kirchhoff–love shell formulations for biological membranes. *Computer methods in applied mechanics and engineering* 293: 328–347.

Tzlil, Shelly, Markus Deserno, William M Gelbart, and Avinoam Ben-Shaul. 2004. A statistical-thermodynamic model of viral budding. *Biophysical journal* 86(4):2037–2048.

Vasan, Ritvik, Shiva Rudraraju, Matthew Akamatsu, Krishna Garikipati, and Padmini Rangamani. 2020. A mechanical model reveals that non-axisymmetric buckling lowers the energy barrier associated with membrane neck constriction. *Soft Matter*.

Voeltz, Gia K, and William A Prinz. 2007. Sheets, ribbons and tubules—how organelles get their shape. *Nature Reviews Molecular Cell Biology* 8(3):258–264.

Vroman, Rozan, Lauw J Klaassen, Marcus HC Howlett, Valentina Cenedese, Jan Klooster, Trijntje Sjoerdsma, and Maarten Kamermans. 2014. Extracellular atp hydrolysis inhibits synaptic transmission by increasing ph buffering in the synaptic cleft. *PLoS biology* 12(5):e1001864.

Wang, Rui, and P Hemachandra Reddy. 2017. Role of glutamate and nmda receptors in alzheimer's disease. *Journal of Alzheimer's Disease* 57(4): 1041–1048.

Wang, Yanqin, Xuehui Zhang, Jinghui Wang, and Yubo Fan. 2022. Viscoelastic modeling of the stress relaxation behavior for the bionic extracellular matrix polymer scaffold. *Medicine in Novel Technology and Devices* 16:100181.

Weingarten, Murray D, Arthur H Lockwood, Shu-Ying Hwo, and Marc W Kirschner. 1975. A protein factor essential for microtubule assembly. *Proceedings of the National Academy of Sciences* 72(5):1858–1862.

Woodcock, Thomas, and Maria Cristina Morganti-Kossmann. 2013. The role of markers of inflammation in traumatic brain injury. *Frontiers in neurology* 4:18.

Xia, Jingsheng, Jason C Lim, Wennan Lu, Jonathan M Beckel, Edward J Macarak, Alan M Laties, and Claire H Mitchell. 2012. Neurons respond directly to mechanical deformation with pannexin-mediated atp release and autostimulation of p2x7 receptors. *The Journal of physiology* 590(10): 2285–2304.

Xing, Shu, Matthew W Grol, Peter H Grutter, S Jeffrey Dixon, and Svetlana V Komarova. 2016. Modeling interactions among individual p2 receptors to explain complex response patterns over a wide range of atp concentrations. *Frontiers in physiology* 7:294.

Xu, Ziwei, Zi-mo Chen, Xiaoyan Wu, Linjie Zhang, Ying Cao, and Pingzheng Zhou. 2020. Distinct molecular mechanisms underlying potassium efflux for nlrp3 inflammasome activation. *Frontiers in immunology* 11:609441.

Yan, Shi Du, XI Chen, Jin Fu, Ming Chen, Huaijie Zhu, Alex Roher, Timothy Slattery, Lei Zhao, Mariko Nagashima, John Morser, et al. 1996. Rage and amyloid-β peptide neurotoxicity in alzheimer's disease. *Nature* 382(6593):685–691.

Yang, Henry TY, S Saigal, A Masud, and RK Kapania. 2000. A survey of recent shell finite elements. *International Journal for numerical methods in engineering* 47(1-3):101–127.

You, Kai, Hui Gu, Zhengwei Yuan, and Xuewen Xu. 2021. Tumor necrosis factor alpha signaling and organogenesis. *Frontiers in Cell and Developmental Biology* 9:727075.

Zareh, Mehrdad, and Xiaoping Qian. 2019. Kirchhoff–love shell formulation based on triangular isogeometric analysis. *Computer Methods in Applied Mechanics and Engineering* 347:853–873.

Zhang, Hengdi, Zaiyi Shen, Brenna Hogan, Abdul I Barakat, and Chaouqi Misbah. 2018. Atp release by red blood cells under flow: model and simulations. *Biophysical journal* 115(11):2218–2229.

Zhao, Qiancheng, Heng Zhou, Xueming Li, and Bailong Xiao. 2019. The mechanosensitive piezo1 channel: a three-bladed propeller-like structure and a lever-like mechanogating mechanism. *The FEBS journal* 286(13): 2461–2470.

Zhao, Yuting, Jianglan Liu, Changsong Yang, Benjamin R Capraro, Tobias Baumgart, Ryan P Bradley, N Ramakrishnan, Xiaowei Xu, Ravi Radhakrishnan, Tatyana Svitkina, et al. 2013. Exo70 generates membrane

curvature for morphogenesis and cell migration. *Developmental cell* 26(3): 266–278.

Zheng, Wei-Mou, and Jixing Liu. 1993. Helfrich shape equation for axisymmetric vesicles as a first integral. *Physical Review E* 48(4):2856.

Zienkiewicz, OC, and D Lefebvre. 1988. A robust triangular plate bending element of the reissner–mindlin type. *International journal for numerical methods in engineering* 26(5):1169–1184.

Zimmerberg, Joshua, and Michael M Kozlov. 2006. How proteins produce cellular membrane curvature. *Nature reviews Molecular cell biology* 7(1): 9–19.

Zou, Jian Y, and Fulton T Crews. 2005. Tnfα potentiates glutamate neurotoxicity by inhibiting glutamate uptake in organotypic brain slice cultures: neuroprotection by nfκb inhibition. *Brain research* 1034(1-2):11–24.